

POLITECNICO DI TORINO

DEPARTMENT OF ELECTRONIC AND TELECOMMUNICATIONS

MASTER IN ELECTRONIC ENGINEERING



MASTER THESIS

---

**Wearable antennas development for  
microwave brain stroke imaging**

---

Advisor  
Prof.ssa Francesca VIPIANA

Candidate  
Silvia SALONIA

Co-Advisor  
Dott. Jorge TOBON

Academic Year 2019 – 2020



# Abstract

The aim of this thesis is to present the design of a novel flexible and compact antenna for the microwave brain stroke imaging system. The design consists in defining the optimal antenna geometry and the matching medium thickness in order to guarantee flexibility and matching between the antenna and the head. This goal is achieved by using CST Microwave Studio software in which the scattering parameters were observed. These simulations exploited several models to obtain the best configuration to be used, starting from a simple model up to a complex model. The accomplishment of the specification through the simulation allows to realize the wearable antennas to verify experimentally if they work correctly. Finally, they were tested close by a 3-D head phantom, filled with a liquid mimicking the brain tissues, to determine if they work properly, if they are able to transmit information and then reveal the presence of a possible target. The measurement process consisted in acquiring the scattering matrix before and after the introduction of a target. Testing reveals that the changing in the transmission coefficient before and after the insertion of the target allows to affirm that the antennas are able to pick up the object with the result that they are flexible and compact.



# Contents

<b>1</b>	<b>Introduction</b>	<b>15</b>
1.1	Background . . . . .	15
1.2	Contribution . . . . .	16
1.3	Outline . . . . .	16
<b>2</b>	<b>Theoretical concepts</b>	<b>17</b>
2.1	Antennas . . . . .	17
2.1.1	Antenna regions . . . . .	17
2.1.2	Antenna field distribution . . . . .	19
2.1.3	Transmission line theory . . . . .	20
2.1.4	Type of antennas . . . . .	24
2.2	Brain stroke . . . . .	25
2.2.1	Method to detect brain stroke . . . . .	26
<b>3</b>	<b>Design Specification</b>	<b>31</b>
3.1	Working frequency range and matching medium selection . . . . .	31
3.2	Substrate and matching material features . . . . .	34
3.3	Number of probes, position and polarization design . . . . .	36
3.4	Issues and their solutions . . . . .	38
<b>4</b>	<b>Numerical Simulations</b>	<b>41</b>
4.1	Model System . . . . .	41
4.1.1	Antenna model . . . . .	41
4.1.2	Head model . . . . .	43
4.2	Results simulations . . . . .	45
4.2.1	Step 1 . . . . .	45
4.2.2	Step 2 . . . . .	48
4.2.3	Step 3 . . . . .	51
4.2.4	Step 4 . . . . .	54
4.2.5	Optimization . . . . .	56
4.3	Results on curved structure . . . . .	61
4.4	Results for transmission . . . . .	67
4.5	Results on head model . . . . .	71
4.5.1	Head model with one antenna . . . . .	71
4.5.2	Head model with two antennas . . . . .	73
4.5.3	Head model with twenty-four antennas . . . . .	77

<b>5</b>	<b>Manufacturing and measurements</b>	<b>87</b>
5.1	MiBraScan system . . . . .	87
5.1.1	VNA and switching matrix . . . . .	87
5.1.2	Final prototype structure . . . . .	88
5.2	Antennas realization and validation . . . . .	89
5.3	Measurements results . . . . .	93
<b>6</b>	<b>Conclusion and future work</b>	<b>105</b>

# List of Figures

2.1	Equivalent circuit for Transmitter (Tx) and Reciver (Rx) systems [3]	17
2.2	Electromagnetic (EM) field . . . . .	18
2.3	Fields distribution [4] . . . . .	19
2.4	Coaxial cable [7] . . . . .	21
2.5	Equivalent electric circuit of a coaxial cable [7] . . . . .	21
2.6	Scheme of impedance transformer [7] . . . . .	22
2.7	Matching network [7] . . . . .	23
2.8	Two-port device and definition of the relevant power waves [7] .	23
2.9	Monopole antenna structure . . . . .	25
2.10	Monopole antenna structure with triangular shape . . . . .	25
2.11	Type of stroke, ischaemic (on left) and haemorrhagic (on right) [9]	26
2.12	Computerized Tomography (CT) device [12] . . . . .	27
2.13	Magnetic Resonance Imaging (MRI) device [13] . . . . .	28
2.14	Signal transmission of breast cancer detection [15] . . . . .	29
3.1	Head model [22] . . . . .	32
3.2	Transmission coefficient [22] . . . . .	34
3.3	Electrical properties of mixture of urethane rubber and graphite powder . . . . .	36
3.4	CN of the discretized scattering operator versus the number and orientation of the probes on surface [1] . . . . .	37
3.5	Discretization error versus the number and orientation of the probes on surface evaluated for infinite and limited Dynamic Range (DR) [1] . . . . .	38
3.6	Position of antennas on head [1] . . . . .	38
4.1	(a) Top side antenna; (b) bottom side antenna . . . . .	41
4.2	Antenna geometry for CST Microwave Studio . . . . .	42
4.3	Dielectric permittivity of <i>head_import</i> . . . . .	43
4.4	Planar head model for CST Microwave Studio . . . . .	43
4.5	Cylinder head model for CST Microwave Studio . . . . .	44
4.6	Complete head model for CST Microwave Studio . . . . .	45
4.7	CST Microwave studio model . . . . .	46
4.8	$S_{11}$ representation . . . . .	47
4.9	Smith Chart . . . . .	47
4.10	Field monitor results . . . . .	48
4.11	CST Microwave Studio model with ABS . . . . .	49
4.12	$ S_{11} $ with ABS . . . . .	49
4.13	CST Microwave Studio model with G30 . . . . .	50

4.14	$ S_{11} $ with G30 . . . . .	50
4.15	$ S_{11} $ of the h and h_pan sweep . . . . .	51
4.16	$ S_{11} $ for material selection . . . . .	52
4.16	$ S_{11} $ for material selection . . . . .	53
4.17	$ S_{11} $ of new and old design . . . . .	54
4.18	$ S_{11} $ of first geometry modification . . . . .	55
4.18	$ S_{11} $ of first geometry modification . . . . .	56
4.19	$ S_{11} $ for material verification (Optimization) . . . . .	57
4.20	$ S_{11} $ of interested curves (Optimization) . . . . .	58
4.21	Results of curve(27) . . . . .	59
4.21	Results of curve(27) . . . . .	60
4.21	Results of curve(27) . . . . .	61
4.22	Results of curve(27) on curved structure . . . . .	61
4.22	Results of curve(27) on curved structure . . . . .	62
4.22	Results of curve(27) on curved structure . . . . .	63
4.23	Results of curve(27) . . . . .	64
4.23	Results of $ S_{11} $ with different bending radius . . . . .	65
4.24	Results of curve(12) . . . . .	65
4.24	Results of curve (12) . . . . .	66
4.25	Results of curve (12) . . . . .	67
4.26	Reflection and transmission of antenna (12) . . . . .	68
4.26	Reflection and transmission of antenna (12) . . . . .	69
4.27	Reflection and transmission of antenna (12) . . . . .	69
4.27	Reflection and transmission of antenna (12) . . . . .	70
4.28	Head model with one antenna for CST Microwave Studio . . . . .	72
4.29	Results on head model with one antenna . . . . .	72
4.29	Results on head model with one antenna . . . . .	73
4.30	Head model with two antennas and no target for CST Microwave Studio . . . . .	74
4.31	S-parameters with two antennas and no target . . . . .	74
4.32	Head model with two antennas and stroke for CST Microwave Studio . . . . .	75
4.33	S-parameters with two antennas and stroke . . . . .	76
4.34	S-parameters without and with stroke . . . . .	76
4.35	Differential signal of $ S_{12} $ . . . . .	76
4.36	Model with twenty-four antennas for CST Microwave Studio . . . . .	77
4.37	Reflection coefficients of the system . . . . .	78
4.38	Graphical representation of the differential matrix . . . . .	85
5.1	First prototype system [21] . . . . .	88
5.2	Actual prototype system [16] . . . . .	88
5.3	Printed antenna . . . . .	89
5.4	Mixture of urethane rubber and graphite powder on the mould . . . . .	90
5.5	Flexibility of thin and thick layers . . . . .	91
5.6	Flexibility of G25 (left) and G35(right) layers . . . . .	91
5.7	Antenna and matching material stick together . . . . .	92
5.8	Structure with connector . . . . .	92
5.9	Final structure . . . . .	92
5.10	Comparison between measured and simulated $S_{11}$ on bigger R . . . . .	93
5.11	Measurement on jar . . . . .	94

5.12 Measured $S_{11}$ on jar . . . . .	94
5.12 Measured $S_{11}$ on jar . . . . .	95
5.13 Comparison of measured $ S_{11} $ on jar . . . . .	95
5.14 Transmission between first and second antenna on jar . . . . .	96
5.15 3D phantom head system . . . . .	96
5.16 Measured $S_{11}$ for all the realized antenna on phantom head . . . . .	97
5.17 Measured S - parameters on phantom head . . . . .	98
5.17 Measured S - parameters on phantom head . . . . .	99
5.17 Measured S - parameters on phantom head . . . . .	100
5.18 Measured S-parameters on phantom head couple antenna 1 and 2	100
5.18 Measured S-parameters on phantom head couple antenna 1 and 2	101
5.19 Measured S-parameters on phantom head couple antenna 1 and 3	101
5.19 Measured S-parameters on phantom head couple antenna 1 and 3	102
5.20 Measured S-parameters on phantom head couple antenna 1 and 5	102
5.20 Measured S-parameters on phantom head couple antenna 1 and 5	103
5.21 Differential signals for the measured antennas . . . . .	103
5.21 Differential signals for the measured antennas . . . . .	104



# List of Tables

3.1	Design specifications . . . . .	31
3.2	Cole-Cole parameters of human head tissues [22] . . . . .	33
3.3	Urethane rubber and graphite powder in 120 g of mixture . . . . .	35
4.1	Parameters list . . . . .	42
4.2	Head parameters . . . . .	44
4.3	Head parameters with curvature . . . . .	44
4.4	Starting parameters list . . . . .	46
4.5	New parameters list . . . . .	54
4.6	Results from the first parametrization sweep of the antenna geometry . . . . .	56
4.7	Results from the first parametrization sweep of the antenna geometry . . . . .	58
4.7	Results from the first parametrization sweep of the antenna geometry . . . . .	58
4.8	Comparison of $ S_{11} $ and bandwidth between curve(27) and curve(28) . . . . .	59
4.9	Optimization on curved structure . . . . .	64
4.10	Comparison of $ S_{11} $ and bandwidth between curve(2), curve(5) and curve(12) with $R = 100$ mm . . . . .	65
4.11	Dielectric properties of blood from 0.8GHz to 1.6GHz . . . . .	75
5.1	Urethane rubber and graphite powder in 100 g of mixture . . . . .	90



# Acronyms

**Tx** Transmitter

**Rx** Receiver

**TL** Transmission Line

**EM** Electromagnetic

**CT** Computerized Tomography

**MRI** Magnetic Resonance Imaging

**MWI** Microwave Imaging

**RF** Radio Frequency

**ABS** Acrylonitrile butadiene styrene

**PI** Polyimide

**VNA** Vector Network Analyser

**SVD** Singular Value Decomposition

**CN** Condition Number

**SNR** Signal-to-noise ratio

**DR** Dynamic Range

**PSF** Point Spread Function

**SP4T** Single-pole-four-throw

**SP6T** Single-pole-six-throw

**SPDT** Single-pole-double-throw



# Chapter 1

## Introduction

### 1.1 Background

Brain stroke is a neurological disease that has a high mortality rate and, even when it is possible to survive, it is in most cases, one of the main causes of disability, dementia and more in general, permanent injuries. This is due to the fact that poor blood flows into the brain causing the death of cerebral cells.

There are two different types of strokes that cause the failure of the brain functionalities: ischaemic (in case of absence of blood flow) or haemorrhagic (due to bleeding into the brain) [1]. To define the therapy to follow, it is important to define what kind of stroke affects the brain and this can be done via different diagnostic methodologies.

The conventional diagnostic methodologies, such as Magnetic Resonance Imaging (MRI) or X-ray Computerized Tomography (CT), are way too powerful and can be harmful for patients, along with being also more expensive and available only in the hospitals [2]. In addition, it is important to note that these methodologies are time-consuming methods and for this reason they are not able to provide a real-time image of the head with the probability of causing the worsening of the disease or also death [1].

An interesting solution should be the realization of a complementary system, in order to have an initial diagnosis of the problem already before the patient's arrive in hospital. In this way, it is possible to prevent severe damages.

Such system should be compact, portable and able to supply a real-time image of head. A high potential is represented by the Microwave Imaging (MWI) for brain stroke monitoring, that is a system that works on the microwave frequencies, characterized by low intensity and non-ionizing radiations that make it one of the safest methods among the already known ones.

A prototype of this system has been realized at the Politecnico di Torino and it is supported by the Italian Ministry of University and Research (MIUR). The project is called "MiBraScan - Microwave Brain Scanner for Cerebrovascular Disease Monitoring" in which a microwave imaging system should be realized, by taking advantage on dielectric properties contrast between brain and stroke tissues.

This prototype is made of 24 antennas, that work as Transmitter (Tx) and Receiver (Rx), placed around a phantom with a head shape and filled with a liquid mimicking the brain tissues. The working frequency range is around 1 GHz. The antennas are connected to a Vector Network Analyser (VNA) through a

switching matrix that allows to compute the transmission coefficients between them. However, some features of this prototype that should be improved are to be more compact and flexible so that the antennas could adapt well to the head shape.

Obviously, the phantom is not included in the final system, but it is used to verify the functionality of the MWI system such that a head shape is given.

## 1.2 Contribution

The main aim of this thesis is to improve the aspects described in 1.1. The actual prototype is in fact made of monopole antennas that are printed on a FR4 substrate. This last is put between two thicker layers of a mixture of urethane rubber and graphite powder to guarantee the matching with the head. Based on these properties, the structure results to be quite rigid and large. Hence, in this thesis novel flexible antennas have been designed, realized and tested. First of all, the antenna is chosen to be printed on a very thin polyimide support. Then, the matching material is projected to guarantee flexibility. Finally, the design of the monopole antenna is revisited to obtain matching between the antenna and the head.

In order to obtain the matching between the new antenna and the head, several simulations were done using CST Microwave Studio software in which the scattering parameters were observed to define reflection and transmission coefficients of antennas. These simulations exploited several models to obtain the best configuration to be used. Starting from a simple model (a parallelepiped) up to a complex model (a head), the parameters characterizing the antenna and the layers were changing until a good matching was obtained.

After the accomplishment of the specification through the simulation, the new antennas and the new layers were realized to verify experimentally if they work correctly. The measures consisted in testing different antennas close by the head phantom (six antennas were tried) singularly or by coupling them to determine if they work properly, if they are able to transmit information and then reveal the presence of a possible target.

## 1.3 Outline

This thesis is divided into three main parts:

- in the first part (Chapter 2) a theoretical background on antennas and brain stroke is proposed. In this way, it is possible to understand the main antennas functionalities and how brain stroke influences the every-day life;
- in the second part, represented by Chapters 3 and 4, the project design specifications are explained, by exploiting the most important steps in choosing them and by simulating the system until their verification;
- the final part (Chapter 5) consists in describing the measurement process by talking about the MiBraScan system and the antenna production.

## Chapter 2

# Theoretical concepts

### 2.1 Antennas

Antennas are important components in telecommunication systems allowing the information propagation in the space between a Tx and a Rx. In particular, they are transducers that allow to couple the circuit and surrounding space admitting the conversion of an electric signal into an electromagnetic wave or vice versa, depending on the communication working mode, so if it is in transmit or receive mode.

From an electrical point of view, the transmitting and receiving systems can be seen as circuits made up of a generator and a load in which the energy transfer must be guided from the generator to the load through a Transmission Line (TL). In particular, it is possible to affirm that the Tx antenna works like a load for its TL, while the Rx antenna works like a generator. The equivalent circuits are the following:

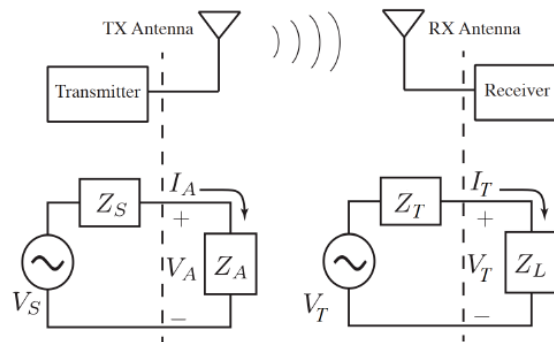


Figure 2.1: Equivalent circuit for Tx and Rx systems [3]

#### 2.1.1 Antenna regions

The surrounding area of an antenna can be subdivided into three regions. In these, their fields distribution are very different. Moreover, their division depends on the antenna dimension and wavelength [4]:

- *reactive near-field* in which the observation point has a distance  $R < 0.62\sqrt{D^3/\lambda}$ ;

- *radiative near-field* in which the observation point has a distance  $0.62\sqrt{D^3/\lambda} \leq R < 2D^2/\lambda$ ;
- *far-field* in which the observation point has a distance  $R > 2D^2/\lambda$ ;

where  $R$  is the distance of the analysed point;  $\lambda$  is the wavelength and  $D$  is the largest antenna dimension. Moreover, to make valid these conditions, it is necessary that "D must also be compared to the wavelength ( $D > \lambda$ )" [4].

The *reactive near-field* is the immediately surrounding area of an antenna, in which the reactive effects of fields predominate. This means that their quadrature components tend to prevail. Moreover, E and H fields are out of phase of  $90^\circ$ , but to guarantee propagation or radiation it is necessary that they are perpendicular and in phase to each other, like in figure below:

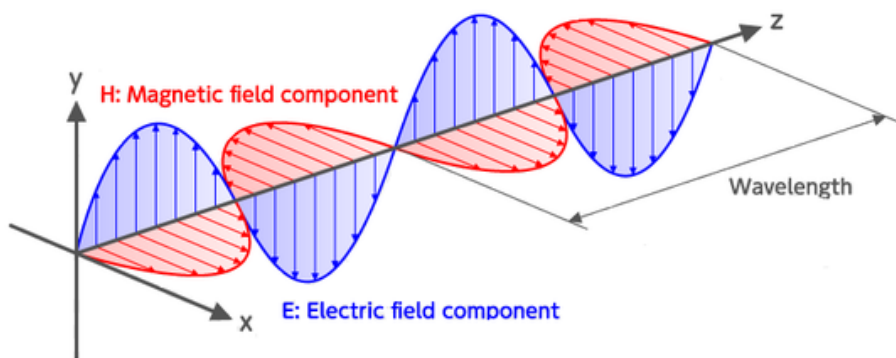


Figure 2.2: EM field

In this region the power flow is very low obtaining a very rapid decay of the reactive energy components [5].

In the *radiative near-field*, also called Fresnel region, the radiative components of the fields start to prevail observing the radiation of the field. Anyway, the electric and the magnetic fields are computed separately since they strongly depends on the distance of the antenna to the analysed point [4].

Finally, in the *far-field* region, also called Fraunhofer region, the radiative components are predominant and the field distributions of the fields are independent on the distance. Therefore, it is possible to compute just one field and obtain the other through the characteristic impedance in free space [5].

The fields distribution of these region are reported in figure 2.3. In it, it is possible to observe that the field distribution is more or less uniform in the reactive near-field and it develops some lobes if it moves toward the far-field region.

The interested region for this thesis is the radiative near-field.

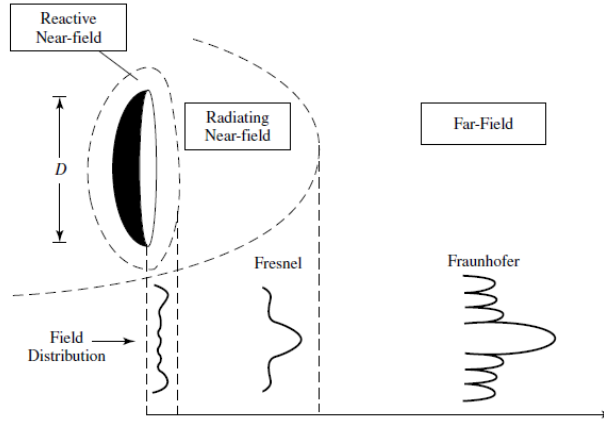


Figure 2.3: Fields distribution [4]

### 2.1.2 Antenna field distribution

For a system the electric and the magnetic fields are solution of the Maxwell's equations [6]:

$$\begin{aligned}\nabla \times \mathcal{E}(\mathbf{r}, t) &= -\frac{\partial}{\partial t} \mathcal{B}(\mathbf{r}, t) - \mathcal{M}(\mathbf{r}, t) \\ \nabla \times \mathcal{H}(\mathbf{r}, t) &= \frac{\partial}{\partial t} \mathcal{D}(\mathbf{r}, t) + \mathcal{J}(\mathbf{r}, t)\end{aligned}\quad (2.1)$$

in which:

- $\mathcal{E}(\mathbf{r}, t)$  is the electric field ( $V/m$ )
- $\mathcal{H}(\mathbf{r}, t)$  is the magnetic field ( $A/m$ )
- $\mathcal{D}(\mathbf{r}, t)$  is the electric induction ( $C/m^2$ )
- $\mathcal{B}(\mathbf{r}, t)$  is the magnetic induction ( $Wb/m^2$ )
- $\mathcal{J}(\mathbf{r}, t)$  is the source of the electric current density ( $A/m^2$ )
- $\mathcal{M}(\mathbf{r}, t)$  is the source of the magnetic current density ( $V/m^2$ )

For real, the magnetic current density is not a real physical quantity, but it is introduced to make symmetrical the system equations.

By applying constitutive relation and Fourier transform, it is possible to express the system in a "simple" way. Indeed, the partial derivative with respect to time is eliminated and the unknowns become just two: the electric and the magnetic fields:

$$\begin{aligned}\nabla \times \mathbf{E}(\mathbf{r}, \omega) &= -j\omega\mu(\omega)\mathbf{H}(\mathbf{r}, \omega) - \mathbf{M}(\mathbf{r}, \omega) \\ \nabla \times \mathbf{H}(\mathbf{r}, \omega) &= j\omega\varepsilon(\omega)\mathbf{E}(\mathbf{r}, \omega) + \mathbf{J}(\mathbf{r}, \omega)\end{aligned}\quad (2.2)$$

in which:

$$\begin{aligned}\mu(\omega) &= \mu_0\mu_r(\omega) \\ \varepsilon(\omega) &= \varepsilon_0\varepsilon_r(\omega)\end{aligned}$$

where  $\mu_0$  and  $\epsilon_0$  are the magnetic permeability and the dielectric permittivity, respectively. While  $\mu_r(\omega)$  and  $\epsilon_r(\omega)$  are the relative permeability and permittivity. Obviously, in free space the relative quantities are equal to 1, but in this thesis the antenna is in contact with a biological tissue. So, these values are different from 1 and they are generally complex. Moreover, since the material is non ferromagnetic, the relative permeability is very close to 1 [6].

Differently from the free space condition, the material between the Tx and Rx antennas is able to absorb and attenuate the fields. In addition, the different antennas and biological tissue dielectric constants introduce some reflection effects reducing the transmission. To this end, to avoid these effects it is important to apply the transmission line theory (section 2.1.3).

This object is a lossy material constitutes of its own relative dielectric constant and conductivity. For this reason, they should be taken into account in the Maxwell's equations:

$$\nabla \times \mathbf{H}(\mathbf{r}, \omega) = j\omega\epsilon(\omega)\mathbf{E}(\mathbf{r}, \omega) + \sigma\mathbf{E}(\mathbf{r}, \omega)$$

that becomes:

$$\nabla \times \mathbf{H}(\mathbf{r}, \omega) = j\omega\tilde{\epsilon}(\omega)\mathbf{E}(\mathbf{r}, \omega)$$

where  $\tilde{\epsilon}(\omega) = \epsilon - j\frac{\sigma}{\omega}$  in which  $\sigma$  is the conductivity of the material.

Moreover, it is possible to evaluate how far the field penetrates into the matter. The penetration depth allows to evaluate how deep the radiation intensity decays to  $1/e$  with respect to the surface quantity. This is inversely proportional to the matter absorption constant:

$$\delta_e = 1/\alpha \tag{2.3}$$

### 2.1.3 Transmission line theory

A conductive material that is able to "guide" the energy transfer from one point to another is called transmission line. Thanks to this behaviour it is possible to radiate an electric field. In particular, to guarantee the maximum energy transfer an impedance matching between generator, TL and load is necessary [7]. In this way, it is possible to reduce the reflection phenomena maintaining low signal attenuation and distortion.

Different types of TL exist:

- coaxial cable that is a cable made of a copper core that is divided by a copper shield thanks to a dielectric material;
- microstrip that is a structure made of a metal strip separated by a ground plane thanks to a dielectric material;
- stripline in which a conductive material is rounded by a dielectric material that separate it from two metal ground plane;
- waveguides are structure that take advantage on the different refractive index of the materials to guarantee the energy transfer.

For the first three structures, the analytical techniques are more or less the same, while they are different for the last one.

The interesting structure for this thesis is the coaxial cable that is used to feed a single antenna. The coaxial cable has a  $50\ \Omega$  characteristic impedance, so the ideal condition is to match the antenna to  $50\ \Omega$ . To do this, it is necessary to apply some expedients. First of all, some background on the TL are proposed. As explained in [7], to describe the TL parameters the equivalent circuit must be obtained.

First of all, the TL of coaxial cable can be represented by two parallel lines as below:

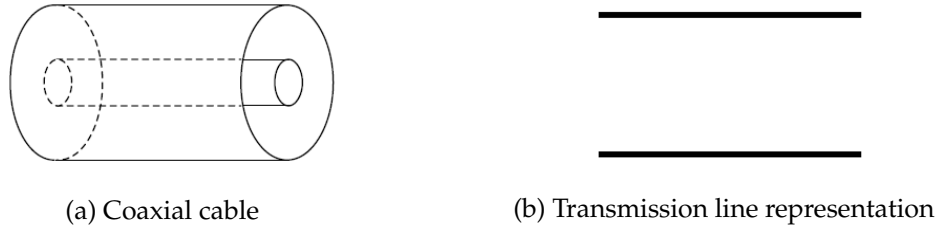


Figure 2.4: Coaxial cable [7]

To obtain the electric quantities the line length should be much lower than the signal wavelength. In other cases, it is difficult to predict the Kirchoff law. Hence, the idea, in this last condition, is to divide the line into small length  $\Delta z \ll \lambda$ . When this condition is accomplished, the structure can be modelled as:

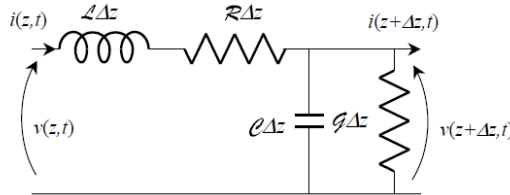


Figure 2.5: Equivalent electric circuit of a coaxial cable [7]

Because of the presence of inductors and capacitors, the quantities describing the circuit are not constant and for this reason they should be represented in function of time and position. By neglecting the impinges wave on the TL, it is possible to describe this system with homogeneous differential equations in which the solution is the combination of a forward and a backward wave. The equation system is:

$$\begin{aligned} \frac{\partial v}{\partial z} + \mathcal{L} \frac{\partial i}{\partial t} &= 0 \\ \frac{\partial i}{\partial z} + \mathcal{C} \frac{\partial v}{\partial t} &= 0 \end{aligned} \quad (2.4)$$

To eliminate the partial derivative, it is possible to apply the Fourier transform

and pass to the frequency domain. The system 2.4 becomes:

$$\begin{aligned} -\frac{d}{dz}V(z, \omega) &= j\mathcal{L}\omega I(z, \omega) \\ -\frac{d}{dz}I(z, \omega) &= jC\omega V(z, \omega) \end{aligned} \quad (2.5)$$

In this way, the system is simpler to solve. The quantities that describe the transfer wave are:

$$\begin{aligned} V(z, \omega) &= V_0^+(\omega)\exp(-jkz) + V_0^-(\omega)\exp(jkz) \\ I(z, \omega) &= I_0^+(\omega)\exp(-jkz) + I_0^-(\omega)\exp(jkz) \end{aligned} \quad (2.6)$$

In both, the first part of the solution express the forward component, while the other the backward. In particular,  $V_0^+(\omega)$  and  $I_0^+(\omega)$  are the amplitude of the forward wave.  $V_0^-(\omega)$  and  $I_0^-(\omega)$  are the amplitude of the backward wave.  $k = \frac{2\pi}{\lambda}$  represents the propagation constant that depends on the wavelength  $\lambda$ . Since from the first equation of 2.5 it is possible to observe that current is proportional to  $dV(\omega, z)/dz$ , it is possible to express  $I_0^\pm(\omega)$  in function of  $V_0^\pm(\omega)$ :

$$\begin{aligned} I_0^+ &= Y_\infty V_0^+(\omega) \\ I_0^- &= -Y_\infty V_0^-(\omega) \end{aligned}$$

where  $Y_\infty$  is the characteristic admittance of the TL. So 2.6 becomes:

$$\begin{aligned} V(z, \omega) &= V_0^+(\omega)\exp(-jkz) + V_0^-(\omega)\exp(jkz) \\ I(z, \omega) &= Y_\infty V_0^+(\omega)\exp(-jkz) - Y_\infty V_0^-(\omega)\exp(jkz) \end{aligned} \quad (2.7)$$

As said before, the ideal condition is to obtain matching between TL and load to avoid the reflection phenomena. This phenomenon comes when the forward wave reaches the end of the TL and it is reflected because of an interface creating the backward wave. To avoid it, the backward wave should be 0 or very small. This condition can be obtained when the load and the characteristic impedances are equal, that is like working with an infinite TL. On the other hand, their discontinuity creates a mismatch condition creating a sort of interface that allows the wave reflection. In both cases it is necessary to evaluate the reflection coefficient that allows to evaluate how much backward wave is present with respect to the forward wave:

$$\Gamma_{in} = \frac{V_0^-}{V_0^+}$$

To obtain  $\Gamma_{in} = 0$ , it is necessary to design matching networks. They will be positioned on the TL and before the load:

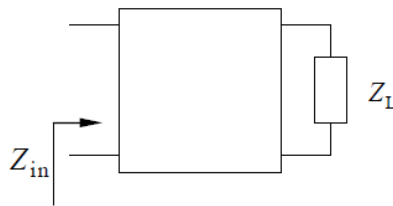


Figure 2.6: Scheme of impedance transformer [7]

The main matching networks are:

- L cells with lumped reactive in which reactive elements are introduced;
- single stub matching network in which a stub is introduced. It is a TL that ends with an open or short circuit and works like a reactance. This matching network can be realized by using double, triple, and so on, stubs;
- $\lambda/4$  matching network in which the TL is designed such that its length is equal to  $\lambda/4$ . In this way, the input normalized characteristic impedance is the inverse of the load one allowing to obtain  $\Gamma_{in} = 0$ .

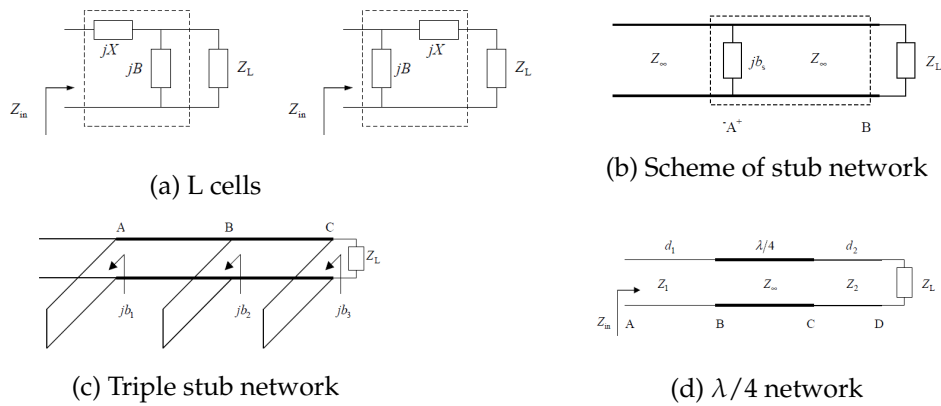


Figure 2.7: Matching network [7]

By working on the Smith chart, that uses the normalized impedances, it is possible to obtain the values of the components necessary for the networks.

In this thesis, to obtain matching between coaxial cable and the antenna, a double stub matching network is used.

In this thesis system, an array of 24 antennas is used that means 24 TL. Hence, it is possible to describe this system with a black box on which 24 TL are connected. To define the behaviour of it, the so called scattering matrix should be defined.

To simplify the study of this system, a 2 port structure is used like in [7]:

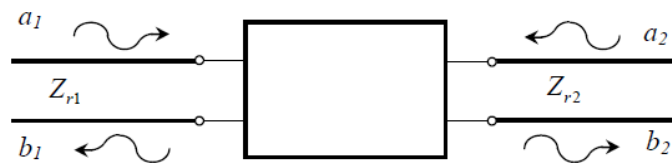


Figure 2.8: Two-port device and definition of the relevant power waves [7]

In this case, the definition of just the reflection coefficient is not sufficient since the quantities of a TL are dependent on those of the other, allowing to define the transmission coefficient, too.

The S-parameters are defined by using power wave amplitude. Hence, the incident and the reflected power wave amplitude must be defined to describe this system:

$$a_i = \sqrt{Y_{ri}}V^+$$

$$b_i = \sqrt{Y_{ri}}V^-$$

So, the equation system that describe the structure is:

$$b_1 = S_{11}a_1 + S_{12}a_2$$

$$b_2 = S_{21}a_1 + S_{22}a_2$$

that for a generic structure can be expressed in matrix form:

$$[b] = [S][a] \quad (2.8)$$

where  $S_{ij} = \frac{b_i}{a_i} \Big|_{a_k=0, k \neq j}$ . This means that to obtain the S-parameters the impedance matching condition is imposed. Moreover, the  $S_{ii}$  parameters represent the reflection coefficients of the general device, so they should be equal to 0 to respect the matching condition. Hence, to obtain it the described matching networks can be used.

The other quantities represent the transmission coefficients that allow to define how many information is transferred from one TL to the other. These allow to define a Tx and Rx antenna and thanks to this transmission, it is possible to detect the target.

#### 2.1.4 Type of antennas

Antennas can be classified in several ways, but in this case they are described depending on their structure.

Different type of antennas exist:

- *wire antennas* in which the current distribution is developed on a seems to be line support;
- *aperture antennas* in which the field distribution is developed on a surface that is called aperture;
- *reflector antennas* that take advantage on the diffraction effect on a metallic surface for the field radiation;
- *printed antennas* in which a radiated metallic structure is separated from the ground plane thanks to some dielectric layers called substrates;
- *array antennas* in which several antennas are positioned on specific spots allowing the improvement of some antennas features;
- *lens antennas* in which suitable lens are designed to guarantee the EM field convergence.

In this thesis a monopole antenna is used. It belongs to *wire antennas* class, but it is obtained in a printed implementation. In particular, it is a omnidirectional antenna that means that it should be able to radiate power in all the surrounding area, by varying its power depending on the angle with respect to the axis.

This kind of antenna is a particular configuration of the dipole antenna. The difference is that the inferior branch is substituted with a conductive plane that works like a ground plane:

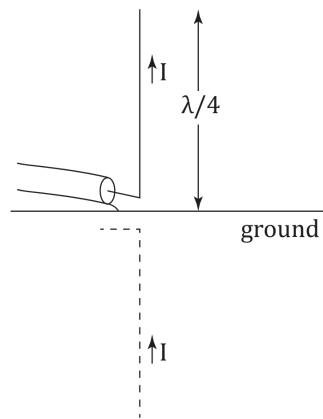


Figure 2.9: Monopole antenna structure

Basically, this structure takes advantage on the image theorem. Practically, the wave radiated from the superior branch are reflected by the ground plane, generating a dipole radiation. The advantage of this structure is that, by considering the same current flow in a dipole, the emitted power is halved. Moreover, the final part of the monopole has a triangular shape in order to guarantee a wide-band condition:

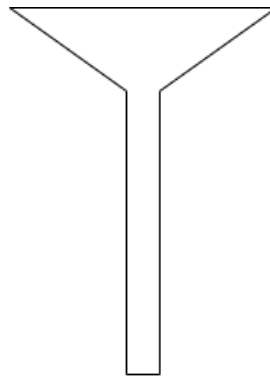


Figure 2.10: Monopole antenna structure with triangular shape

## 2.2 Brain stroke

Brain stroke is a neurological disease that has a high mortality rate and, even when it is possible to survive, it is in most cases, one of the main causes of disability, dementia and more in general, permanent injuries. This is due to the fact that a variation of blood flow takes place in head, by causing cerebral cells suffering and death. The average cerebral blood flow is of 49 mg/100 g of tissue. The gravity of this disease depends on some factors, like the time interval from the starting illness and the affected area. Indeed, in this last condition, different collateral effect are presents because of the interested zone. Moreover, as explained in [8], time is an important factor since every minute that pass from the starting stroke, about 1.9 million of neurons, 14 milliard of synapsis and 12 km of nervous fibres are lost. While every 4 minutes the probability of having

higher disability increases. And every 6 minutes the probability of lose your own autonomy increases, too.

The principle causes of brain stroke are the following [8]:

- the obstruction of arterial vessel due to other diseases;
- the formation of emboli or foreign material within the circulatory system;
- other diseases.

For this reason, brain stroke can be of two different types:

- *ischaemic* that is the more frequent (about 85%). In this case the lower flow is due to the blood vessels closure due to the presence of blood clot or emboli in the circulatory system;
- *haemorrhagic* due to the blood loss on brain causing an haemorrhage.

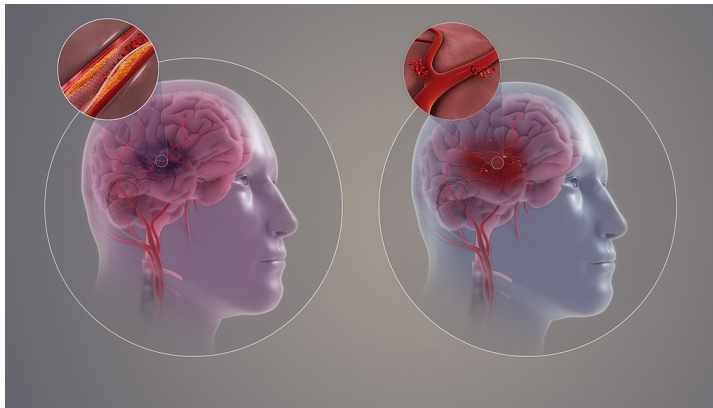


Figure 2.11: Type of stroke, ischaemic (on left) and haemorrhagic (on right) [9]

Depending on the stroke type different diagnosis and treatments are done. Generally, for the first case, a pharmacological therapy is done to melt the colt, while in the other it is necessary to intervene surgically [8].

Globally, stroke represents the second cause of death and the third of disability [10]. Hence, on 15 million people contract brain stroke every year. About 5 million of them dead, while the other 5 million are subjected to permanent injuries [11].

### 2.2.1 Method to detect brain stroke

When a brain stroke comes it is important that the patient goes to the hospital as soon as possible. Here, the patient is subjected to some tests, such as physical and blood exams. But, to detect and determine the nature of the illness it is important to reconstruct the internal head tissues images. The conventional methods to detect them are mainly two:

- CT;
- MRI.

### Computerized Tomography

CT is a method that takes advantage on a X-rays narrow beam. The process consists on the rotation of a tube that shoots the beam on the patient. The X-rays are detected by detectors that are positioned on the opposite site of the beam source. They are able to produce signals that are processed to generate the imaging of internal tissues[12].

In particular, data do not generate a organ 3D image, but it realizes some 2D slices. They can be stacked together later in order to obtain the whole image. Obviously, not all the organs are easy to reconstruct since they are made of tissues that absorb X-rays in a way that makes imaging difficult . Therefore, some pharmacological agents visible to rays are used [12].

Anyway, this type of method presents an important issue. X-rays are ionizing radiation that have sufficient energy to tear away electrons from atoms or molecules. About that, some unwanted effect on tissues can be obtained. In particular, this risk increases if the patient is frequently subjected to this exposure.



Figure 2.12: CT device [12]

### Magnetic Resonance Imaging

MRI is a method that uses non-ionizing radiation. The device that allows to do MRI is composed by magnets that create high magnetic field. It is able to align protons present in the body. Then, a Radio Frequency (RF) current is applied to stimulate protons. After, the current is turned off and protons tend to realign to the magnetic field. To realize the image of tissue, MRI takes advantage on the energy release of protons from the on to off RF current. This energy is detected by sensors. Obviously, the time necessary to obtain image depends on the one needed for protons energy release [13].

Also in this case, it is possible to inject pharmacological agents that in this case allow to accelerate protons release and so time.

The big problem with this method is that it needs high magnetic fields, hence it is very powerful. Moreover, this method is too time-consuming.



Figure 2.13: MRI device [13]

### Microwave Imaging System

The conventional methods present some limits. Therefore, to overcome them a new imaging system method should be developed. In particular, the main goal is to realize a system that is compact and portable such that a pre-hospital diagnosis can be done, differently from the previous systems.

The solution can be the MWI system that is still matter of research, so a commercial and adopted system is not produced yet.

MWI is an imaging technique that has been evolved in order to detect hidden objects in a structure by taking advantage on Electromagnetic (EM) waves that work in microwave regime, that goes from about 300 MHz to 300 GHz. MWI technique is able to provide an imaged object by solving a nonlinear inverse problem. This one is converted into a linear inverse problem by using the Born approximation. But, when the problem is too expensive or when no approximation is necessary, it is possible to apply iterative solvers.[14]

A MWI system consists of a hardware and a software part. The first allows to collect the data measurements. This collection is possible thanks to a Tx antenna that is feed to generate an EM field that will penetrate into the the sample under test. This field is then picked up by a Rx antenna. To detect the object, the S-parameters are calculated as explained in section 2.1.3. Indeed, if matter is made of non-homogeneous material, EM wave will be reflected, allowing to detect the difference in the dielectric properties between the illness and the surrounding area [14].

Generally, this system is made of several antennas that are able to increase the spatial resolution of the system. But the antennas that are close to each other, because of coupling effect may scheme off the signal reducing the probability to detect the object. Hence, to overcome this problem, the idea should be to feed just one antenna per time that works as a Tx antenna. All the others will work in sequence as Rx antennas. In this way, just two antennas per time will scan the object under test. When all the antennas had worked as Tx, all the collected data will be processed thanks to the software part.

This type of process is used for several applications. But the interesting one is the medical that is matter of research, yet. Therefore, it could be a very useful method for the detection of breast cancer, brain stroke and so on. This is

due to the fact that these malignant tissues present dielectric properties that are very different from the surrounding tissues. So, the detection can be significant. Practically, "Microwave images for medical applications are maps of the electrical property distributions in the body" [15].

In the particular case of the medical application, a typical system is described in [15] in which a breast cancer is detected. Essentially, the energy wave coming from the Tx antenna is able to cross the breast it is detected by the Rx on the opposite side:

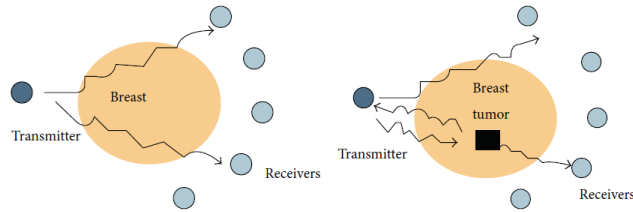


Figure 2.14: Signal transmission of breast cancer detection [15]

As said, due to different dielectric properties between breast and surrounding area, reflections can be recorded by Tx leading to scattering of the incident wave. This effect, changes the energy detected by Rx. All this process allows to generate the image from the information of detected energies.

This system presents some advantages [16]:

- it uses non - ionizing radiation allowing to make repeatable imaging avoiding the risk of tissues damages;
- it is compact and portable guaranteeing a pre - hospital diagnosis;
- low cost for both production and data process, hence it is possible to obtain a real-time evaluation of the problem.

Anyway, two types of this system have been tested on humans, yet [16]:

1. Strokefinder, developed by Medfield Diagnostic [17, 18]. This system allows to recognise if the stroke is ischaemic or haemorrhagic thanks to a database that has been realized by observing different stroke cases. It does not provide a head imaging, but it is simple and compact;
2. EMTensor Brain Scanner [19]. This system, differently on the first, allows to obtain the head imaging. But it is a very complex system since it is composed by a too high number of antennas that makes the data process expensive and slow.

The ideal condition, is to obtain a good trade-off to realize a system that is able to make the image maintaining the data process no more complex and able to discern the type of stroke.



## Chapter 3

# Design Specification

In this chapter, the design specification to be verified are presented. The design of the antenna is a real challenge because of the complexity of human head tissues that are lossy. This means that they strongly attenuate the EM signal and so it penetrates lower inside the head. Moreover, the inverse relation between frequency band and antenna size introduces some problems that influence the physical size of the antenna itself, changing the number of antennas around the head [20]. However, the idea is to realize a flexible antenna, for this reason it is important to introduce some specifications also for the antenna substrate. A summary of the specifications are reported below:

Working frequency	
Resonance frequency	1 GHz
Bandwidth @-10 dB	> 400 MHz
Substrate material	
Thickness	< 10 mm
Flexibility and robustness to bending	
Compatibility with human head tissues	
Antenna design	
Planar monopole antenna	
Length	48 mm
Width	30 mm

Table 3.1: Design specifications

In the successive sections, the main steps to obtain these specifications are described.

### 3.1 Working frequency range and matching medium selection

In this section, the selection of the working frequency range and the matching medium of the system is discussed. Their selection is treated together in order to guarantee the best trade-off between the wave penetration inside the head and the imaging resolution [1, 21]. Indeed, the penetration depth of the wave is inversely proportional to the absorption coefficient, that means it is inversely proportional to the working frequency. Hence, the working frequency range

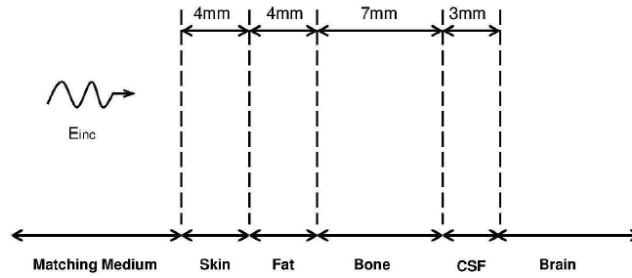
should be chosen such that it is a low range. Unfortunately, low frequencies are associated to large wavelengths that means that a low spacial image resolution is obtained, so the stroke should not be detected. For this reason, a trade-off should be obtained to guarantee the detection of the stroke.

To this end, it is good practice to study the materials that characterize the head in the TL theory. This study is carried out in paper [22] in which the evaluated range is the one that goes from 0.1 GHz to 10 GHz, since the application is the one of the microwave range.

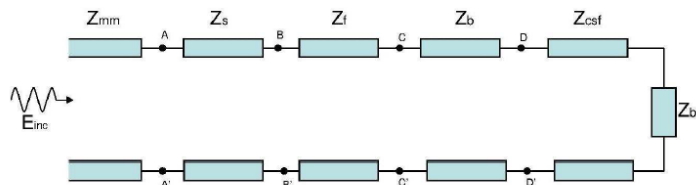
In this study the head is modeled with five planar layers that present different dielectric properties and length. These are:

1. skin;
2. fat;
3. cortex bone;
4. cerebrospinal fluid;
5. brain region.

In particular, in the brain region it is important to guarantee the maximum penetration of the incoming field. The model is the following one:



(a) Simplified layered model of human head



(b) Corresponding transmission line model

Figure 3.1: Head model [22]

In figure 3.1b the corresponding TL model is reported in which each head tissue is characterized by a proper characteristic impedance  $Z_n = \sqrt{\mu_0/\epsilon_0\epsilon_n}$  where  $\epsilon_n$  is the complex permittivity of the n-th section. Moreover, also the dispersive behaviour of the biological tissues must be taken into account by using the single-pole Cole-Cole model:

$$\epsilon(\omega) = \epsilon'(\omega) - j\epsilon''(\omega) = \epsilon_\infty + \frac{\Delta\epsilon}{1 + j\omega\tau^{1-\alpha}} + \frac{\sigma_i}{1 + j\omega\epsilon_0} \quad (3.1)$$

where:  $\omega$  is the angular frequency,  $\epsilon_\infty$  is the high frequency permittivity,  $\Delta\epsilon$  is the magnitude of the dispersion,  $\tau$  is the relaxation time constant,  $\alpha$  is the parameter that allows for the broadening of the dispersion and  $\sigma_i$  is the static ionic conductivity. For each tissue, these quantities are:

Tissue	$\epsilon_\infty$	$\Delta\epsilon$	$\tau$	$\alpha$	$\sigma_i$
Dry Skin	4	32	7.23e-12	0	0.0002
Fat	2.5	3.0	7.96e-12	0.2	0.01
Cortex bone	2.5	10	13.26e-12	0.2	0.02
Grey matter	4	45	7.96e-12	0.1	0.02
White matter	4	32	7.96e-12	0.1	0.02

Table 3.2: Cole-Cole parameters of human head tissues [22]

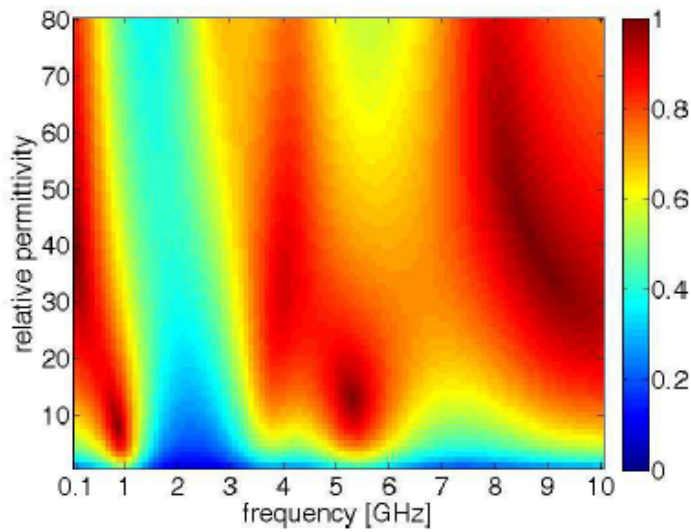
The quantities of cerebrospinal fluid is not available for the Cole Cole model in literature, so they are taken form in which  $\epsilon_{CSF} = 69.3$  and  $\sigma_{CSF} = 0.4\text{S/m}$ . Regarding the brain region, it is composed by grey and white matter, so this means that the brain electric properties are defined by averaging them.

After the definition of these quantities, it is possible to apply the TL formalism to determine the transmission coefficient  $T = 1 + \Gamma$ . It allows to compute the power of the incoming field that penetrates into the head.  $\Gamma$  is the reflection coefficient at the interface between the matching medium and skin (section AA’):

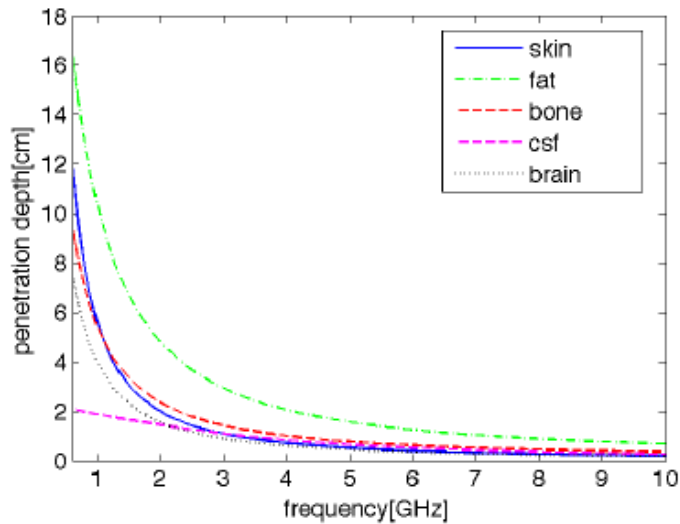
$$\Gamma = \frac{Z_{AA'} - Z_{mm}}{Z_{AA'} + Z_{mm}} \quad (3.2)$$

At this point, it is possible to observe why the selection of the working frequency range and the matching medium is done together. Indeed, to compute the transmission coefficient it is important to define the characteristic impedance of the coupling medium in which its dielectric constant is assumed to be real and to span from air to water  $\epsilon_{mm} = [1 \div 80]$ . By doing these consideration, the transmission coefficient in figures 3.2 is obtained.

Considering figure 3.2a, in which the amplitude of the transmission coefficient is plotted, it is possible to affirm that a sort of forbidden band exists in the  $1.5 \div 4\text{GHz}$  range since  $|T|$  is lower than 0.5 and, so, this operating conditions seems to be useless. Probably, its presence is due to the strong difference between the dielectric properties of cortex bone, fat layers and CSF that create a strong mismatch. At this end, the useful working frequency ranges are: the one that goes from 0.1 GHz to 1.5 GHz and the one that goes from 4 GHz to 10 GHz. But, by observing figure 3.2b, it is possible to observe that over 4 GHz the penetration depth is very low. So, it is not convenient to work over this frequency since the incoming field do not penetrate properly on the brain and the stroke detection becomes difficult. At the same time, it is not convenient to work with very low frequencies because of the low imaging resolution. The idea is choose the range that goes from 0.8 GHz to 1.2 GHz, in which a high transmission is obtained with matching medium that has relative permittivity higher than 20. For this reason, the chosen matching medium is a mixture of urethane rubber and graphite powder with a permittivity of  $\epsilon_{mm} = 23.1$  and a conductivity of  $\sigma_{mm} = 0.3\text{S/m}$ , at the operating frequency of 1 GHz.



(a) The transmission coefficient as a function of frequency and dielectric constant of the lossless matching medium



(b) Skin depth for human head tissues

Figure 3.2: Transmission coefficient [22]

### 3.2 Substrate and matching material features

The new designed antenna will be printed on a Polyimide (PI) substrate that is employed in different engineering fields because of its interesting properties. Anyway, for this project, PI is used as a support for the antenna, so its dielectric properties are more or less negligible. But, like reported in [23], it presents:

- excellent dielectric properties, in which the relative dielectric constant might vary between 3.1 and 3.5;
- great thermal stability, so this means that there is the possibility to fabricate materials that uses high temperature processes;
- low coefficient of thermal expansion because of its molecular structure;

- high chemical resistance;
- very good mechanical properties, indeed it presents an elongation at break of 90% that can be translated into a good flexibility. This material has a flexural modulus, the property that measure the flexibility of a plastic material, of  $(2.48 \div 4.1)GPa$ . Obviously, this last properties depends also on the thickness of the material: thicker is less flexible is, but in this case the material has a thickness of  $150\mu m$  so it is quite thin to be flexible;
- transparency to a lot of microwave application;
- low losses.

Initially, this material was largely used in aerospace and automotive fields because of the properties mentioned above, but because of its biocompatibility and biostability, it can be employed also in medical field, that is the interest one for this thesis.

As said in paragraph 3.1, to match the antenna and the head tissues, the matching material should present a relative dielectric constant higher than 20. But, to maintain a flexible and compact structure, an idea to control the dielectric properties of PI is to introduce a matching material made of mixtures of urethane rubber and graphite powder.

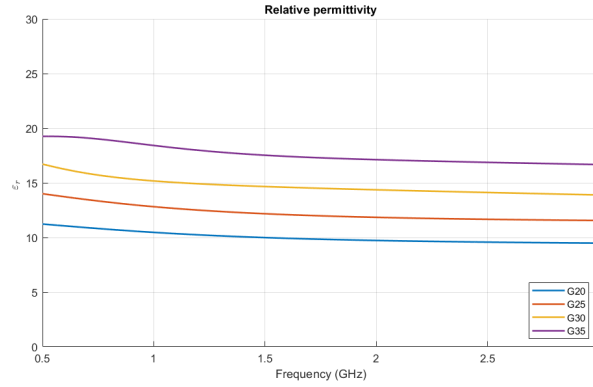
Urethane rubber is a material that belongs to the rubber family and it is extremely versatile in different engineering fields since it presents the best performances with respect to the natural rubber and also than some metals. This is due to the fact that it presents a high resistance to heat and elasticity, so it is a flexible structure. An interesting advantage is that it is an elastomer that resists to: radiation; abrasion; impact; ozone, oxygen and oil attack and chemical reaction. Moreover, the high abrasion resistance is the properties that make this material the best with respect to other rubber type, indeed, it is 10 times resistant than them [24]. The disadvantage of this material is that its relative dielectric constant is much lower than 20 at 1 GHz, so to increase it, it is possible to introduce graphite powder, that increase also the conductivity of urethane rubber [16].

In this case, the flexibility of urethane rubber is highly influenced by the graphite powder that will be added in the mixture: higher the graphite concentration is less flexible the structure is. By doing some studies, it was observed that by adding a percentage of graphite powder of 20%, 25%, 30% and 35% than the total mixture weight, the elongation of the urethane rubber is guaranteed if its thickness is lower than 10 mm. By supposing that 120 g of mixture are necessary, for each percentage the weight of urethane rubber and graphite powder are:

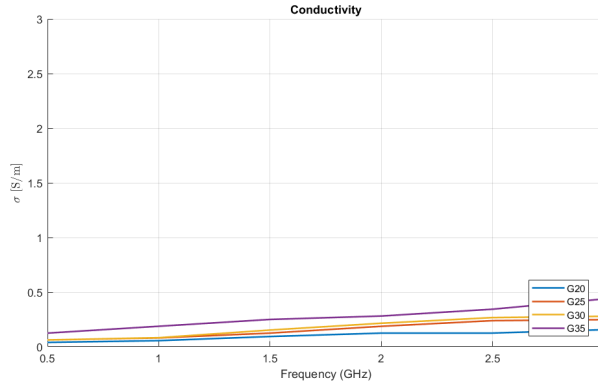
Percentage	Urethane rubber (g)	Graphite powder(g)
G20	96	24
G25	90	30
G30	84	36
G35	78	42

Table 3.3: Urethane rubber and graphite powder in 120 g of mixture

Finally, the relative dielectric constant and the conductivity are:



(a) Relative dielectric constant



(b) Conductivity

Figure 3.3: Electrical properties of mixture of urethane rubber and graphite powder

### 3.3 Number of probes, position and polarization design

The number, position and polarization of the antennas are explained in [1], and they are determined such that a proper data acquisition and a good spacial resolution are guaranteed for the image reconstruction.

Paper [1] said that this design was taking out by using the Singular Value Decomposition (SVD) of the operator that expresses linearity between  $\Delta S(\mathbf{r}_p, \mathbf{r}_q)$  and  $\Delta\chi$ :

$$\Delta S = \mathcal{S}(\Delta\chi) \quad (3.3)$$

where  $\Delta S(\mathbf{r}_p, \mathbf{r}_q)$  is the difference between the scattering matrices before and after the stroke,  $\Delta\chi$  is the electric contrast variation due to the stroke evolution,  $r_p$  is the position of Rx antenna and  $r_q$  is the position of Tx antenna.

This linearisation can be taken into account because the stroke is localized in a small region and so also the electric contrast. Hence, the Born approximation is considered and the linearisation of  $\Delta\chi$  can be taken into account. This linear operator is defined on a continuous surface on which the antennas can present any position. For this reason, it is possible to discretize the problem rewriting

3.3 as:

$$[y] = [S_d][x] \quad (3.4)$$

where  $[S_d]$  is the operator  $\mathcal{S}$  discretization with kernel  $-j\omega\epsilon_b/4\mathbf{E}_b(\mathbf{r}_m, \mathbf{r}_p) \cdot \mathbf{E}_b(\mathbf{r}_m, \mathbf{r}_q)$ . To determine the number of antennas, their position and polarization, two quantities were evaluated: the Condition Number (CN) of  $[S_d]$  and the discretization error  $\epsilon_s$ .

To guarantee the inversion of 3.4 such that it is not influenced by noise and model error, the CN should be small. Hence, in paper [1] the CN was evaluated by considering the number of antennas and the polarization:

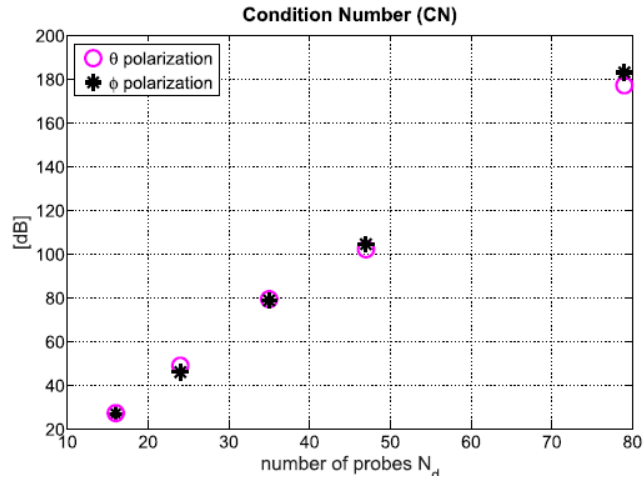


Figure 3.4: CN of the discretized scattering operator versus the number and orientation of the probes on surface [1]

By increasing the number of element, the CN increases due to interference effect between antennas. But, since a standard measurement system presents an Signal-to-noise ratio (SNR) and DR of 90 dB, it is good practice to have a CN that is below this value. For this reason, the threshold was fixed to  $N_b = 48$ . The polarization is independent for these condition.

For the position and the polarization, the discretization error should be taken into account since it tends to change by changing them. This value should be as lower as possible and its behaviour is reported in 3.5.

The motivation to use a limited dynamic range is due to the fact that the differential signal due to the stroke has a margin of 20 dB before going under the measurement system dynamic range. So, this will influence the number of elements, the polarization and position. For real, at laboratory, a new measurement system is present that has 110 dB DR, so the margin for the differential signal is not 20 dB, yet, but it is about 40 dB. Anyway, from figure 3.5, the best conditions are those with 24 to 48 antennas. But, by using 48 probes, the CN and the hardware complexity tends to increase. So the good trade off is to use 24 antennas in which the polarization is independent.

Everything was then verified through the Point Spread Function (PSF) of  $[S_d]$ , obtaining the structure in figure 3.6.

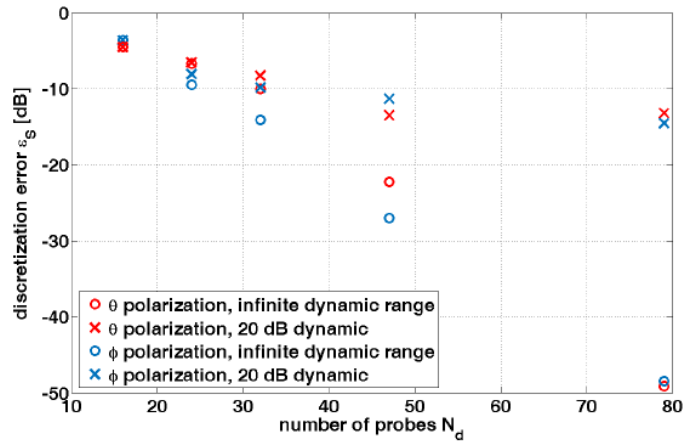


Figure 3.5: Discretization error versus the number and orientation of the probes on surface evaluated for infinite and limited DR [1]

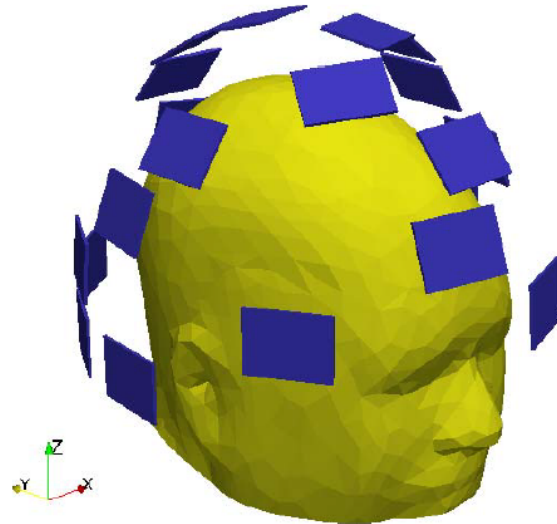


Figure 3.6: Position of antennas on head [1]

### 3.4 Issues and their solutions

A prototype of this system is present at the Politecnico di Torino. But some features of it should be improved such that a more compact and flexible system can be obtained. About that, in this section the main solutions are described.

The principal project for this work is the one described in paper [16] that is composed by 24 monopole antennas that are built up on a helmet which presents the same shape of the upper part of the head. These antennas are printed on a 1.6 mm FR4 substrate. The main problem of this system is the use of this type of material. Indeed, by using FR4 with that thickness, means that the substrate is rigid, so the flexibility of the structure is not verified. However, in this condition, the antenna is not able to be perfectly skin-tight, introducing some empty spaces between the antenna and the head. The presence of them will create unwanted reflections that might overlap with the useful scattered signal [20]. Moreover, another important problem is the difficulty in making the system portable, be-

cause this type of material needs a bulky platform. Hence, the mixture of urethane rubber and graphite powder is several centimetre depth.

A first solution for this was proposed by the previous thesis student, [25], in which different flexible materials were proposed. The solution to FR4 was to use PI substrate that is a flexible and robust material but it presents a lower relative permittivity, for this reason it needs a conductive part that allows the antenna to be matched with the brain tissues. The prototype of this last project introduces some interesting results also if the specifications were not verified, so unfortunately, also this prototype presents some problems.

First of all, the production of the antenna was a handmade production, so the antenna was hand cut and this might introduce higher uncertainties on the system with respect to a printed one. Indeed the solution to this is to print the antenna on a PI substrate to reduce the uncertainties.

Another issue was the use of a model system that is very far from the real case, for example this one do not consider the Acrylonitrile butadiene styrene (ABS) layer that describes the phantom thickness, that is important since it screen off the antenna effect. In the new prototype, it is important to introduce also this layer in the simulations.

Finally, a thickness of mixture of urethane rubber and graphite powder of just 5 mm was considered, so this make the antenna less matched with the brain tissues, so the idea is to increase this quantity such that it remains lower that 10 mm.



## Chapter 4

# Numerical Simulations

This chapter explains how the system to realize was modelled and simulated such that the specifications can be satisfied before its physical realization. To do this, the CST Microwave Studio software was used. In this environment the materials were described by specific permittivity ( $\epsilon$ ) and conductivity ( $\sigma$ ), while the structures were defined by using a geometrical parametric list. The aim of this part is to improve and optimize the system studied before, as said in Chapter 3.4.

### 4.1 Model System

Before talking about the results obtained in the simulations, it is necessary to describe the model used for the study. Moreover, some changes have been done with respect to the previous project.

#### 4.1.1 Antenna model

The reference antenna is the one reported in [21] and as following:

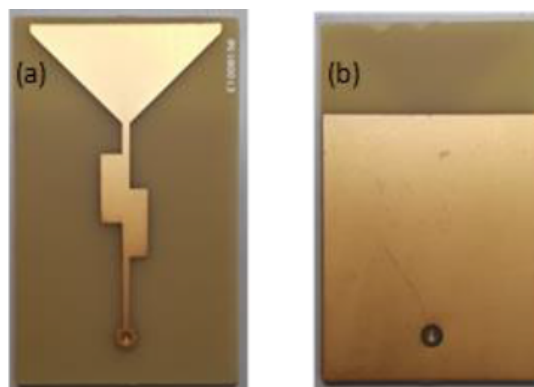


Figure 4.1: (a) Top side antenna; (b) bottom side antenna

The antenna that should be realized is a wideband monopole antenna, printed on a PI substrate. The top side of the antenna is characterized by a TL made up of a double stub structure that allows to match the circuit. This one ends with a radiating part that has a triangular shape to guarantee the wideband condition. The figure reported in 4.1(b) represents the bottom side of the antenna and

so the ground plane, [21]. Moreover, the antenna was positioned between two rectangular portions, of height  $h$  and  $h_{pan}$ , made up of a mixture of urethane rubber and graphite powder. Depending on their weight ratio it is possible to obtain a more or less flexible structure. Moreover, their relative permittivity and conductivity are reported in figures 3.3. These two portions allow to match the antenna with head tissues.

Obviously the antenna structure is a conductive material and it is made of copper annealed.

To model this structure, a parametric list was compiled such that the quantities could be changed time after time to obtain the best solution. As a matter of fact, the antenna geometry in CST Microwave Studio was realized in this way:

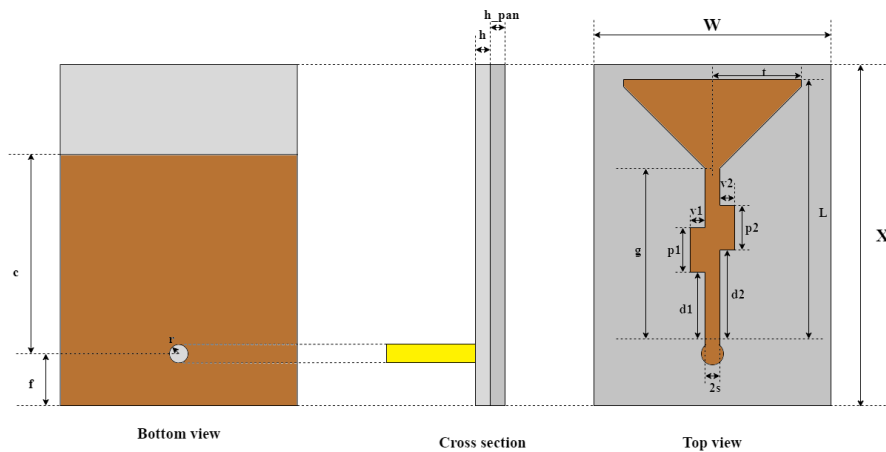


Figure 4.2: Antenna geometry for CST Microwave Studio

The final conditions obtained for the structure presents the following features:

Parameter	Size (mm)
X	48.00
W	30.00
c	35.00
f	6.00
r	1.50
L	40.50
g	32.00
t	12.64
s	0.50

Parameter	Size (mm)
h	5.00
h_pan	4.00
d1	13.97
d2	11.58
p1	12.00
p2	10.47
v1	4.35
v2	2.59

Table 4.1: Parameters list

These were obtained by doing different examinations that allow to obtain the best matching condition, where the most significant are reported in the chapter 4.2. Moreover, another simulation that was done is the one that allows to choose the weight ratio between the urethane rubber and graphite powder for the two rectangular portions. The final solution for them is of using G35 for the top part and G25 for the other.

### 4.1.2 Head model

To model the head, different conditions were simulated to define the situation that can be presented.

Firstly, an initial matching condition was obtained by using a simple model of the head that was built like a parallelepiped that had the dimensions similar to the one of a head. Then, the simulations were done by using a cylinder for the head model to take into account the curvature of it. Therefore, these experiments used different radius  $R$  to describe the best and the worst conditions for the studying, like in paper [20].

In both cases, an important improvement was introduced with respect to the previous project. Indeed, a material of ABS, of height  $Phan$ , was positioned between the antenna system and the brain to simulate the presence of plastic in the phantom available in laboratory.

Finally, the material used for the head is composed by a material called *head\_import* that is obtained by doing the average of the dielectric properties of the head tissues:

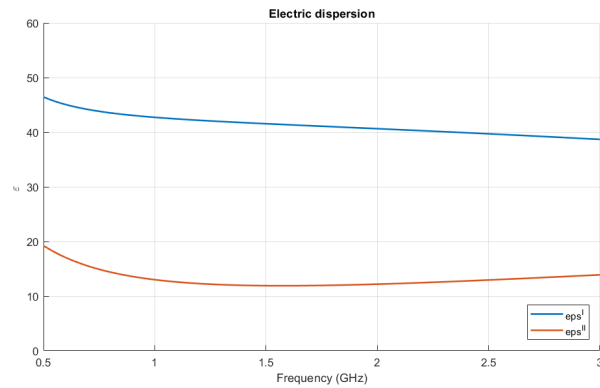


Figure 4.3: Dielectric permittivity of *head\_import*

The first condition is represented as follow:

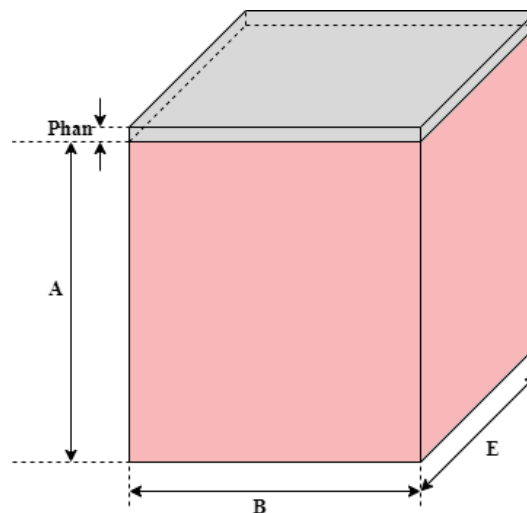


Figure 4.4: Planar head model for CST Microwave Studio

where:

Parameter	Size (mm)
A	200.00
B	160.00
E	120.00
Phan	3.00

Table 4.2: Head parameters

The same was done to simulate the curvature, but in this case the head was modelled with a cylinder as follow:

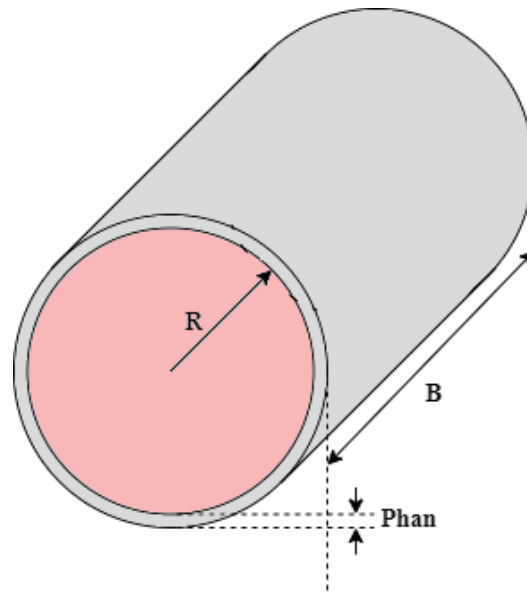


Figure 4.5: Cylinder head model for CST Microwave Studio

where:

Parameter	Size (mm)
R	100.00
B	160.00
Phan	3.00

Table 4.3: Head parameters with curvature

For the final verification, one and two antennas were positioned on a real head model in CST Microwave Studio. It is made up of ABS, to model the liquid container, and the *head\_import* material:

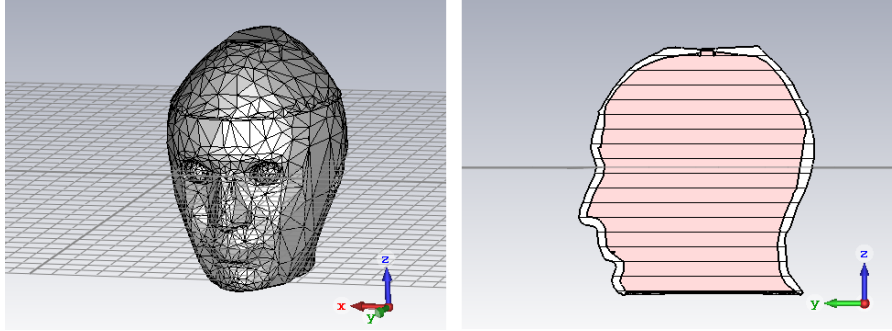


Figure 4.6: Complete head model for CST Microwave Studio

## 4.2 Results simulations

In this part, the most important simulations results are reported. Their principle goal is to obtain a structure that is able to verify the specifications reported in chapter 3.

These simulations were played by paying attention on the design parameters, where the finals are reported in table 4.1. By changing them time to time, it was possible to obtain a structure that respect the design specifications. Moreover, these results can be divided into two parts:

- the first is necessary to define the antenna parameters;
- the second is necessary to define the best couple of the rectangular portions to guarantee the matching condition between the antenna and the biological tissues.

### 4.2.1 Step 1

The starting point of these simulations is the previous structure that has to be improved. As explained in chapter 3.4, the antenna was designed and adapted by using a model that did not consider some important conditions. They are:

- the layer of ABS, that is important to model the thickness of the phantom;
- the second rectangular portion.

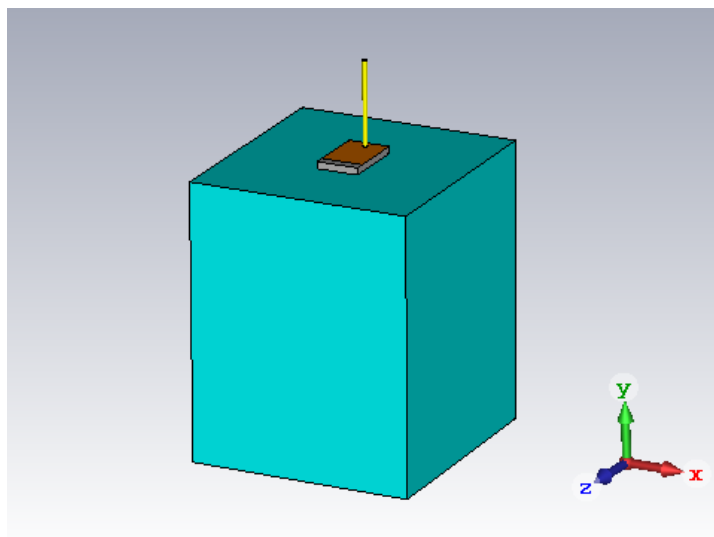
In this case the starting parameters were reported in tables 4.4.

The rectangular portion that was considered was the one positioned between the ground plane and the top part of the antenna, so the one with thickness  $h$ , that was made of G25. The model obtained in CST Microwave studio was the one in figure 4.7:

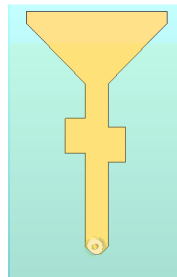
In this case, the quantities that were studied were:  $S_{11}$ , the Smith chart (to study the impedance at 1GHz), the maximum electric field at 1GHz, the power flow at 1GHz and the surface current at 1GHz that were simulated by using the time domain solver. The final results are the following:

Parameter	Size (mm)	Parameter	Size (mm)
X	48.00	s	2.00
W	30.00	h	5.00
c	35.00	d1	14.5
f	6.00	d2	16.00
r	1.50	p1	6.00
L	40.50	p2	6.00
g	28.00	v1	2.94
t	12.64	v2	3.40

Table 4.4: Starting parameters list

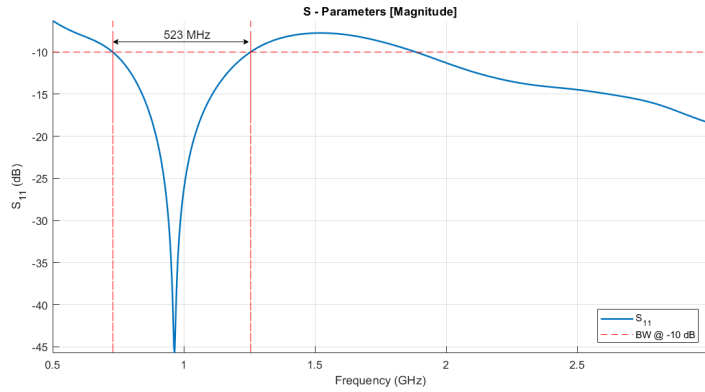


(a) CST Microwave studio complete model

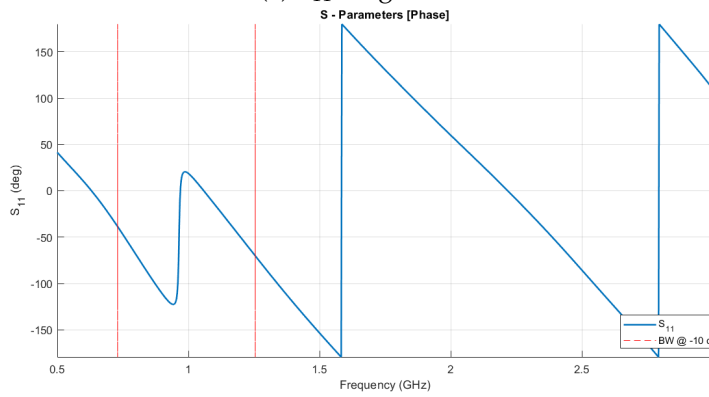


(b) CST Microwave studio antenna model (Top part)

Figure 4.7: CST Microwave studio model



(a)  $S_{11}$  Magnitude



(b)  $S_{11}$  Phase

Figure 4.8:  $S_{11}$  representation

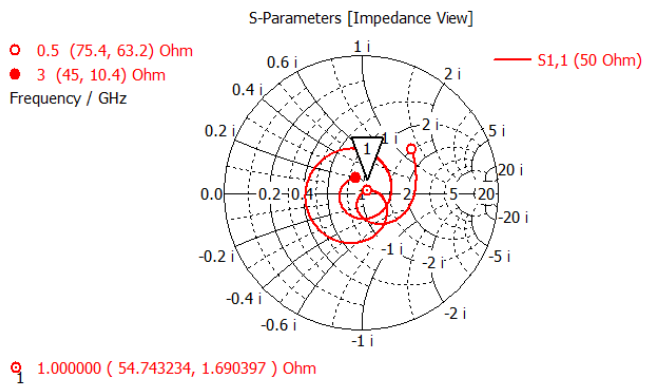
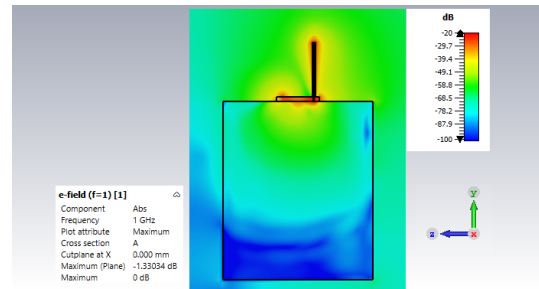
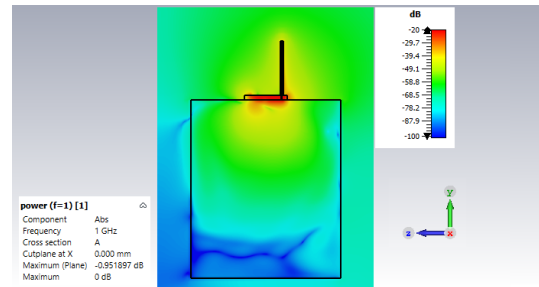


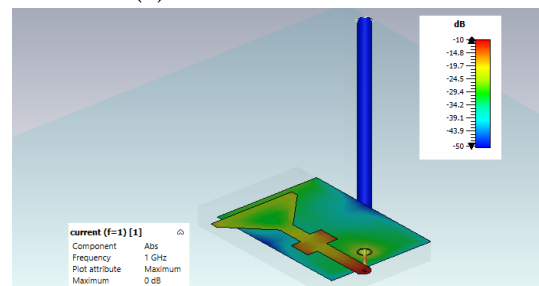
Figure 4.9: Smith Chart



(a) Maximum electric field in dBMax



(b) Power flow in dBMax



(c) Maximum surface current in dBMax

Figure 4.10: Field monitor results

## 4.2.2 Step 2

After the first step, the model was changed by firstly introducing: an ABS layer, to model the thickness of the phantom. Then, the second rectangular portion, positioned between the top part of the antenna and the ABS layer, was added, too. To do this, it is important that the thickness of this portion is chosen such that the total depth of those is less than 10 mm to guarantee flexibility.

In this case, just the  $|S_{11}|$  quantity was observed because, with respect to the previous step, the matching condition is surely lost and for this reason it is more important to reach first the matching condition and, when it is so, evaluate also the electric field, the power flow and the surface current. Moreover, by doing so, it is possible to reduce the time simulation since no field monitors are set up.

### Step 2: ABS layer introduction

As said, the first thing was the introduction of the ABS layer that is modelled with a thickness of  $Phan = 3$  mm and the simulation was done without the second rectangular portion. Hence, the top part of the antenna was in directly

contact with the ABS layer.

The model with the ABS layer is the following:

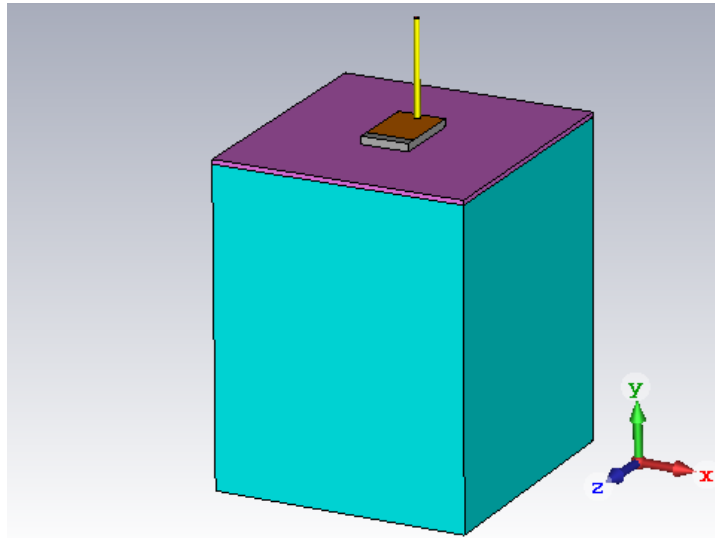


Figure 4.11: CST Microwave Studio model with ABS

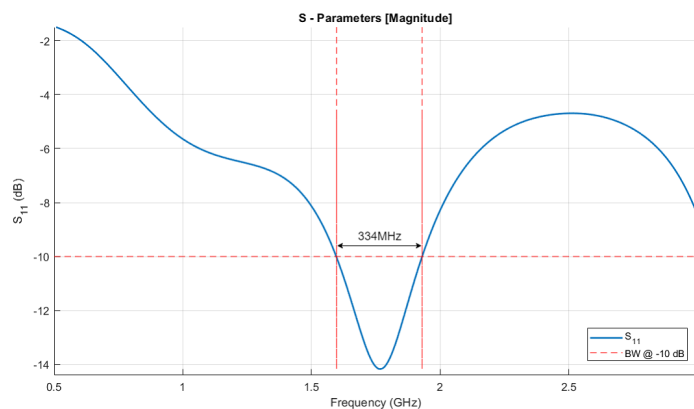


Figure 4.12:  $|S_{11}|$  with ABS

Comparing the figures 4.8a and 4.12 it is possible to observe that, as expected, the  $|S_{11}|$  loses its properties in frequency, so it is not matched at 1GHz yet, and magnitude, that means that is slightly away from the zero reflection condition. This is due to the presence of the ABS layer that makes less effective the antenna job.

### Step 2: Rectangular portion layer introduction

After the previous introduction, also the second rectangular portion was introduced, by using a thickness of  $h_{pan} = 5$  mm and it was made up of G30. In this way, the top part of the antenna is positioned between the two rectangular portions.

The model with the new portion layer is the following:

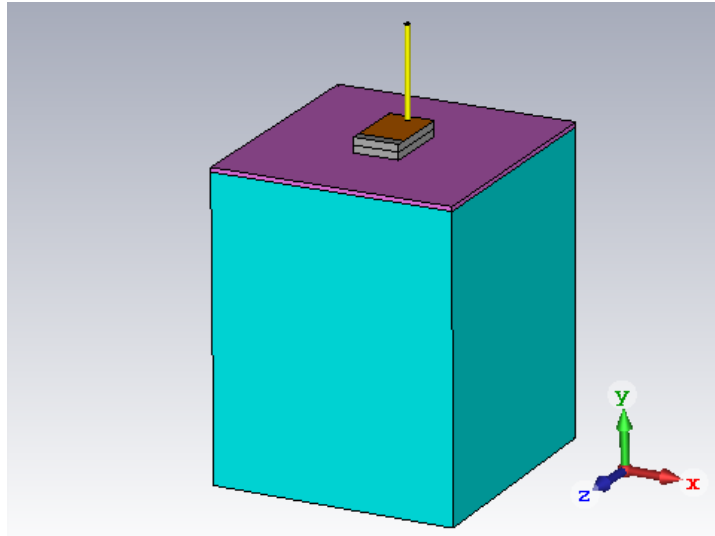
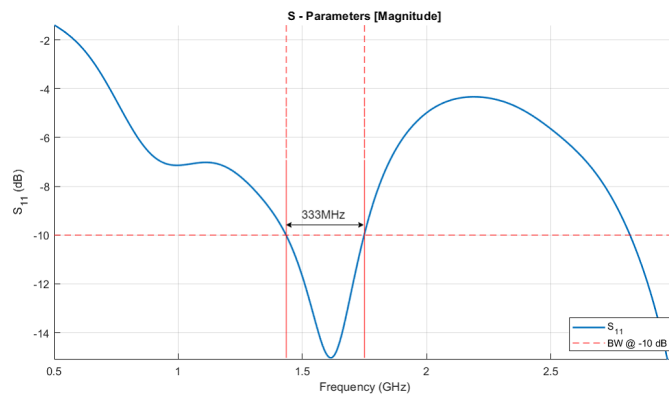


Figure 4.13: CST Microwave Studio model with G30

Figure 4.14:  $|S_{11}|$  with G30

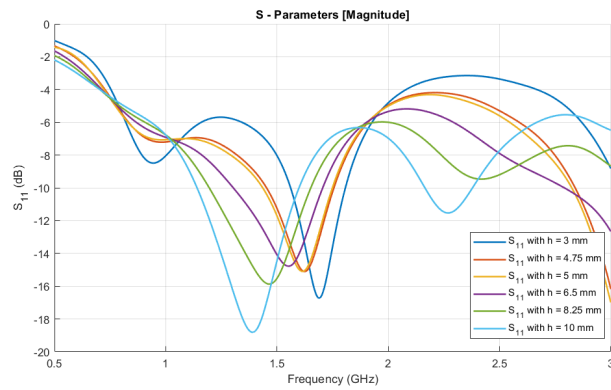
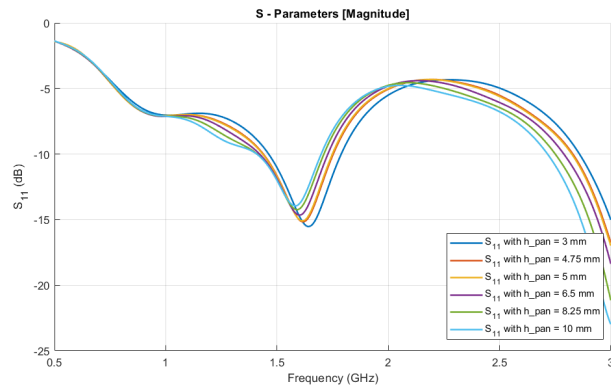
In this case, it is possible to affirm that the magnitude of the  $S_{11}$  is better with respect to the case in which the rectangular portion is not added (as it has been seen by comparing figures 4.12 and 4.14). But it is still far from the condition that should be achieved. This improvement is due to the presence of this additional layer that makes the antenna more conductive.

Before continuing with the other steps, a sweep on the thickness of the rectangular portions ( $h$  and  $h_{pan}$ ) was simulated to observe if a better condition than this last one was present, taking into account that:

- their sum should be less than 10 mm, otherwise the flexibility is lost;
- in the G30 the flexibility is less with respect to the G25, because of higher graphite powder present in it, so thinner is better.

To evaluate these quantities, the simulations were done by firstly fixing  $h_{pan}$  and varying  $h$ . After,  $h$  was fixed and  $h_{pan}$  was varied, obtaining the results reported in 4.15.

From figure 4.15a it is possible to determine the thickness of the top layer defined by  $h$ . Observing this figure, it is possible to affirm that by increasing  $h$

(a) Sweep of  $h$  (top portion)(b) Sweep of  $h_{pan}$  (bottom portion)Figure 4.15:  $|S_{11}|$  of the  $h$  and  $h_{pan}$  sweep

the  $|S_{11}|$  tends to become small and it moves toward the interesting matching frequency; on the contrary, by decreasing it the minimum peak moves toward higher frequencies. In real, by choosing a dimension that is higher than 5 mm, considering that  $h_{pan} = 5$  mm, is not a good choice since the sum of  $h$  and  $h_{pan}$  will be higher than 10 mm so the flexibility will be lost. The idea is to choose  $h = 4$  mm to guarantee a good  $|S_{11}|$  behaviour and a good flexibility. The same can be said for  $h_{pan}$  and for this reason, also in this case,  $h_{pan} = 4$  mm.

### 4.2.3 Step 3

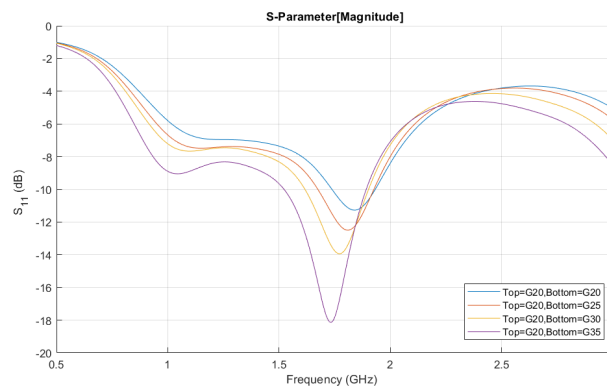
After the definition of  $h$  and  $h_{pan}$ , the simulations were run to determine what couple of urethane rubber and graphite powder is better to reach the matching condition. These portion were selected by choosing between: G20; G25; G30 and G35 (described in chapter 3.2).

This control was done to observe if it is possible to obtain the matching condition without changing the antenna geometry.

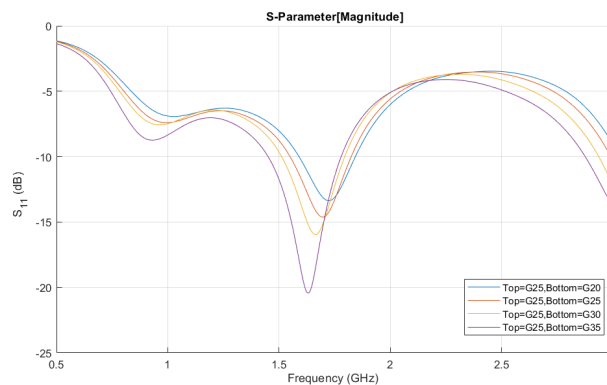
The idea to chose the "best" couple between the two portions, was to simulate all the combination. Their plots were put together considering the same type of top portion; finally, the best solution of each graph was reported on a final graph to make the comparison.

For figures 4.16a, 4.16b and 4.16c, the best conditions are the one represented by: G20/G35; G25/G35 and G30/G35, respectively, where the first component is the top portion and the second is the bottom. In these cases, the selection was done because they represent the best conditions in term of bandwidth at  $-10$  dB, the minimum value of  $|S_{11}|$  and the position of this last one in term of frequency. For figure 4.16d, the best condition is considered to be the one composed by G35/G25 because it represents the good trade - off between the bandwidth at  $-10$  dB, the minimum value of  $|S_{11}|$  and the position of this last one in term of frequency.

The comparison is reported in 4.16e. The best solution seems to be the one composed by G35/G25, but, initially, the idea is to select the couple made up of G25/G35 because it has a slightly bigger bandwidth and it could represent a good compromise for the minimum value of  $|S_{11}|$  and the position of this last one in term of frequency.

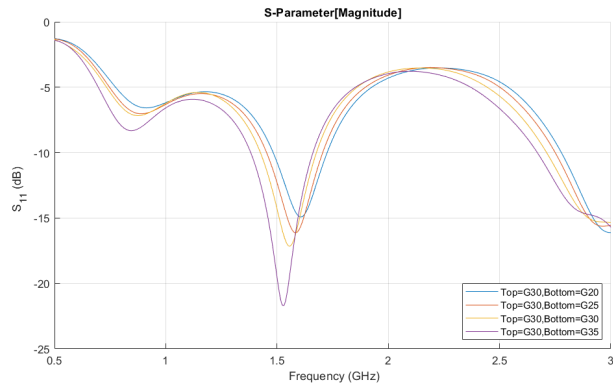


(a) Top portion G20

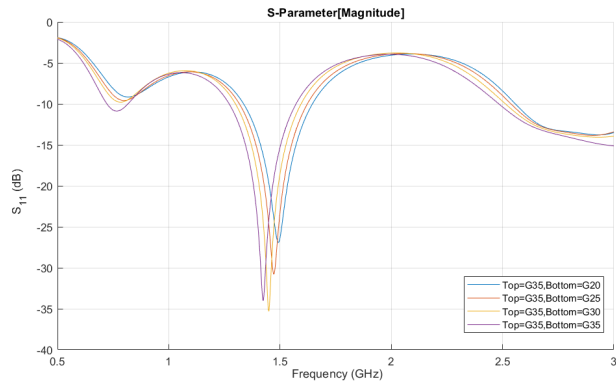


(b) Top portion G25

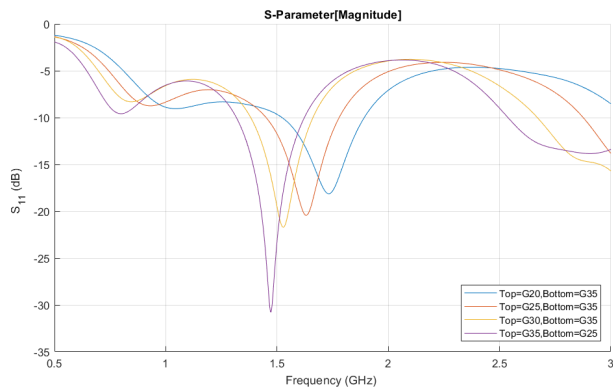
Figure 4.16:  $|S_{11}|$  for material selection



(c) Top portion G30



(d) Top portion G35



(e) Final comparison between the best solution

Figure 4.16:  $|S_{11}|$  for material selection

#### 4.2.4 Step 4

The selection of material for the two rectangular portions improved the matching condition, but it is not reached yet, for this reason it was necessary to change the geometry to reach the matching condition.

First of all, the geometry was improved like the structure reported in figure 4.1, by using the following values:

Parameter	Size (mm)
L	40.50
g	28.00
t	12.64
s	0.50
d1	9.09
d2	13.59
p1	9.00
p2	9.00
v1	2.44
v2	2.90

Table 4.5: New parameters list

The result was:

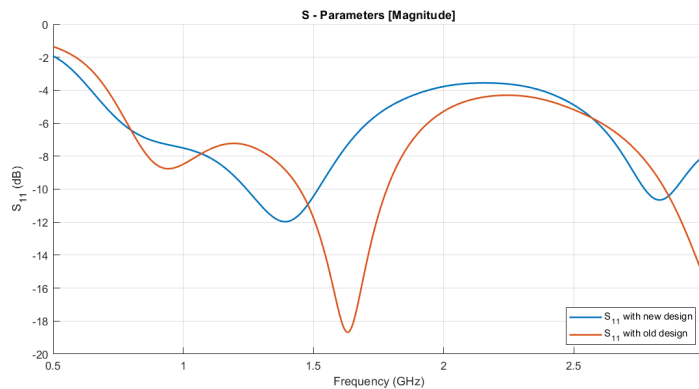
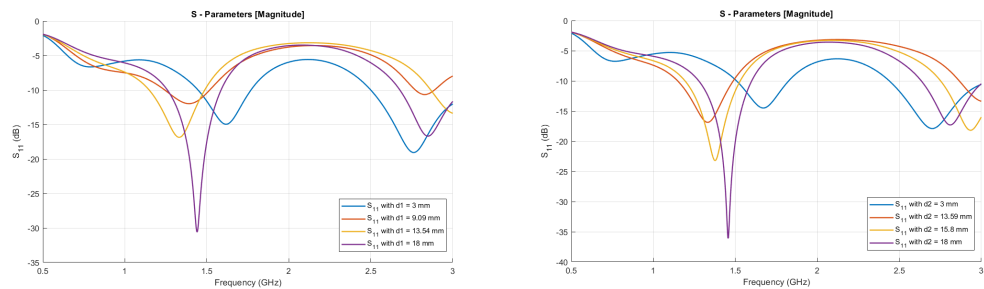


Figure 4.17:  $|S_{11}|$  of new and old design

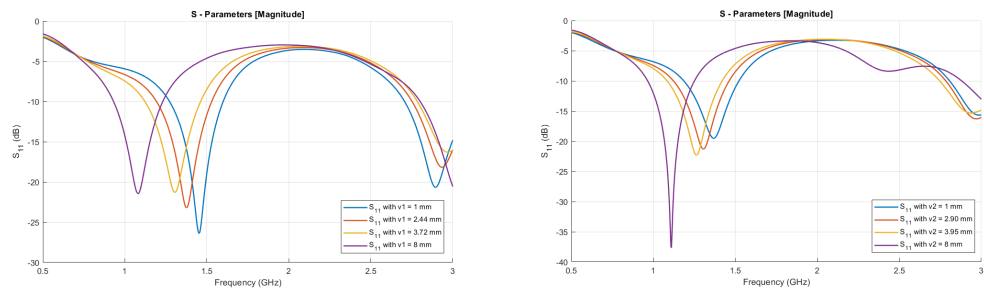
From the graph above, it is possible to observe that the  $|S_{11}|$  of the new design becomes worse since a slightly bigger reflection is present with respect to the old version; but the advantage is that the matching condition tends to move toward 1 GHz, so, from this condition, a new design was defined. For this reason, each parameter reported in table 4.5, was changed by applying the parametrization sweep in which three or four points were observed such that smaller and bigger quantities, with respect to the one reported in the table, were evaluated. By changing time by time, so fixing all the quantities and varying just one of them, it is possible to obtain a better geometry before the optimization, as reported in the figures 4.18.

For each graph, all the curves are evaluated and between them the condition that seems the best was chosen. This selection takes into account some things, such that the trade-off between the minimum value of the  $|S_{11}|$ , the position

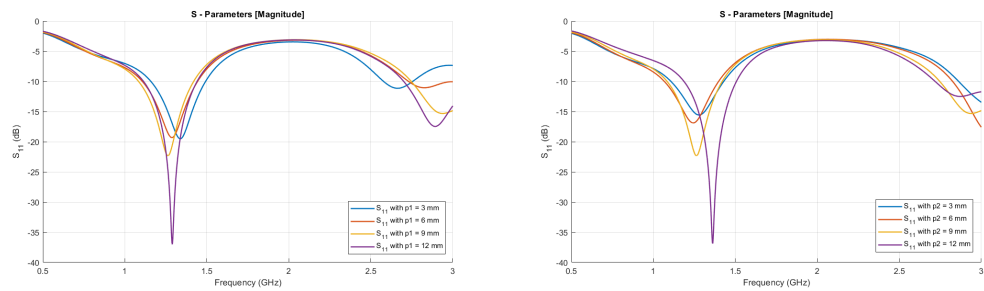
of this last one in term of frequencies and, finally, the desired matching condition at 1 GHz. In some cases, also the dimension of the quantity was taken into account to avoid large surfaces that could cause problems during printing, for example, they might introduce stubs that are too big and so they introduce some problems from an electromagnetic point of view. Rather, they can create an additional electromagnetic field. In particular, this last condition was taken into account for the determination of  $v1$ ,  $v2$ ,  $p1$  and  $p2$  that are the quantities that define the geometry of the two stubs. While  $d1$  and  $d2$  define the distance of them from the input, so they consider just the trade-off condition. Also the determination of  $t$ ,  $L$  and  $s$  uses the trade-off condition.



(a) Variation of  $d1$  and  $d2$

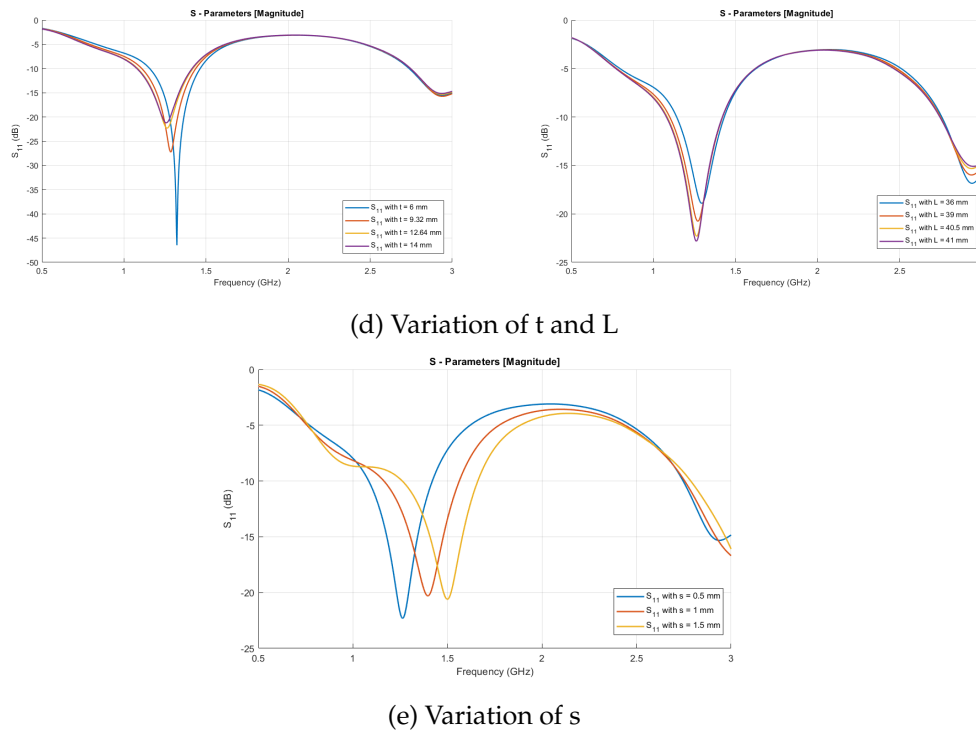


(b) Variation of  $v1$  and  $v2$



(c) Variation of  $p1$  and  $p2$

Figure 4.18:  $|S_{11}|$  of first geometry modification

Figure 4.18:  $|S_{11}|$  of first geometry modification

The final structure from this evaluation presents the following dimensions:

Parameter	Size (mm)
L	40.50
g	28.00
t	12.64
s	0.50
d1	13.54
d2	15.80
p1	9.00
p2	9.00
v1	3.72
v2	3.95

Table 4.6: Results from the first parametrization sweep of the antenna geometry

Comparing tables 4.5 and 4.6, it is possible to observe that the quantities  $L$ ,  $t$ ,  $p1$  and  $p2$  remain the same before and after the sweep. Indeed, looking at figures 4.18c and 4.18d the effect of the sweep was not so important and for this reason the same dimension was maintained. Also  $s$  is equal, but in this case the reason is that, from figure 4.18e, the effect of 0.5 mm is better than the other two.

## 4.2.5 Optimization

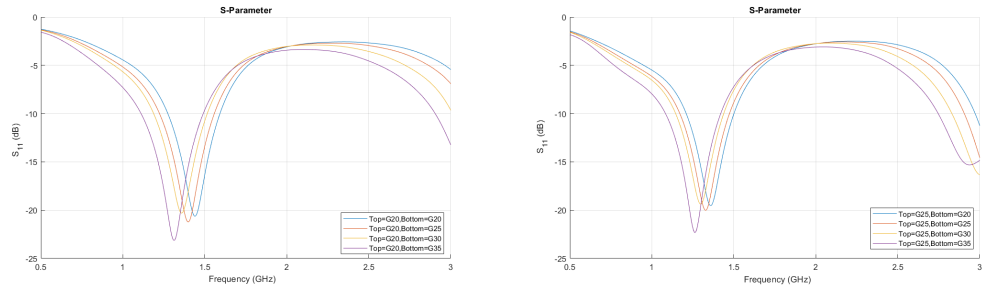
The optimization step consists of two important steps:

- verify if the materials of the two rectangular portions gives the best per-

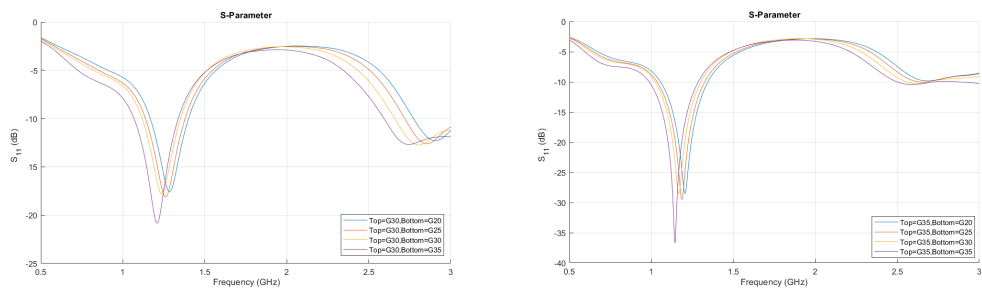
formances;

- try to reach the matching condition at  $f = 1$  GHz.

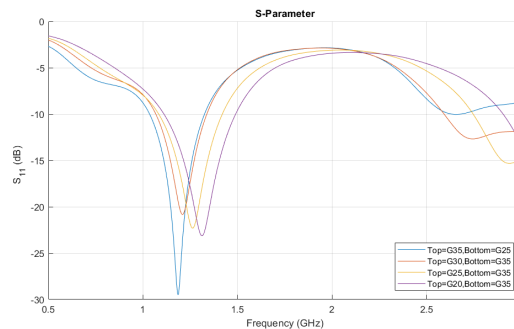
The idea to verify the couple material was to simulate every type of couple possible and try to compare all the solution. The images were put together considering the same type of top portion; the best condition of each graph was then reported in other graph in which the comparison between the best solutions was done, like in figures 4.19.



(a) Verification for top G20 (left) and G25(right)



(b) Verification for top G30 (left) and G35(right)



(c) Final comparison between the best solution

Figure 4.19:  $|S_{11}|$  for material verification (Optimization)

From this evaluation, the couple that was chosen was the one composed by the top portion made up of G35 and the bottom one made up of G25.

Regarding the optimization of the antenna design, the optimization tool of CST Microwave studio was used, in which it is possible to set up some goals to obtain the desired condition. The goals were set up such that:

- the bandwidth at  $S_{11} = -10$  dB is equal to  $BW = 550$  MHz;
- the magnitude of  $S_{11}$  at  $f = 1$  GHz is less than  $-30$  dB.

Unfortunately, this tool did not verify these two conditions, but considering all the results obtained by it, it was possible to change the parameters such that the matching condition could be reached also if the set up goals were not verified. A lot of simulations were done to reach the matching condition, but just the most interested curves are reported:

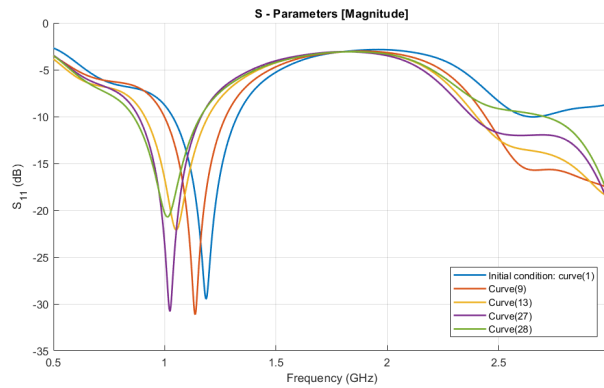


Figure 4.20:  $|S_{11}|$  of interested curves (Optimization)

in which the parameters that define them are the following:

Curve	d1 (mm)	d2 (mm)	p1 (mm)	p2 (mm)	v1 (mm)	v2 (mm)
(1)	13.54	15.80	9.00	9.00	3.72	3.95
(9)	13.54	15.80	9.00	6.00	4.02	4.45
(13)	13.54	15.80	9.00	6.00	4.02	4.45
(27)	13.54	14.80	11.00	9.00	4.50	4.50
(28)	13.54	12.80	11.00	9.00	4.50	4.50

Table 4.7: Results from the first parametrization sweep of the antenna geometry

Curve	g (mm)	h (mm)	h_pan (mm)
(1)	28.00	4.00	4.00
(9)	28.00	5.70	4.00
(13)	32.00	5.70	4.00
(27)	32.00	5.70	4.00
(28)	32.00	5.70	4.00

Table 4.7: Results from the first parametrization sweep of the antenna geometry

From figure 4.20, the selection had been done between the curve (27) and (28). To accomplish the final design of the antenna, the decision was done by evaluating: the module of  $S_{11}$  at 1 GHz and the bandwidth.

Curve (27) presents a lower  $S_{11}$  magnitude than curve (28), that is better since the reflection effect is less and so this means that the electric field will penetrate better. On the other hand, the curve (28) seems to be perfectly matched and it presents a higher bandwidth with respect to curve(27).

Finally, the chosen design is the one defined by the curve(27). Moreover, as reported in table 4.7, h was chosen to be equal to 5.70 mm, but to product the G35 portion there is the millimetre precision, for this reason the final simulation

Curve	$S_{11}$ @1 GHz	BW@-10 dB
(27)	-24 dB	280.17 MHz
(28)	-20 dB	302.52 MHz

Table 4.8: Comparison of  $|S_{11}|$  and bandwidth between curve(27) and curve(28)

was done by imposing  $h = 5.00$  mm to guarantee more flexibility with respect to  $h = 6.00$  mm. The images below report the maximum electric field, the power flow, the maximum surface current at 1 GHz, the  $S_{11}$  (in magnitude and phase) and the Smith chart:

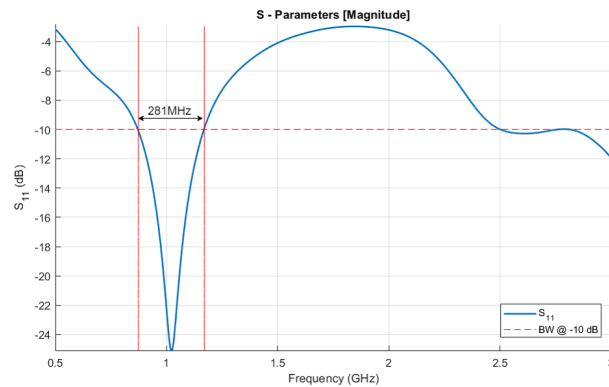
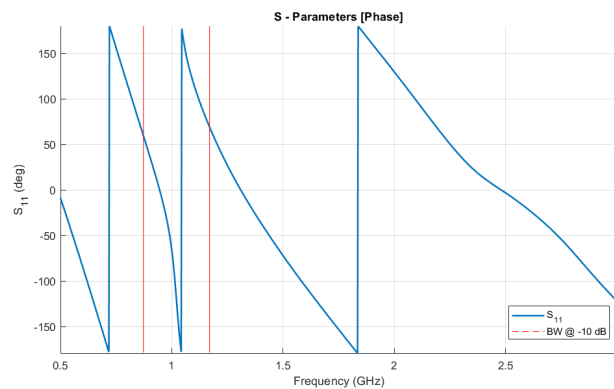
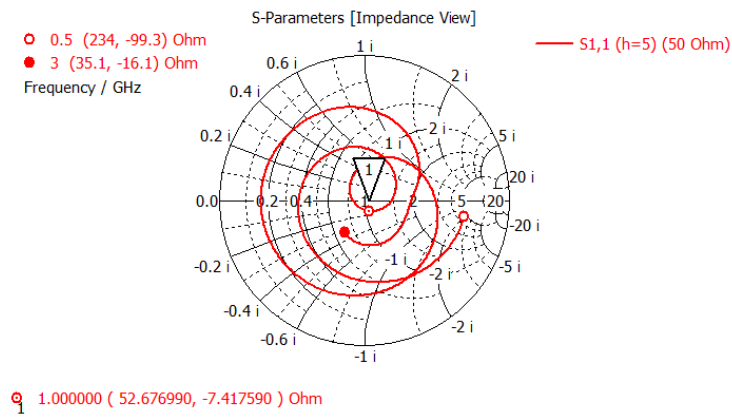
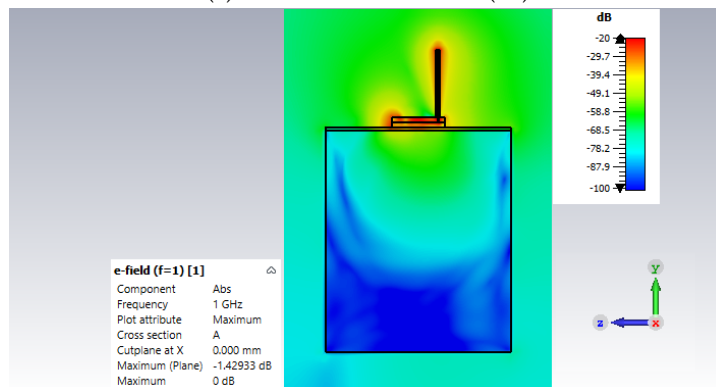
(a)  $|S_{11}|$  of curve(27)(b)  $S_{11}$  phase of curve(27)

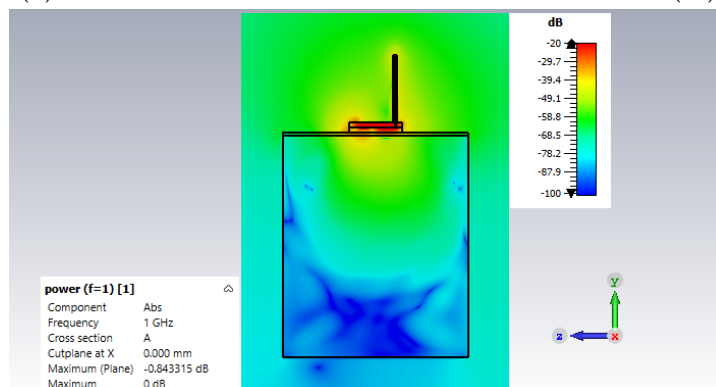
Figure 4.21: Results of curve(27)



(c) Smith chart of curve (27)

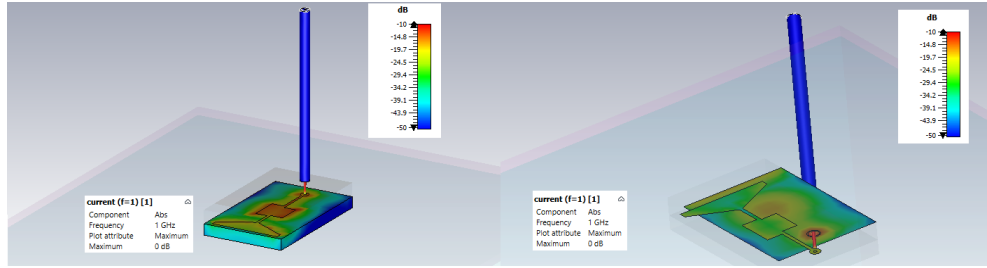


(d) Maximum electric field in dBMax at 1 GHz of curve (27)



(e) Power flow in dBMax at 1 GHz of curve (27)

Figure 4.21: Results of curve(27)



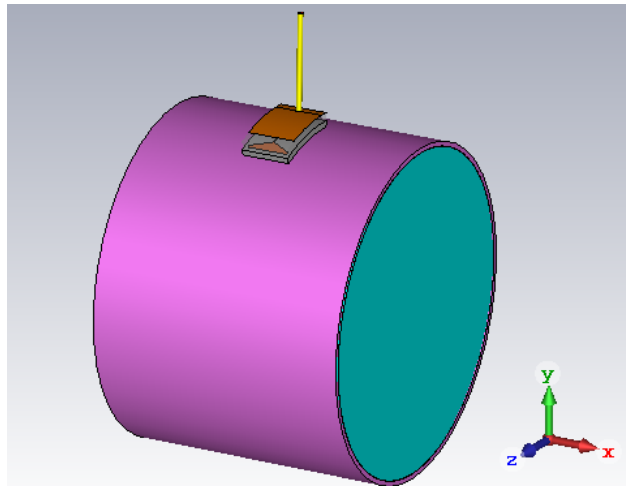
(f) Maximum surface current in dBMax at 1 GHz of curve (27)

Figure 4.21: Results of curve(27)

### 4.3 Results on curved structure

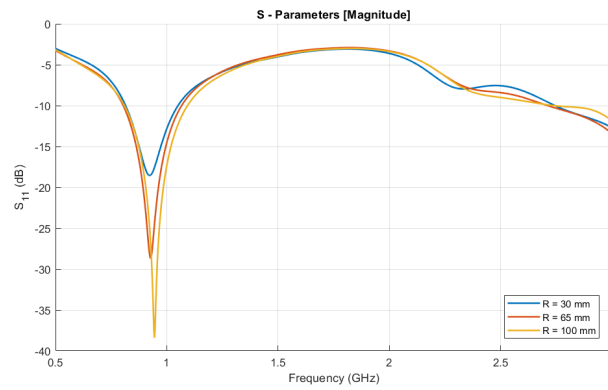
As known, the proposed antenna is flexible because it has to be attached to human head, for this reason it is important to simulate the proposed antenna on a curved structure that should model the head curvature. To this end, the idea is to model the head with a cylinder of different bending radius  $R$  [20], like in figure 4.5. This radius  $R$  is defined on an average human head model [20].

In this case, it was chosen to simulate  $R = 30, 65, 100\text{mm}$ . As the planar structure, the quantities that were evaluated, just for  $R = 100\text{mm}$ , were:  $S_{11}$ , the Smith chart to study the impedance, the maximum electric field, the power flow and the maximum surface current at 1 GHz. The most important thing is that the matching condition is maintained with respect to the planar structure.

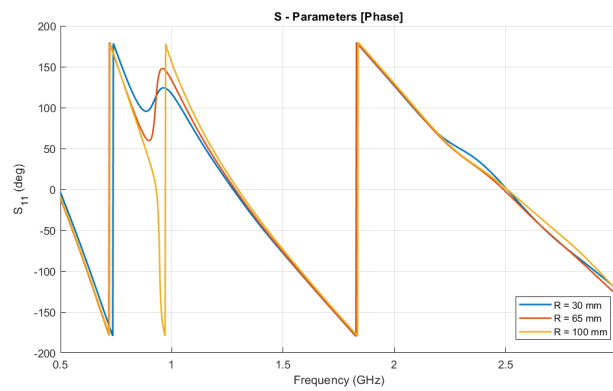


(a) CST Microwave studio model

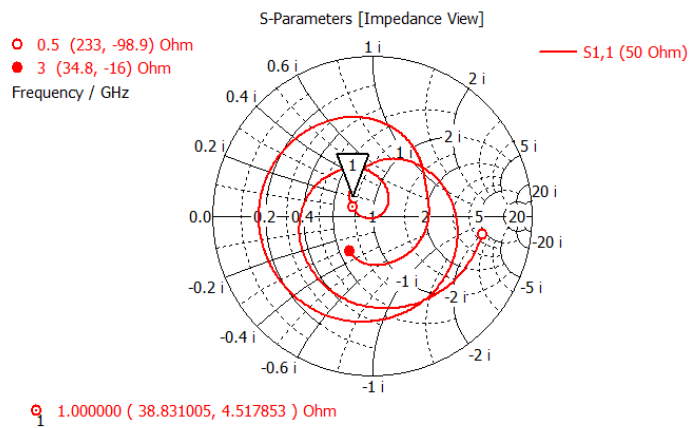
Figure 4.22: Results of curve(27) on curved structure



(b)  $|S_{11}|$  with different bending radius

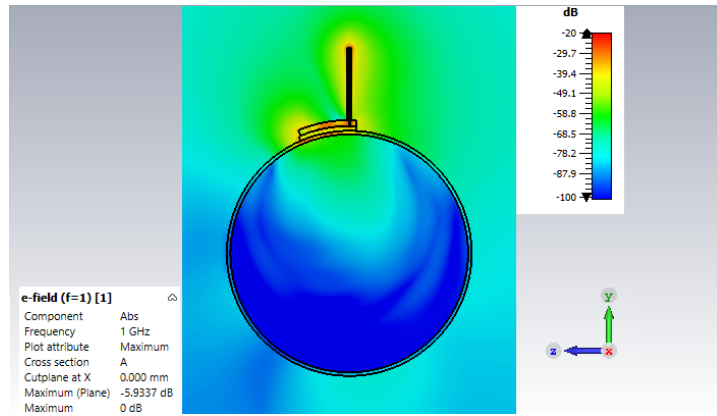


(c)  $S_{11}$  phase with different bending radius

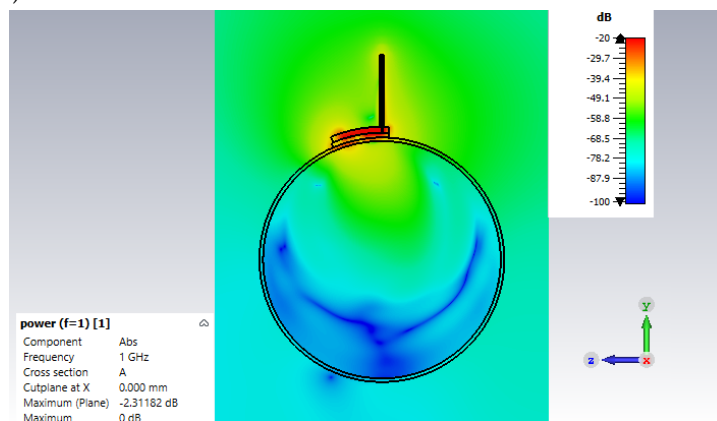


(d) Smith Chart

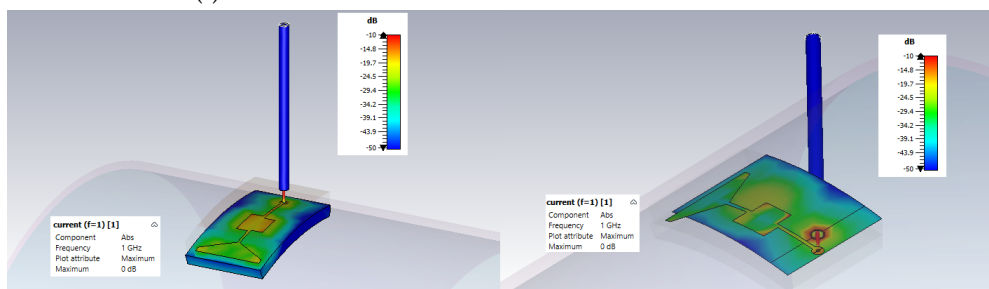
Figure 4.22: Results of curve(27) on curved structure



(e) Maximum electric field in dBMax at 1 GHz with  $R = 100$  mm



(f) Power flow in dBMax at 1 GHz with  $R = 100$  mm



(g) Maximum surface current in dBMax at 1 GHz with  $R = 100$  mm

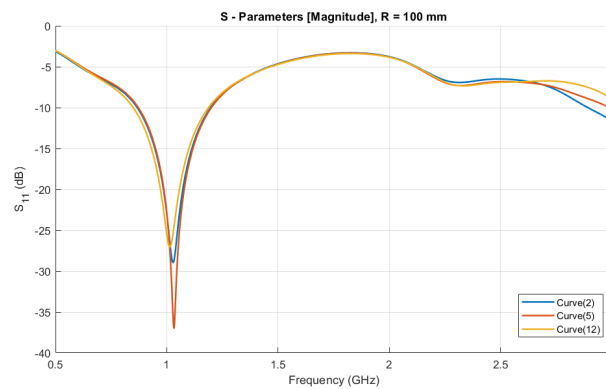
Figure 4.22: Results of curve(27) on curved structure

Since the real application is on a curved structure, the idea is to obtain a better matching condition starting from the antenna defined until now, and doing the optimization, parameter per parameter, on the curved structure itself. The best solutions were three and they were the following:

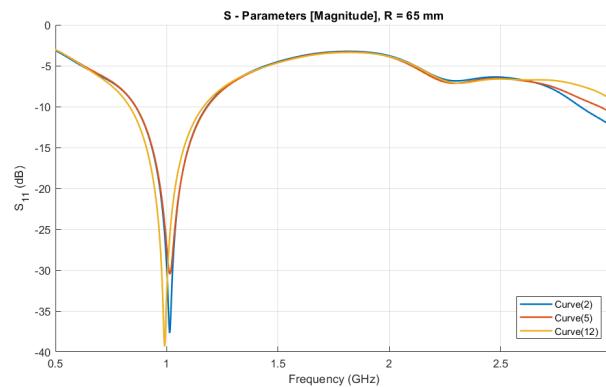
Curve	d1 (mm)	d2 (mm)	p1 (mm)	p2 (mm)	v1 (mm)	v2 (mm)
(2)	15.53	12.31	11.00	9.00	3.40	3.95
(5)	15.53	12.03	11.68	10.74	3.12	3.95
(12)	13.97	11.58	12.00	10.47	4.35	2.59

Table 4.9: Optimization on curved structure

In figures 4.23, the curves in table 4.9 are reported for different bending radius.

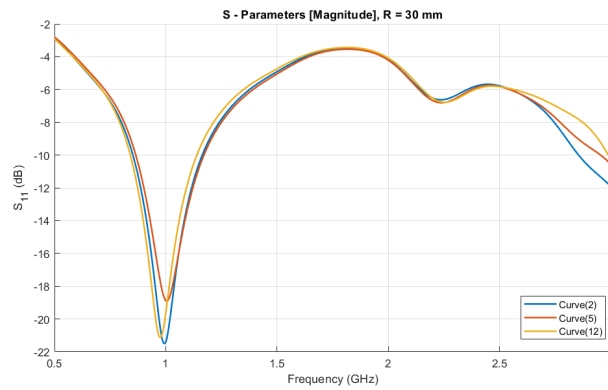


(a)  $|S_{11}|$  with  $R = 100$  mm



(b)  $|S_{11}|$  with  $R = 65$  mm

Figure 4.23: Results of curve(27)

(c)  $|S_{11}|$  with  $R = 30$  mmFigure 4.23: Results of  $|S_{11}|$  with different bending radius

Comparing them, it is possible to report the most important quantities necessary to define what curve can be selected and reported in table 4.10, from which the choice falls in curve (12) that seems to be more matched.

Curve	$ S_{11} $ @1 GHz	BW@-10 dB
(2)	$\approx -23$ dB	$\approx 330$ MHz
(5)	$\approx -22.8$ dB	$\approx 329$ MHz
(12)	$\approx -25.5$ dB	$\approx 338$ MHz

Table 4.10: Comparison of  $|S_{11}|$  and bandwidth between curve(2), curve(5) and curve(12) with  $R = 100$  mm

Also for this selection,  $S_{11}$ , the Smith chart to study the impedance, the maximum electric field, the power flow and the maximum surface current at 1 GHz were reported in figure 4.24.

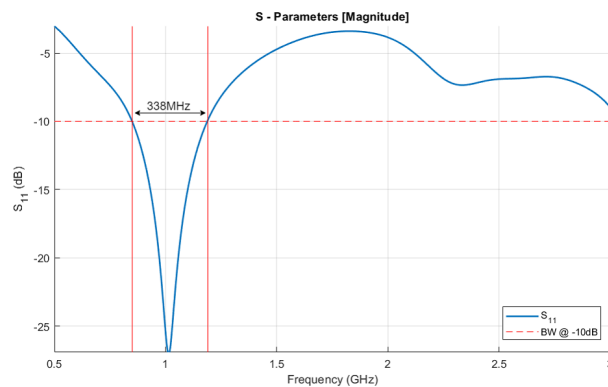
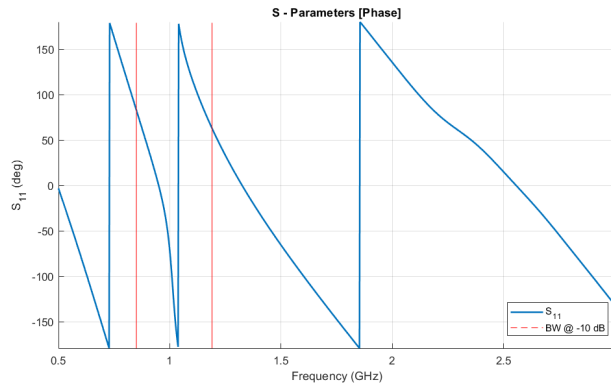
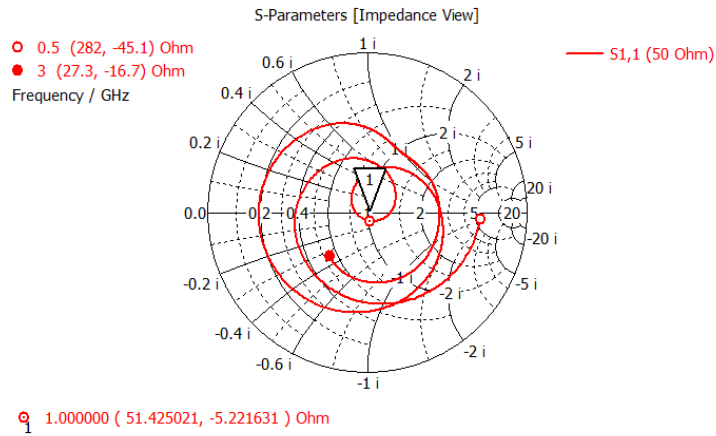
(a)  $|S_{11}|$  with  $R = 100$  mm

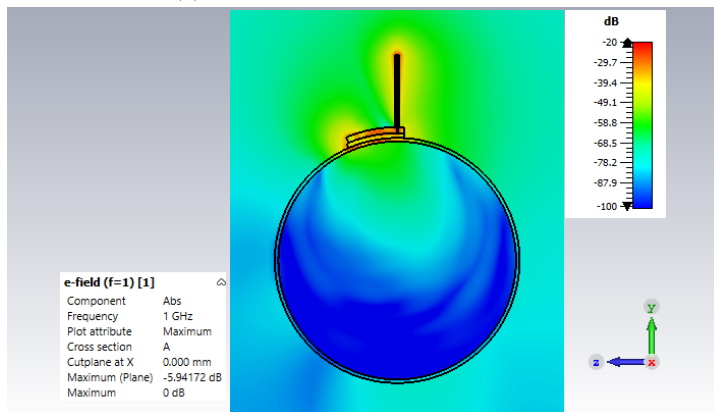
Figure 4.24: Results of curve(12)



(b)  $S_{11}$  phase with  $R = 100$  mm



(c) Smith chart with  $R = 100$  mm



(d) Maximum electric field in dBMax with  $R = 100$  mm

Figure 4.24: Results of curve (12)

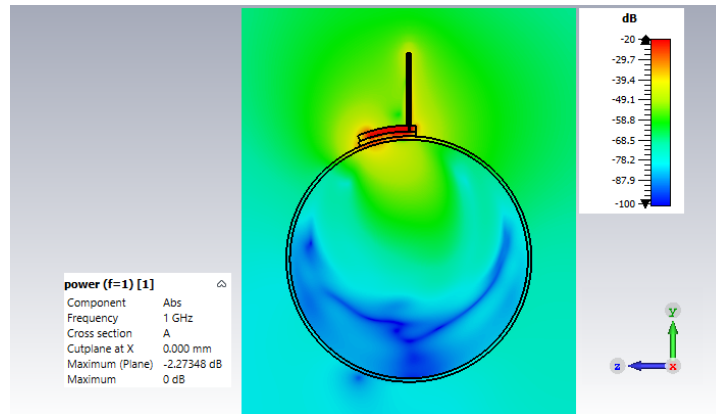
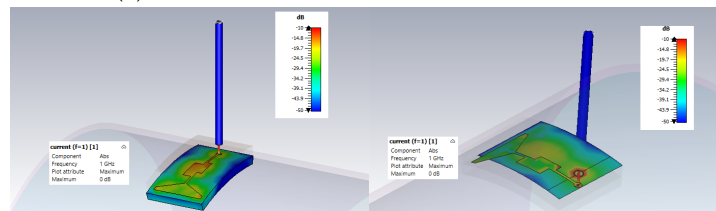
(a) Power flow in dBMax with  $R = 100$  mm(b) Maximum surface current in dBMax with  $R = 100$  mm

Figure 4.25: Results of curve (12)

#### 4.4 Results for transmission

Finally, the last step was the evaluation of the transmission coefficients,  $S_{12}$  and  $S_{21}$ , that were evaluated by considering two antennas positioned on two opposite sides of the head model.

The transmission coefficients allow to describe the information transmission between a Tx and Rx antenna. Closer to 0 dB is better because better is the information transmission. But at the same time, it is important that these quantities are higher than  $-110$  dB to guarantee that signal does not go to the noise band. Indeed, the DR of the measurement system is of 110 dB.

As said in 3.3, to detect an object between the two antennas it is necessary to evaluate the S-parameters before and after the stroke. By doing the difference between them, it is possible to evaluate the evolution of the stroke itself.

Below, the simulations of the antenna obtained in chapter 4.3, on plane and curved structure, are reported:

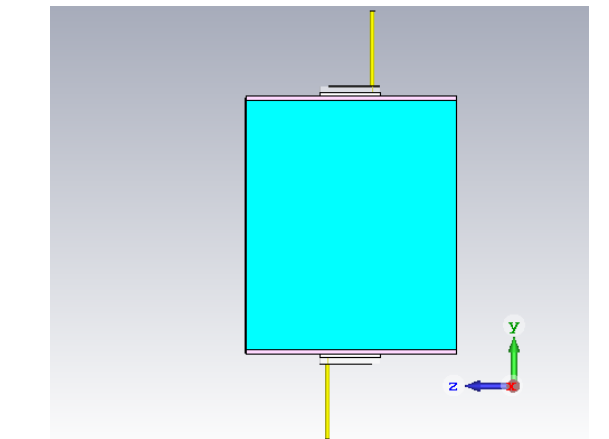
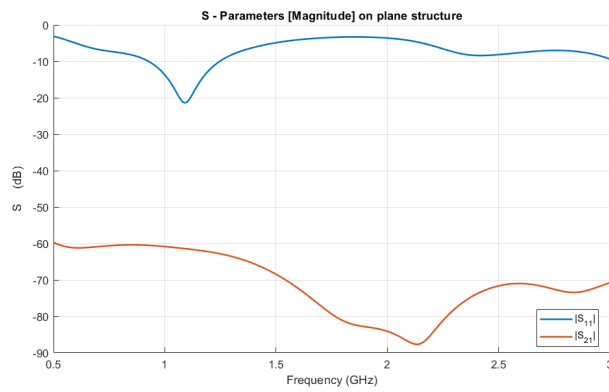
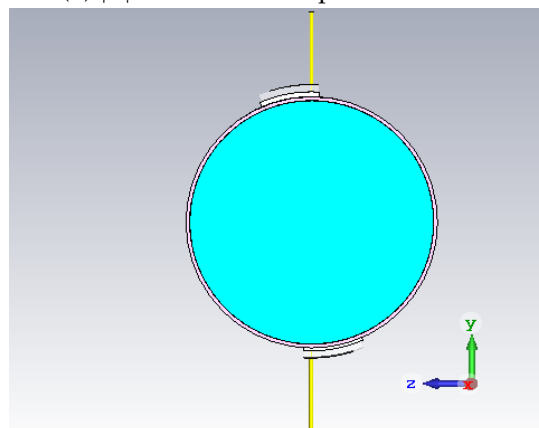
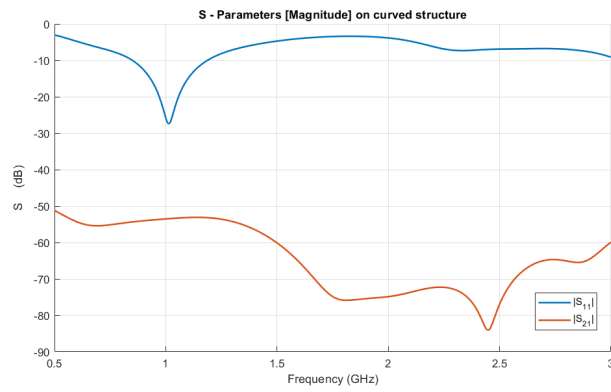
(a)  $|S|$  - Parameter on plane structure(b)  $|S|$  - Parameter on plane structure(c)  $|S|$  - Parameter on curved structure with  $R = 100$  mm

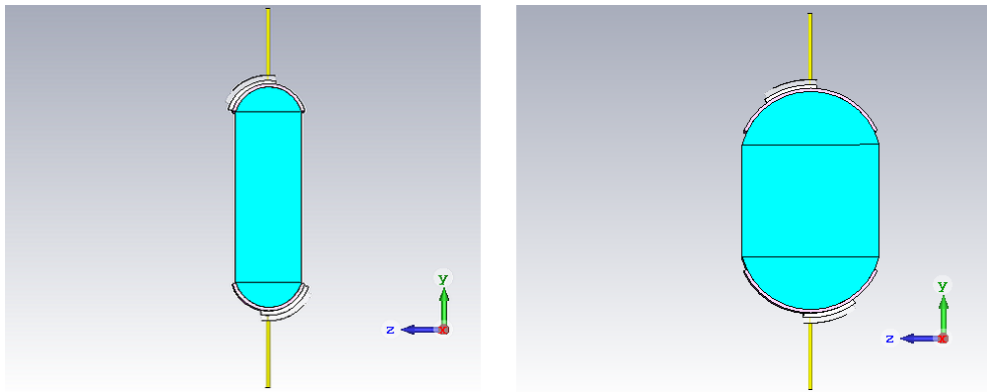
Figure 4.26: Reflection and transmission of antenna (12)



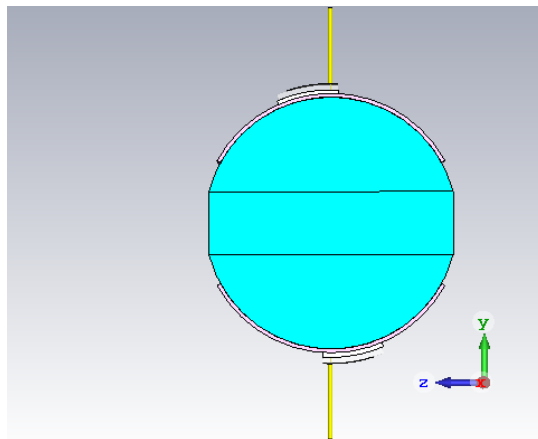
(d)  $|S|$  - Parameter on curved structure with  $R = 100$  mm

Figure 4.26: Reflection and transmission of antenna (12)

Moreover, the transmission was evaluated also for different radius curvature, by maintaining the same distance between the antennas (that is 200 mm):



(a) Transmission structure with  $R = 30$  mm (left) and  $R = 65$  mm(right)



(b) Transmission structure with  $R = 100$  mm

Figure 4.27: Reflection and transmission of antenna (12)

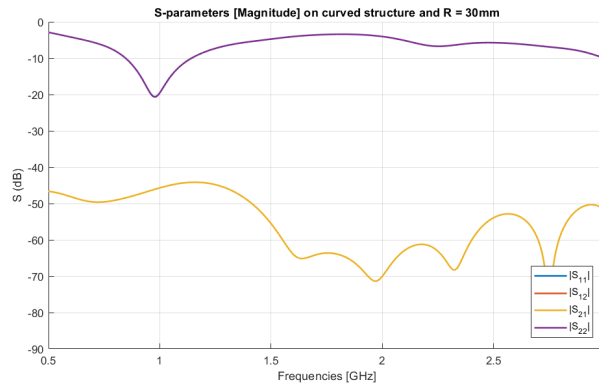
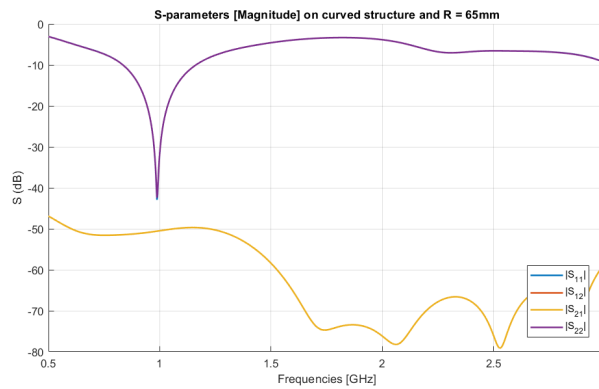
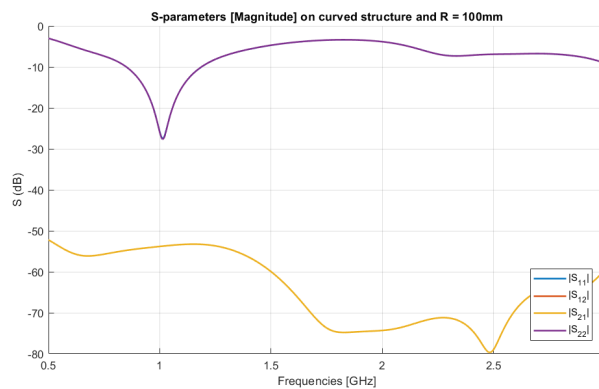
(c)  $|S|$ -Parameters on curved structure with  $R = 30$  mm(d)  $|S|$ -Parameters on curved structure with  $R = 65$  mm(e)  $|S|$ -Parameters on curved structure with  $R = 100$  mm

Figure 4.27: Reflection and transmission of antenna (12)

For this part, just a verification was done. Therefore, it was observed if  $|S_{12}|$  and  $|S_{21}|$  are above  $-110$  dB. The detection of the target was done in the successive section 4.5, in which the complete model of the head was used.

## 4.5 Results on head model

In this simulation part the model was made complex. Indeed, a structure that simulates the head shape was realized. Moreover, also the presence of a target was evaluated.

This model is reported in figure 4.6 in which an external layer made of ABS is filled with a material mimicking the brain tissues. In particular, four type of simulations were done:

1. by using just one antenna;
2. by using two antennas without any target;
3. by using two antennas introducing something mimicking the stroke;
4. by using all the 24 antennas.

Unfortunately, this model still presents some problems that are not so relevant, but they could affect the final results. One of this problem is that the head shape was realized by using triangles elements, like in figure 4.6. Therefore, the software does not allow to bend the antenna on the ABS layer since the structure must be perfectly curved. By not simulating the antenna flexibility some air gaps can be introduced slightly modifying the final results. To solve this problem, some solutions were taken into account:

- for the first three examinations, the antennas were positioned such that there were as few as possible air gaps between the antenna and the ABS;
- for the last one, the bottom portion of urethane rubber and graphite powder was increased and inserted with ABS layer to avoid air pockets.

Obviously, these solutions were applied only at the simulation level, but not at the realization level.

### 4.5.1 Head model with one antenna

The first step is to validate the functionality of the designed antenna on a head model and prove that is similar to the results obtained in the simple models.

For this system, both magnitude and phase of  $S_{11}$  were evaluated and also the Smith Chart. The simulated system is the following:

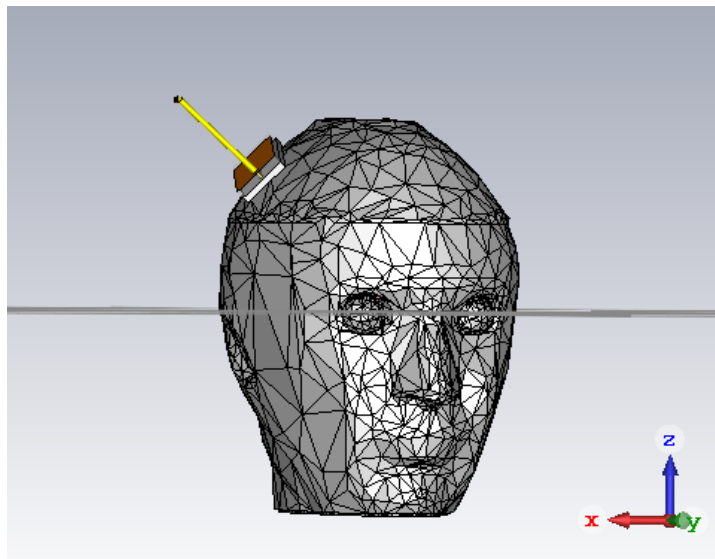


Figure 4.28: Head model with one antenna for CST Microwave Studio

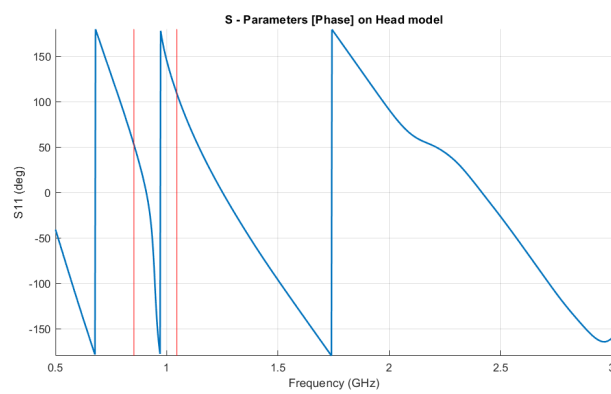
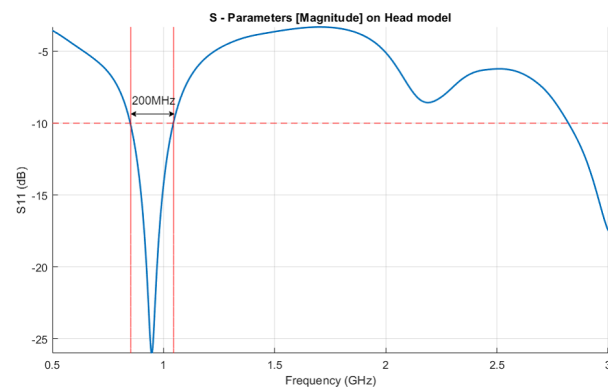
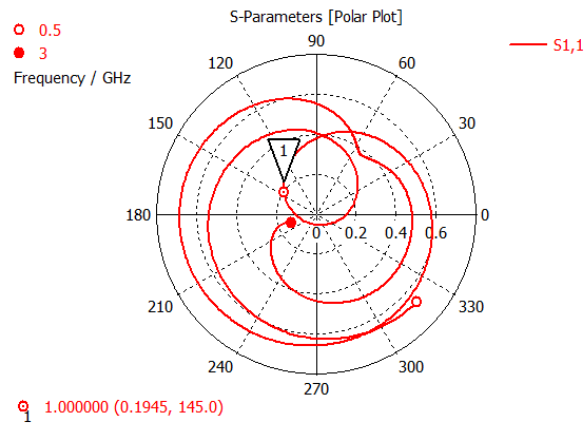


Figure 4.29: Results on head model with one antenna



(c) Smith Chart

Figure 4.29: Results on head model with one antenna

Comparing figure 4.24a (that is the simulation of just one antenna on curved structure) with 4.29a, it is possible to observe that the trend of  $|S_{11}|$  is similar. In the first case the reflection coefficient allows to affirm that the system is slightly more matched and the bandwidth at  $-10$  dB is bigger than the other. Anyway, it is necessary to take into account that in the second case no flexibility is considered. So, this can explain the careless difference between the two cases. As observed from the simple models, it is possible that by considering the bending, the two conditions can be very similar.

In any case, it is possible to affirm that the functionality of the system is the expected one.

#### 4.5.2 Head model with two antennas

This part is probably the more interested since the detection of the stroke is studied.

The system was modelled such that two antennas were opposite one to the each other. In this way, more material is present between them, so the signal should be more attenuated. This means that if the object is detected in this condition, it is surely detect also when the signal is less attenuated.

This situation was evaluated in two conditions:

1. the model do not consider any target;
2. in the model was introduced an object that seems a stroke.

By doing these, it is possible to observe if the model is able to detect the presence of an object within the head tissues. Therefore, the evaluation is done by taking into consideration the S-parameters of the two conditions. By calculating

the differential signal of the two it is possible to affirm that the system is able to reveal the target. In particular, this evaluation is done on the transmission coefficients that are those that allow the transfer information between two antennas. The differential signal is computed by doing the difference of  $|S_{12}|$  (or  $|S_{21}|$ ) after the stroke and  $|S_{12}|$  (or  $|S_{21}|$ ) before the stroke:

$$\Delta S_{12} = S_{12,stroke} - S_{12,NOstroke}$$

Obviously, it is necessary that this signal does not go below  $-100$  dB to not fall in the noise range.

The first condition gives the following results:

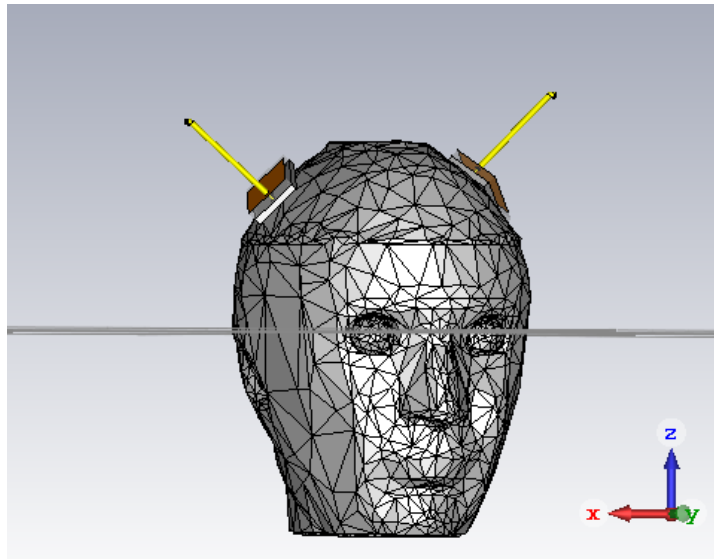


Figure 4.30: Head model with two antennas and no target for CST Microwave Studio

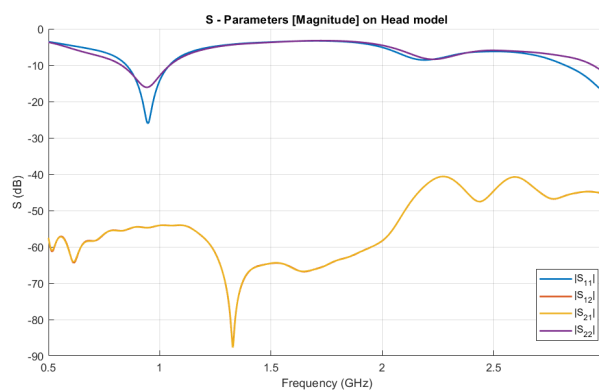


Figure 4.31: S-parameters with two antennas and no target

The difference on the reflection coefficients can be due to the fact that the second antenna is positioned in a part that presents higher air pockets than the first one. Then, the stroke was introduced. To model it a sphere of 15 mm radius is used. Its material was created on CST Microwave Studio such that it presents a relative dielectric constant  $\epsilon_r = 61.06$  and a conductivity  $\sigma = 1.5829S/m$ . These

values are valid at 1 GHz for blood. Indeed, they are values that changes with frequency, but considering a band that goes from 0.8 GHz to 1.6 GHz these are:

Frequency(GHz)	Conductivity $\sigma(S/m)$	Relative permittivity $\epsilon_r$
0.80	1.4956	61.70
0.89	1.5331	61.39
0.98	1.5727	61.13
1.07	1.6145	60.89
1.16	1.6584	60.67
1.24	1.7047	60.46
1.33	1.7531	60.28
1.42	1.8037	60.08
1.51	1.8566	59.91
1.60	1.9117	59.74

Table 4.11: Dielectric properties of blood from 0.8GHz to 1.6GHz

From the table above it is possible to claim that these values are not so difference from those proposed. Moreover, since the interested frequency is 1GHz, it is possible to model this material by considering  $\epsilon_r$  and  $\sigma$  as constants.

The results are the following:

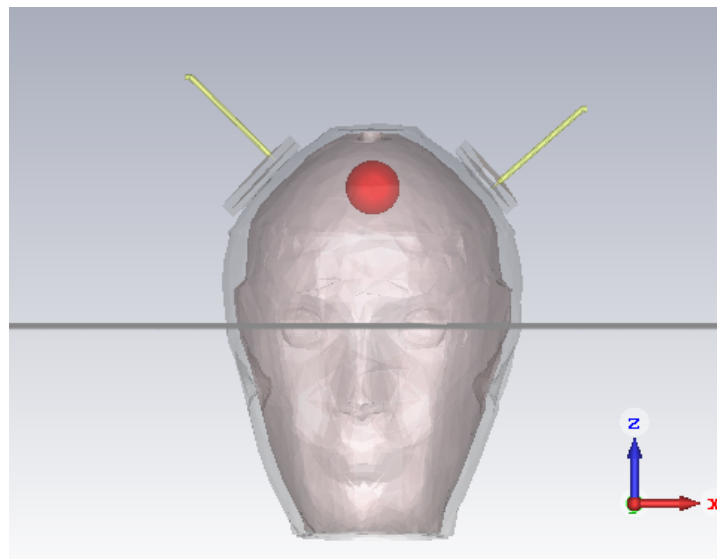


Figure 4.32: Head model with two antennas and stroke for CST Microwave Studio

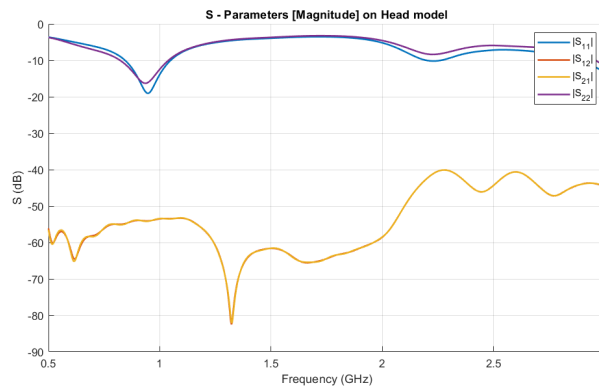


Figure 4.33: S-parameters with two antennas and stroke

By putting together the graphs in figures 4.31 and 4.33, it is possible to observe a difference on the transmission coefficients:

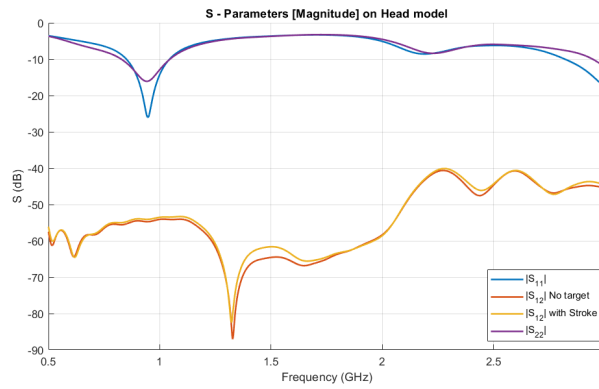
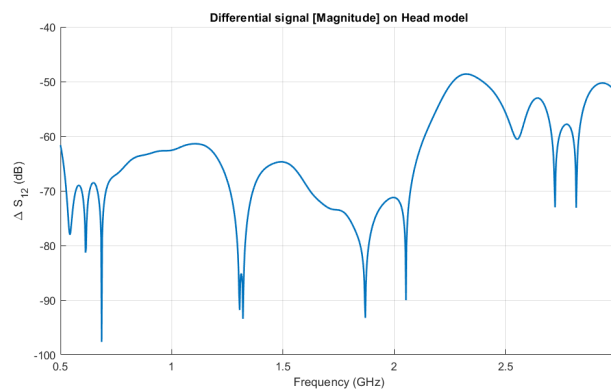


Figure 4.34: S-parameters without and with stroke

Their differential signal is:

Figure 4.35: Differential signal of  $|S_{12}|$ 

in which the  $|S|$ -parameters (in dB) at 1 GHz are:

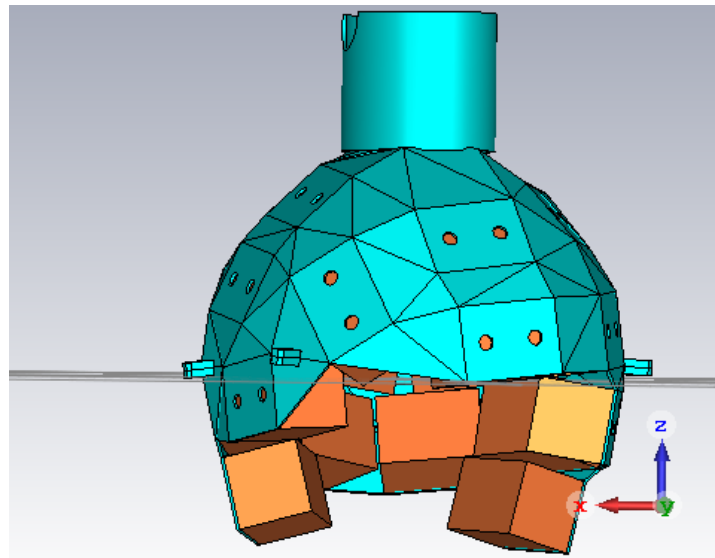
$$S_{NOstroke} = \begin{bmatrix} -14.22 & -54.10 \\ -54.09 & -12.87 \end{bmatrix}$$

$$S_{stroke} = \begin{bmatrix} -13.89 & -53.44 \\ -53.51 & -12.44 \end{bmatrix}$$

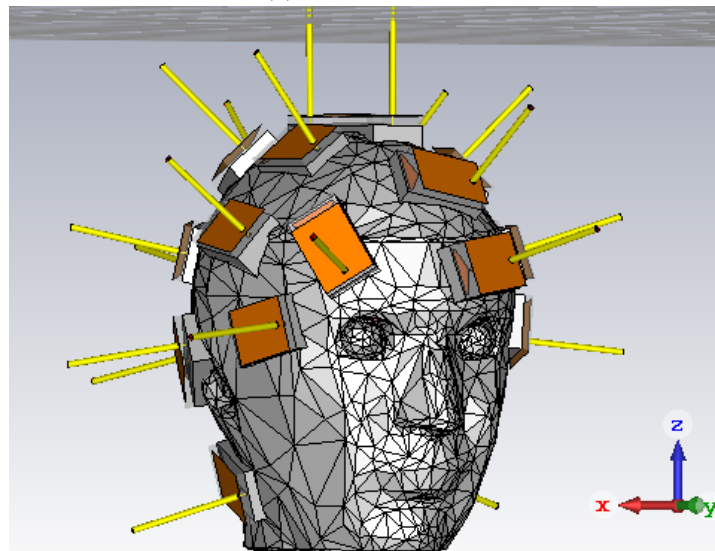
$$\Delta S = \begin{bmatrix} -25.16 & -62.57 \\ -61.97 & -22.65 \end{bmatrix}$$

### 4.5.3 Head model with twenty-four antennas

Finally, twenty-four antennas were positioned by using a specific scheme defined by a helmet like in figure 4.36.



(a) Helmet model



(b) Complete structure

Figure 4.36: Model with twenty-four antennas for CST Microwave Studio

For this simulation the frequency domain solver was used since the time one needs a very big number of meshcells, so the simulation can be very long. To pass from the time domain solver to the frequency a verification on the model

with two antennas was done to be sure that the new solver is able to give results that are compatible between the two. The verification was accomplished.

For this simulation 576 elements must be obtained in which the  $S_{ii}$  parameters are the reflection coefficients of the system and the  $S_{ij}$  are the transmission coefficients.

Since the model is not so accurate, it was observed the general behaviour of the system trying to understand it:

- the reflection coefficients are similar;
- the transmission coefficients respect the reciprocity theorem, so  $S_{ij} = S_{ji}$ ;
- there is a difference on the transmission coefficients before and after the stroke at 1GHz, trying to obtain two matrices 24x24.

Regarding the reflection coefficients it is possible to affirm that their behaviour is similar for all the antennas, obtaining:

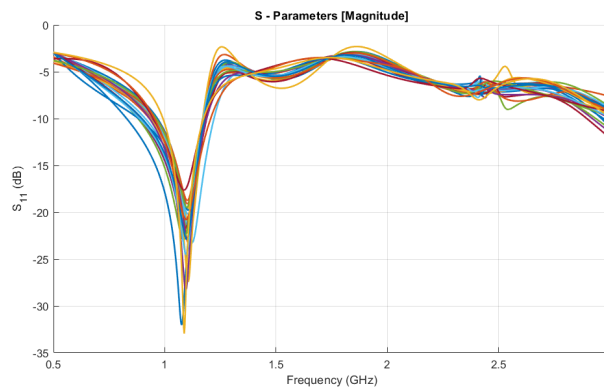
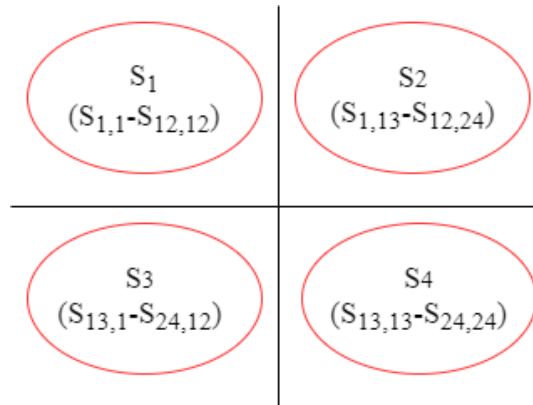


Figure 4.37: Reflection coefficients of the system

The S-parameters of the system without and with the stroke at 1 GHz and their differential signal are computed. They are 24x24 matrices. Hence, to make the matrices easier to read, they have been divided into four sub-matrices 12x12 in which:

- the first reports the elements from  $|S_{1,1}|$  to  $|S_{12,12}|$ ;
- the second reports the elements from  $|S_{1,13}|$  to  $|S_{12,24}|$ ;
- the third reports the elements from  $|S_{13,1}|$  to  $|S_{24,12}|$ ;
- the fourth reports the elements from  $|S_{13,13}|$  to  $|S_{24,24}|$ ;

in which the reflection coefficients are on the diagonal of the first and the fourth sub-matrices. All the others are the transmission coefficients. Moreover, because of the reciprocity theorem, the transpose of the second sub-matrix should be equal to the third sub-matrix.



**S-parameters without stroke:**

abs(S1) =

-11.32	-35.78	-37.93	-27.18	-46.31	-38.19	-37.48	-32.02	-36.65	-42.54	-32.00	-39.05
-35.78	-12.54	-34.75	-31.88	-42.61	-39.68	-32.28	-38.03	-32.58	-41.40	-33.25	-36.89
-37.93	-34.75	-12.31	-27.13	-42.02	-32.12	-33.21	-35.16	-34.25	-43.38	-30.75	-35.97
-27.18	-31.88	-27.13	-16.54	-36.07	-31.56	-29.13	-36.89	-32.83	-40.70	-26.81	-29.59
-46.31	-42.61	-42.02	-36.07	-11.82	-53.65	-54.49	-39.15	-36.34	-48.33	-35.85	-36.71
-38.19	-39.68	-32.12	-31.56	-53.65	-12.11	-33.55	-34.59	-43.76	-42.33	-45.36	-40.65
-37.48	-32.28	-33.21	-29.13	-54.49	-33.55	-12.54	-31.54	-34.59	-39.97	-34.69	-33.18
-32.02	-38.03	-35.16	-36.89	-39.15	-34.59	-31.54	-12.34	-33.00	-51.34	-33.43	-41.17
-36.65	-32.58	-34.25	-32.83	-36.34	-43.76	-34.59	-33.00	-12.26	-44.95	-31.74	-37.82
-42.54	-41.40	-43.38	-40.70	-48.33	-42.33	-39.97	-51.34	-44.95	-11.61	-32.47	-42.89
-32.00	-33.25	-30.75	-26.81	-35.85	-45.36	-34.69	-33.43	-31.74	-32.47	-13.53	-32.74
-39.05	-36.89	-35.97	-29.59	-36.71	-40.65	-33.18	-41.17	-37.82	-42.89	-32.74	-12.26

abs(S2) =

-33.31	-41.69	-28.88	-53.63	-38.92	-31.50	-39.27	-36.45	-38.01	-39.99	-35.14	-33.60
-34.55	-40.18	-31.22	-43.08	-29.73	-30.50	-33.81	-28.29	-45.52	-45.06	-34.57	-35.31
-29.52	-32.19	-27.71	-41.13	-36.89	-28.78	-36.68	-32.77	-29.92	-31.09	-39.19	-29.82
-24.39	-34.79	-22.92	-41.50	-43.96	-23.86	-35.25	-28.53	-28.09	-39.80	-29.65	-26.21
-46.54	-46.65	-36.17	-43.47	-46.62	-43.93	-40.47	-40.86	-45.26	-46.85	-33.74	-40.66
-33.13	-39.87	-27.56	-47.53	-34.92	-32.62	-40.21	-37.17	-50.24	-46.80	-41.72	-34.51
-33.78	-39.51	-29.47	-55.14	-26.98	-29.29	-31.69	-29.20	-41.49	-47.03	-34.26	-37.20
-61.49	-51.09	-29.47	-48.81	-30.67	-35.02	-39.93	-32.94	-42.90	-35.87	-38.02	-35.40
-36.48	-33.28	-31.14	-40.92	-29.88	-40.82	-31.26	-28.31	-32.28	-32.14	-38.90	-32.23
-46.60	-42.08	-43.26	-46.95	-44.25	-40.10	-54.04	-44.94	-42.27	-47.98	-39.88	-43.10
-35.08	-31.38	-24.05	-39.95	-33.13	-24.19	-35.30	-30.58	-32.46	-35.51	-30.90	-27.65
-31.86	-40.53	-32.26	-41.70	-52.87	-30.36	-37.72	-32.23	-42.06	-45.96	-35.80	-31.40

abs(S3) =

-33.31	-34.55	-29.52	-24.39	-46.54	-33.13	-33.78	-61.49	-36.48	-46.60	-35.08	-31.86
-41.69	-40.18	-32.19	-34.79	-46.65	-39.87	-39.51	-51.09	-33.28	-42.08	-31.38	-40.53
-28.88	-31.22	-27.71	-22.92	-36.17	-27.56	-29.47	-29.47	-31.14	-43.26	-24.05	-32.26
-53.63	-43.08	-41.13	-41.50	-43.47	-47.53	-55.14	-48.81	-40.92	-46.95	-39.95	-41.70
-38.92	-29.73	-36.89	-43.96	-46.62	-34.92	-26.98	-30.67	-29.88	-44.25	-33.13	-52.87
-31.50	-30.50	-28.78	-23.86	-43.93	-32.62	-29.29	-35.02	-40.82	-40.10	-24.19	-30.36
-39.27	-33.81	-36.68	-35.25	-40.47	-40.21	-31.69	-39.93	-31.26	-54.04	-35.30	-37.72
-36.45	-28.29	-32.77	-28.53	-40.86	-37.17	-29.20	-32.94	-28.31	-44.94	-30.58	-32.23
-38.01	-45.52	-29.92	-28.09	-45.26	-50.24	-41.49	-42.90	-32.28	-42.27	-32.46	-42.06
-39.99	-45.06	-31.09	-39.80	-46.85	-46.80	-47.03	-35.87	-32.14	-47.98	-35.51	-45.96
-35.14	-34.57	-39.19	-29.65	-33.74	-41.72	-34.26	-38.02	-38.90	-39.88	-30.90	-35.80
-33.60	-35.31	-29.82	-26.21	-40.66	-34.51	-37.20	-35.40	-32.23	-43.10	-27.65	-31.40

	-11.82	-31.05	-28.40	-41.71	-44.90	-29.95	-35.69	-35.68	-31.21	-32.22	-39.23	-27.88
	-31.05	-11.96	-34.15	-40.72	-49.55	-35.62	-37.07	-36.24	-32.18	-29.28	-37.40	-31.55
	-28.40	-34.15	-14.73	-46.22	-30.33	-26.55	-39.81	-32.75	-29.55	-31.70	-28.40	-25.57
	-41.71	-40.72	-46.22	-11.37	-41.90	-43.69	-38.32	-36.95	-39.67	-38.62	-42.90	-41.80
	-44.90	-49.55	-30.33	-41.90	-12.18	-31.02	-33.86	-27.71	-40.30	-38.25	-38.10	-37.66
	-29.95	-35.62	-26.55	-43.69	-31.02	-13.57	-32.39	-28.85	-38.47	-43.00	-31.11	-30.98
abs(S4) =	-35.69	-37.07	-39.81	-38.32	-33.86	-32.39	-12.18	-28.89	-43.59	-39.39	-39.07	-35.26
	-35.68	-36.24	-32.75	-36.95	-27.71	-28.85	-28.89	-14.01	-46.63	-46.31	-32.90	-36.07
	-31.21	-32.18	-29.55	-39.67	-40.30	-38.47	-43.59	-46.63	-12.46	-38.34	-39.56	-33.13
	-32.22	-29.28	-31.70	-38.62	-38.25	-43.00	-39.39	-46.31	-38.34	-11.87	-35.15	-37.80
	-39.23	-37.40	-28.40	-42.90	-38.10	-31.11	-39.07	-32.90	-39.56	-35.15	-12.72	-34.79
	-27.88	-31.55	-25.57	-41.80	-37.66	-30.98	-35.26	-36.07	-33.13	-37.80	-34.79	-13.01

**S-parameters with stroke:**

	-11.40	-37.21	-46.60	-30.38	-49.90	-43.14	-40.56	-32.57	-37.69	-44.88	-33.20	-40.50
	-37.21	-12.16	-34.73	-36.23	-43.20	-43.04	-34.37	-37.97	-32.67	-43.17	-35.72	-38.67
	-46.60	-34.73	-12.63	-27.22	-42.82	-31.79	-34.11	-35.61	-31.72	-41.97	-34.06	-35.89
	-30.38	-36.23	-27.22	-15.91	-36.23	-32.56	-30.35	-37.78	-31.96	-39.39	-30.36	-30.87
	-49.90	-43.20	-42.82	-36.23	-11.90	-55.51	-53.38	-38.43	-35.85	-48.54	-35.38	-36.65
	-43.14	-43.04	-31.79	-32.56	-55.51	-12.28	-33.63	-35.21	-40.76	-43.66	-52.53	-39.90
abs(S1) =	-40.56	-34.37	-34.11	-30.35	-53.38	-33.63	-12.42	-31.81	-35.45	-41.33	-38.25	-34.27
	-32.57	-37.97	-35.61	-37.78	-38.43	-35.21	-31.81	-12.39	-33.79	-52.08	-35.14	-40.63
	-37.69	-32.67	-31.72	-31.96	-35.85	-40.76	-35.45	-33.79	-12.49	-45.45	-32.90	-36.62
	-44.88	-43.17	-41.97	-39.39	-48.54	-43.66	-41.33	-52.08	-45.45	-11.47	-33.35	-43.57
	-33.20	-35.72	-34.06	-30.36	-35.38	-52.53	-38.25	-35.14	-32.90	-33.35	-13.10	-34.53
	-40.50	-38.67	-35.89	-30.87	-36.65	-39.90	-34.27	-40.63	-36.62	-43.57	-34.53	-12.27

$$\text{abs}(S_2) = \begin{bmatrix} -37.23 & -46.43 & -29.32 & -48.62 & -36.88 & -35.32 & -43.50 & -37.88 & -39.10 & -40.47 & -37.33 & -34.27 \\ -35.72 & -40.00 & -33.55 & -43.24 & -30.98 & -33.35 & -35.82 & -30.06 & -49.74 & -44.58 & -36.99 & -37.98 \\ -28.31 & -30.59 & -31.31 & -39.39 & -36.90 & -28.93 & -37.90 & -34.62 & -31.58 & -32.12 & -41.86 & -32.64 \\ -25.34 & -33.62 & -26.07 & -40.30 & -48.03 & -25.25 & -36.05 & -30.05 & -29.96 & -40.55 & -31.70 & -28.82 \\ -47.48 & -46.09 & -36.88 & -43.00 & -48.67 & -44.22 & -40.18 & -40.80 & -44.68 & -46.80 & -33.57 & -40.56 \\ -33.11 & -39.93 & -29.60 & -45.66 & -36.36 & -34.38 & -41.81 & -39.37 & -57.23 & -43.24 & -41.35 & -38.05 \\ -34.93 & -40.89 & -31.96 & -54.99 & -28.07 & -30.23 & -33.22 & -31.39 & -40.09 & -45.15 & -36.23 & -37.45 \\ -45.11 & -46.01 & -30.68 & -48.14 & -31.20 & -35.38 & -40.91 & -33.20 & -42.72 & -35.77 & -37.90 & -37.75 \\ -33.71 & -32.04 & -33.27 & -39.09 & -29.45 & -39.57 & -31.98 & -28.84 & -33.56 & -33.14 & -40.12 & -34.02 \\ -49.13 & -41.83 & -45.37 & -46.71 & -45.44 & -40.53 & -51.49 & -45.33 & -43.93 & -48.95 & -41.12 & -45.90 \\ -41.84 & -32.91 & -25.79 & -40.71 & -34.77 & -25.85 & -38.78 & -33.35 & -34.00 & -35.96 & -32.43 & -29.18 \\ -31.37 & -40.32 & -34.89 & -41.20 & -63.47 & -31.71 & -37.81 & -32.29 & -44.79 & -47.66 & -37.18 & -32.62 \end{bmatrix}$$

$$\text{abs}(S_3) = \begin{bmatrix} -37.23 & -35.72 & -28.31 & -25.34 & -47.48 & -33.11 & -34.93 & -45.11 & -33.71 & -49.13 & -41.84 & -31.37 \\ -46.43 & -40.00 & -30.59 & -33.62 & -46.09 & -39.93 & -40.89 & -46.01 & -32.04 & -41.83 & -32.91 & -40.32 \\ -29.32 & -33.55 & -31.31 & -26.07 & -36.88 & -29.60 & -31.96 & -30.68 & -33.27 & -45.37 & -25.79 & -34.89 \\ -48.62 & -43.24 & -39.39 & -40.30 & -43.00 & -45.66 & -54.99 & -48.14 & -39.09 & -46.71 & -40.71 & -41.20 \\ -36.88 & -30.98 & -36.90 & -48.03 & -48.67 & -36.36 & -28.07 & -31.20 & -29.45 & -45.44 & -34.77 & -63.47 \\ -35.32 & -33.35 & -28.93 & -25.25 & -44.22 & -34.38 & -30.23 & -35.38 & -39.57 & -40.53 & -25.85 & -31.71 \\ -43.50 & -35.82 & -37.90 & -36.05 & -40.18 & -41.81 & -33.22 & -40.91 & -31.98 & -51.49 & -38.78 & -37.81 \\ -37.88 & -30.06 & -34.62 & -30.05 & -40.80 & -39.37 & -31.39 & -33.20 & -28.84 & -45.33 & -33.35 & -32.29 \\ -39.10 & -49.74 & -31.58 & -29.96 & -44.68 & -57.23 & -40.09 & -42.72 & -33.56 & -43.93 & -34.00 & -44.79 \\ -40.47 & -44.58 & -32.12 & -40.55 & -46.80 & -43.24 & -45.15 & -35.77 & -33.14 & -48.95 & -35.96 & -47.66 \\ -37.33 & -36.99 & -41.86 & -31.70 & -33.57 & -41.35 & -36.23 & -37.90 & -40.12 & -41.12 & -32.43 & -37.18 \\ -34.27 & -37.98 & -32.64 & -28.82 & -40.56 & -38.05 & -37.45 & -37.75 & -34.02 & -45.90 & -29.18 & -32.62 \end{bmatrix}$$

	-11.92	-30.08	-31.86	-40.63	-42.86	-31.57	-37.38	-42.23	-32.87	-33.38	-41.25	-29.74
	-30.08	-12.07	-38.30	-39.65	-43.31	-35.71	-38.33	-38.02	-33.55	-30.01	-38.42	-33.30
	-31.86	-38.30	-14.20	-50.69	-30.71	-29.84	-48.10	-35.93	-31.24	-32.06	-30.04	-27.34
	-40.63	-39.65	-50.69	-11.78	-40.73	-43.91	-38.71	-37.51	-40.16	-38.97	-42.90	-42.99
	-42.86	-43.31	-30.71	-40.73	-12.30	-33.58	-35.55	-28.93	-41.48	-37.68	-40.41	-39.75
	-31.57	-35.71	-29.84	-43.91	-33.58	-13.20	-34.38	-31.30	-42.31	-40.71	-33.25	-34.14
abs(S4) =	-37.38	-38.33	-48.10	-38.71	-35.55	-34.38	-12.09	-30.15	-45.42	-40.16	-42.40	-38.15
	-42.23	-38.02	-35.93	-37.51	-28.93	-31.30	-30.15	-13.64	-43.40	-44.76	-35.60	-40.61
	-32.87	-33.55	-31.24	-40.16	-41.48	-42.31	-45.42	-43.40	-12.34	-38.51	-40.11	-34.63
	-33.38	-30.01	-32.06	-38.97	-37.68	-40.71	-40.16	-44.76	-38.51	-11.82	-34.85	-38.53
	-41.25	-38.42	-30.04	-42.90	-40.41	-33.25	-42.40	-35.60	-40.11	-34.85	-12.59	-35.90
	-29.74	-33.30	-27.34	-42.99	-39.75	-34.14	-38.15	-40.61	-34.63	-38.53	-35.90	-12.94

**Differential signal:**

	-28.43	-41.32	-38.57	-30.01	-48.81	-39.87	-40.43	-41.30	-43.34	-46.34	-38.17	-44.53
	-41.32	-23.01	-58.49	-33.87	-51.56	-42.37	-36.47	-56.65	-49.25	-46.15	-36.87	-41.62
	-38.57	-58.49	-23.89	-43.87	-49.78	-43.26	-40.47	-45.23	-35.28	-47.55	-33.48	-53.26
	-30.01	-33.87	-43.87	-24.58	-50.69	-38.44	-35.23	-44.23	-39.36	-45.25	-29.34	-35.52
	-48.81	-51.56	-49.78	-50.69	-29.61	-58.22	-59.84	-46.56	-45.57	-61.52	-45.23	-54.81
	-39.87	-42.37	-43.26	-38.44	-58.22	-26.35	-50.84	-43.38	-43.79	-48.10	-46.28	-47.86
abs(diff_S1)=	-40.43	-36.47	-40.47	-35.23	-59.84	-50.84	-28.09	-43.83	-42.05	-45.66	-37.22	-39.74
	-41.30	-56.65	-45.23	-44.23	-46.56	-43.38	-43.83	-32.22	-40.79	-59.43	-38.29	-49.99
	-43.34	-49.25	-35.28	-39.36	-45.57	-43.79	-42.05	-40.79	-25.13	-54.59	-38.06	-42.81
	-46.34	-46.15	-47.55	-45.25	-61.52	-48.10	-45.66	-59.43	-54.59	-26.37	-39.81	-51.24
	-38.17	-36.87	-33.48	-29.34	-45.23	-46.28	-37.22	-38.29	-38.06	-39.81	-23.36	-37.45
	-44.53	-41.62	-53.26	-35.52	-54.81	-47.86	-39.74	-49.99	-42.81	-51.24	-37.45	-38.66

abs(diff\_S2)=

-35.57	-43.47	-39.07	-50.27	-41.16	-33.83	-41.32	-41.97	-44.52	-49.73	-39.15	-42.04
-40.80	-53.94	-35.03	-57.38	-35.75	-33.68	-38.12	-33.03	-47.58	-54.42	-38.27	-38.70
-34.47	-35.71	-30.19	-44.21	-62.34	-43.30	-42.77	-37.38	-34.92	-37.85	-42.57	-33.04
-31.48	-39.90	-25.79	-46.45	-46.13	-29.48	-42.94	-33.83	-32.64	-47.79	-33.89	-29.66
-53.67	-55.28	-44.39	-52.91	-50.88	-55.71	-52.12	-59.95	-53.65	-66.67	-47.58	-56.66
-56.81	-58.59	-31.82	-50.23	-40.43	-37.41	-45.33	-41.18	-51.21	-45.77	-52.14	-37.06
-40.09	-45.17	-33.08	-69.65	-33.52	-36.40	-36.97	-33.22	-45.68	-49.70	-38.64	-49.80
-45.21	-47.63	-35.61	-56.61	-40.15	-45.99	-46.89	-45.24	-56.76	-51.96	-53.27	-39.18
-36.97	-38.08	-35.25	-43.73	-39.66	-45.56	-39.44	-37.73	-38.19	-38.98	-44.99	-36.95
-50.17	-54.38	-47.42	-59.34	-50.45	-50.34	-55.01	-55.52	-47.24	-55.00	-45.93	-46.34
-36.11	-36.66	-28.87	-47.89	-38.15	-29.15	-37.89	-33.85	-37.69	-45.56	-36.19	-32.92
-41.06	-53.49	-35.67	-50.91	-53.27	-36.12	-54.61	-50.48	-45.36	-50.86	-41.44	-37.51

abs(diff\_S3)=

-35.57	-40.80	-34.47	-31.48	-53.67	-56.81	-40.09	-45.21	-36.97	-50.17	-36.11	-41.06
-43.47	-53.94	-35.71	-39.90	-55.28	-58.59	-45.17	-47.63	-38.08	-54.38	-36.66	-53.49
-39.07	-35.03	-30.19	-25.79	-44.39	-31.82	-33.08	-35.61	-35.25	-47.42	-28.87	-35.67
-50.27	-57.38	-44.21	-46.45	-52.91	-50.23	-69.65	-56.61	-43.73	-59.34	-47.89	-50.91
-41.16	-35.75	-62.34	-46.13	-50.88	-40.43	-33.52	-40.15	-39.66	-50.45	-38.15	-53.27
-33.83	-33.68	-43.30	-29.48	-55.71	-37.41	-36.40	-45.99	-45.56	-50.34	-29.15	-36.12
-41.32	-38.12	-42.77	-42.94	-52.12	-45.33	-36.97	-46.89	-39.44	-55.01	-37.89	-54.61
-41.97	-33.03	-37.38	-33.83	-59.95	-41.18	-33.22	-45.24	-37.73	-55.52	-33.85	-50.48
-44.52	-47.58	-34.92	-32.64	-53.65	-51.21	-45.68	-56.76	-38.19	-47.24	-37.69	-45.36
-49.73	-54.42	-37.85	-47.79	-66.67	-45.77	-49.70	-51.96	-38.98	-55.00	-45.56	-50.86
-39.15	-38.27	-42.57	-33.89	-47.58	-52.14	-38.64	-53.27	-44.99	-45.93	-36.19	-41.44
-42.04	-38.70	-33.03	-29.66	-56.66	-37.06	-49.80	-39.18	-36.95	-46.34	-32.92	-37.51

abs(diff\_S4)=

-28.14	-37.06	-31.01	-47.22	-47.11	-35.03	-40.61	-36.76	-36.19	-38.49	-43.51	-32.45
-37.06	-27.93	-36.26	-46.24	-44.48	-52.89	-43.05	-40.97	-37.87	-37.40	-44.23	-36.32
-31.01	-36.26	-23.58	-48.13	-41.14	-29.29	-40.51	-35.60	-34.48	-42.69	-33.43	-30.32
-47.22	-46.24	-48.13	-21.82	-47.01	-56.80	-48.92	-46.13	-49.42	-49.71	-72.90	-47.98
-47.11	-44.48	-41.14	-47.01	-27.92	-34.54	-38.77	-33.82	-46.52	-46.76	-41.93	-41.83
-35.03	-52.89	-29.29	-56.80	-34.54	-24.17	-36.73	-32.51	-40.79	-44.59	-35.21	-33.85
-40.61	-43.05	-40.51	-48.92	-38.77	-36.73	-29.24	-34.89	-48.22	-47.27	-41.79	-38.39
-36.76	-40.97	-35.60	-46.13	-33.82	-32.51	-34.89	-24.48	-46.21	-49.99	-36.24	-37.94
-36.19	-37.87	-34.48	-49.42	-46.52	-40.79	-48.22	-46.21	-27.84	-52.53	-48.81	-38.49
-38.49	-37.40	-42.69	-49.71	-46.76	-44.59	-47.27	-49.99	-52.53	-30.95	-46.58	-45.86
-43.51	-44.23	-33.43	-72.90	-41.93	-35.21	-41.79	-36.24	-48.81	-46.58	-27.64	-41.25
-32.45	-36.32	-30.32	-47.98	-41.83	-33.85	-38.39	-37.94	-38.49	-45.86	-41.25	-31.20

in which the graphical representation of the differential matrix can be obtained as follow:

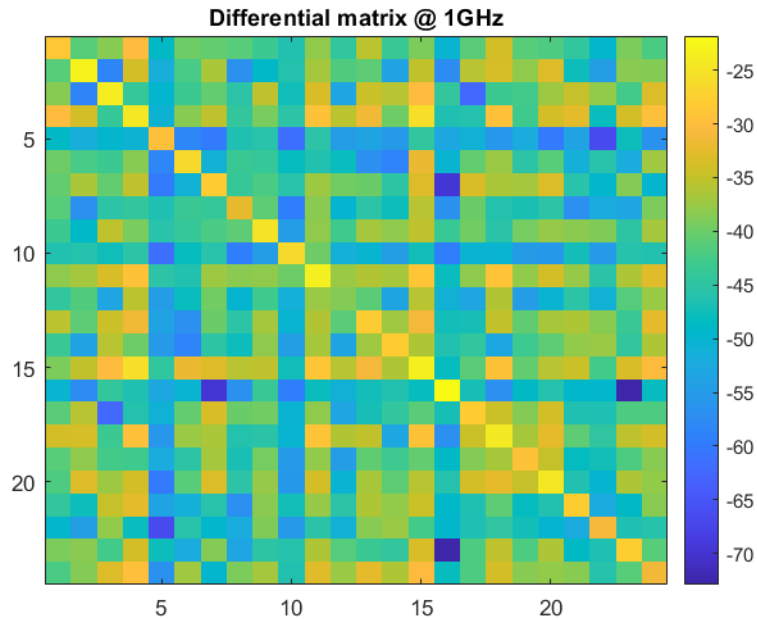


Figure 4.38: Graphical representation of the differential matrix

From these values it is possible to affirm that the reciprocity theorem is verified. In addition, since the differential signal is higher than  $-110$  dB, it does not fall into noise range. So, the information propagation allows to detect the target. The points in which the differential signal is lower, means that the antennas

are further away. Hence, the signal is more attenuated and the detection target probability tends to decrease.

## Chapter 5

# Manufacturing and measurements

In this chapter, the most important results of the project are reported. However, before describing them, it is important to talk about the system available at the Politecnico laboratory that allows to test the antennas and to exploit how the antennas were realized.

### 5.1 MiBraScan system

The MiBraScan system is composed by 24 monopole antennas that are positioned around an ABS phantom head.

#### 5.1.1 VNA and switching matrix

To obtain the head imaging, it is necessary to obtain the scattering matrix before and after the stroke. It is possible to acquire them by using a VNA that is connected to the antennas through a 2x24 switching matrix.

The VNA presents two ports and for this reason, to feed the antennas it needs the switching matrix. As said in [21], this last consists of:

- two Single-pole-four-throw (SP4T);
- eight Single-pole-six-throw (SP6T);
- twenty - four Single-pole-double-throw (SPDT).

SP4T is a switch of four choices that allows to select a set of antennas. This set is composed by six antennas, so by a SP6T, a switch of six selections, it is possible to select the antenna to connect to the port. Finally, the SPDT is a switch of two choices that allows to connect the antenna to port 1 or 2.

For the measurements the process is the following: the system active just an antenna in Tx mode while the other 23 work in sequence in Rx mode. In this way, it is possible to evaluate time after time the S-parameters of a couple of antennas that work in Tx and Rx mode. This process is done until the antennas have been worked in Tx mode. All the S-matrices are combined to obtain a matrix of 576 elements.

### 5.1.2 Final prototype structure

The first prototype consists of an ABS phantom that was immersed on a mixture of Triton X-100 and water in the volume percentage 70/30. Initially, this matching material was chosen because it is stable, easy to prepare and it has a dielectric constant of about 20 [21]. The antennas were printed on FR4 substrate and distanced 2.5 cm from phantom to guarantee matching [1].



Figure 5.1: First prototype system [21]

The actual prototype substitutes the liquid matching material with a solid one that presents a dielectric constant around 20. This is a mixture of urethane rubber and graphite powder. This last is built around the FR4 substrate with dimensions  $(5 \times 5 \times 7) \text{cm}^3$ .



Figure 5.2: Actual prototype system [16]

The structure that was realized and described in the successive sections allow to substitute the actual brick with a new one that is compact and flexible. Probably it can be the new system prototype.

## 5.2 Antennas realization and validation

In this section, the antennas development is exploited.

As said in chapter 3, the antenna is chosen to be printed on a very thin PI support. Hence, the features of the antenna geometry were sent to a company that deals with the printing of PCB circuits. In particular, a great challenge was to find a company that allows to print flexible antennas on a PI substrate, since in most cases companies prefer to print on rigid or semi-flexible structure. The printed antennas are reported below:

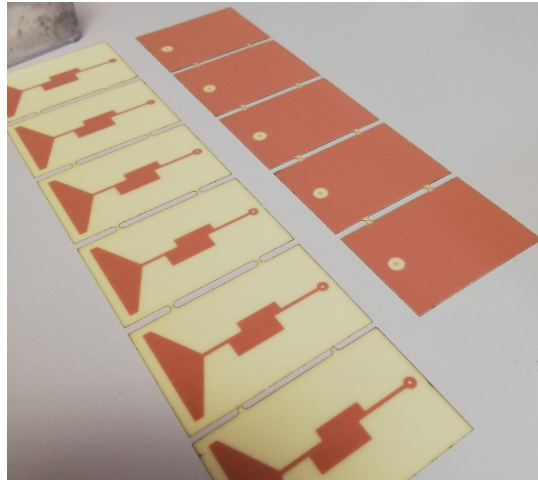


Figure 5.3: Printed antenna

In figure 5.3, the top sheets represent the ground plane, while the bottom one represent the top side of the antennas. These sheets are made up of 150  $\mu\text{m}$  PI, but the brown parts represent the metallic part of the antennas made up of copper.

Once the antennas were realized, they were glued to the portions of urethane rubber and graphite powder that are necessary in order to obtain matching between the antennas and the head. As said in section 4.2.5, these are made up of G25 and G35 that means that:

- for G25 it is necessary the 25% of graphite powder with respect to the total mixture weight, while the 75% is of urethane rubber;
- for G35 it is necessary the 35% of graphite powder with respect to the total mixture weight, while the 65% is of urethane rubber.

The mixture was prepared by defining the total weight that should be obtained and then the weight of the single materials were calculated. When the mixture was obtained, it was positioned on a mould waiting for solidification:



Figure 5.4: Mixture of urethane rubber and graphite powder on the mould

In particular, the mixture quantity necessary for the moulds in figure 5.4 is about 100 g that means:

Percentage	Urethane rubber (g)	Graphite powder(g)
G25	75	25
G35	65	35

Table 5.1: Urethane rubber and graphite powder in 100 g of mixture

Moreover, by observing figure 5.4, the bottom mould allows to obtain a portion that is thicker than the top one. Hence, it is possible to verify that the flexibility of the layer depends also on the thickness and not only on the graphite powder percentage. Indeed, in figure 5.5 it is proved that thinner the layer is more flexible is. A comparison can be done also between G25 and G35 blocks with the same thickness: the one with less graphite powder should be more flexible than the other. This proof is reported in figure 5.6.

Since a thicker layer was produced, it was then cut to obtain layers of 5 cm thick for both G35 and G25. For real, in 4.2.2 was said that the G25 layer should be 4 cm thick, but for simplicity it was realized 5 cm thick because of the mould thickness.

After the realization of the layers, it was possible to stick together the PI substrate and the matching materials (the one made up of G35) by using a super glue, as in figure 5.7. Regarding the G25 layer, it was then inserted by applying a pressure against the head.

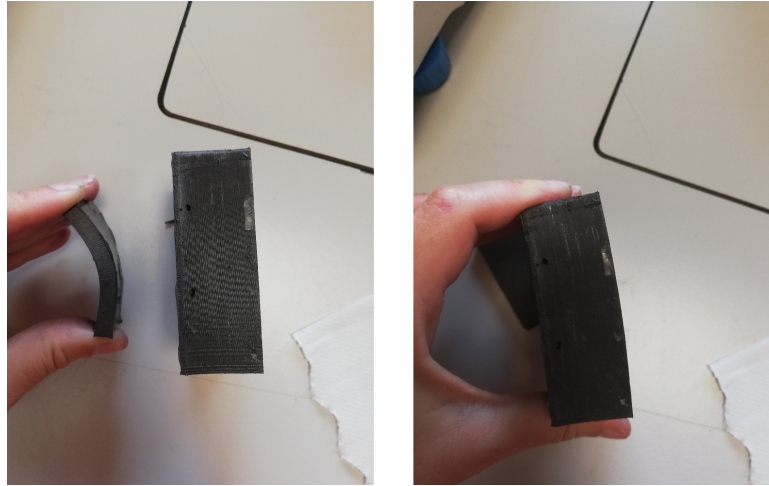


Figure 5.5: Flexibility of thin and thick layers

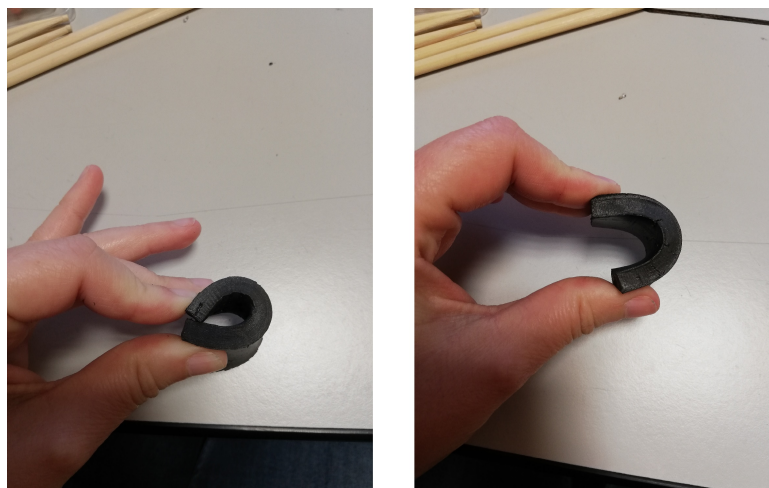


Figure 5.6: Flexibility of G25 (left) and G35(right) layers

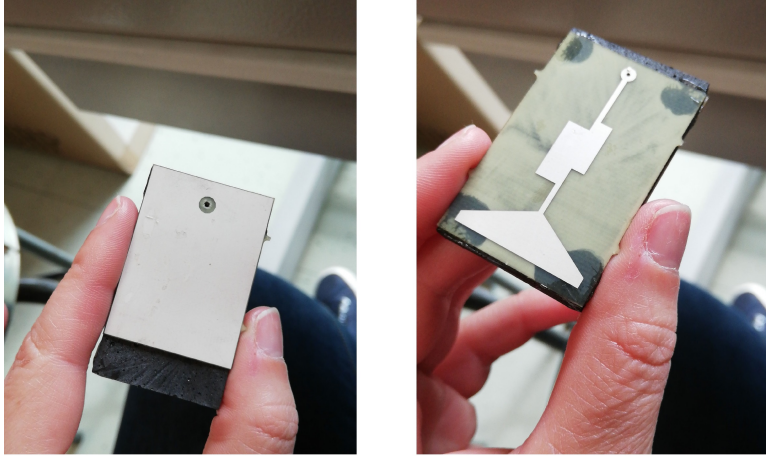


Figure 5.7: Antenna and matching material stick together

The antenna can be feed by welding a connector that allows to connect the antenna to the VNA:

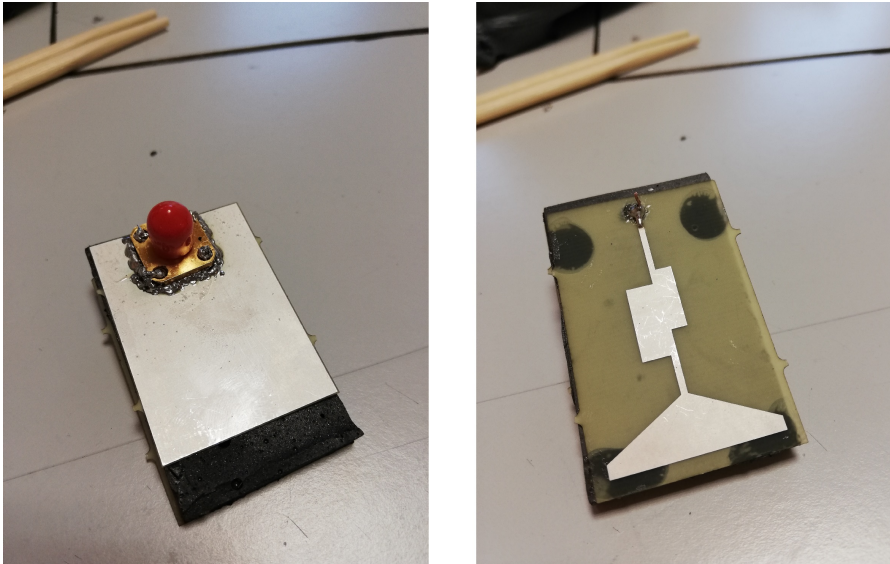


Figure 5.8: Structure with connector

The final structure and the proof of its flexibility is reported below:

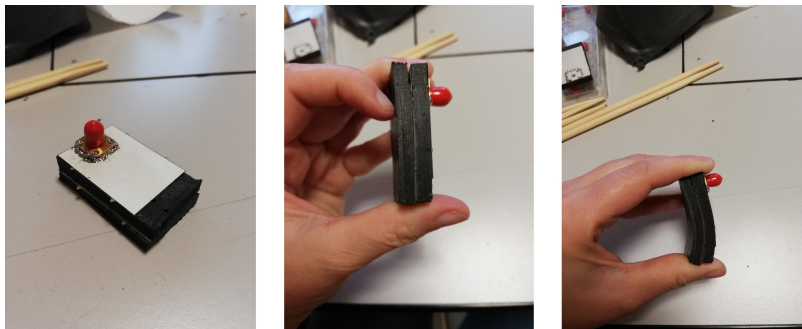


Figure 5.9: Final structure

### 5.3 Measurements results

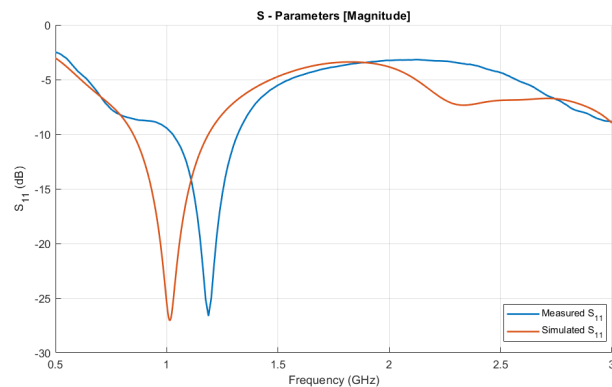
Following the process reported in section 5.2, six antennas were realized and tested.

The measurements consisted of two main steps:

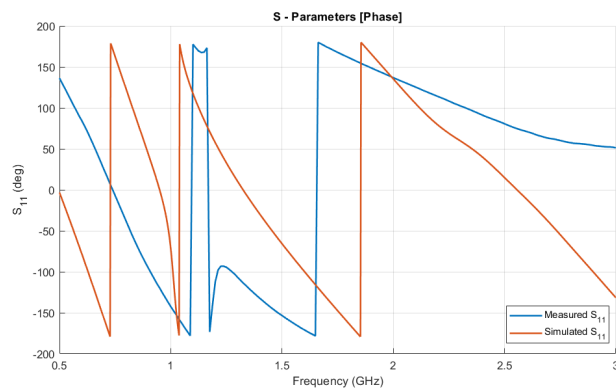
1. some antennas were tested by putting them close to a plastic jar filled by a liquid mimicking the brain tissues;
2. all the antennas were tested by putting them close to an ABS 3D phantom head filled by a liquid mimicking the brain tissues.

The first step was done to observe an operating principle of the antennas, while the other was necessary to study the working antennas on a more realistic system.

Starting from the first step, just three antennas were tested singularly or by coupling them in order to study the scattering parameters. Moreover, in this condition it was possible to exploit the effect of the decreasing radius curvature since the jar is composed by a bigger and a smaller radius. This is an interesting thing since in section 4.3 three different curvature were studied, but the radius of the jar are not the same to the simulated one. Anyway, a comparison between the higher curved structures has been done to observe the compatibility between the measured and the simulated condition. Indeed:



(a)  $S_{11}$  Magnitude



(b)  $S_{11}$  phase

Figure 5.10: Comparison between measured and simulated  $S_{11}$  on bigger R

During the testing the antenna was pressed against the head by using tape. This measurement was done in this condition:



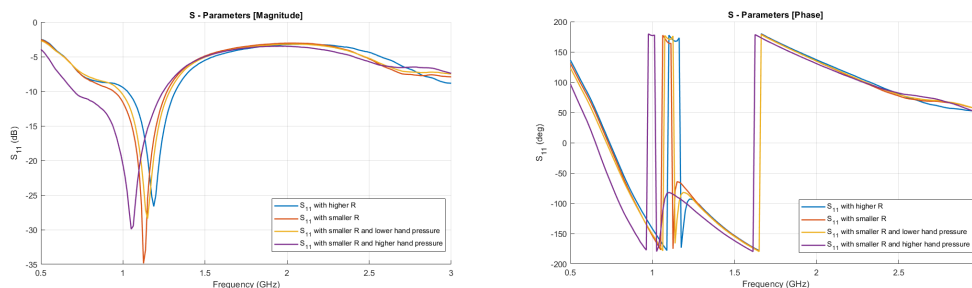
Figure 5.11: Measurement on jar

Observing figure 5.10a, it is possible to see that the behaviour of  $|S_{11}|$  is similar, but its measured minimum value moves toward higher frequencies. Probably, this is due to big radius of the jar that is higher than the simulated one. In addition, the pressure of the antenna against the jar is not as the wanted one, that should be higher, and for this reason the measured minimum peak is at slightly high frequency.

In particular, for this experiment four different cases were exploited:

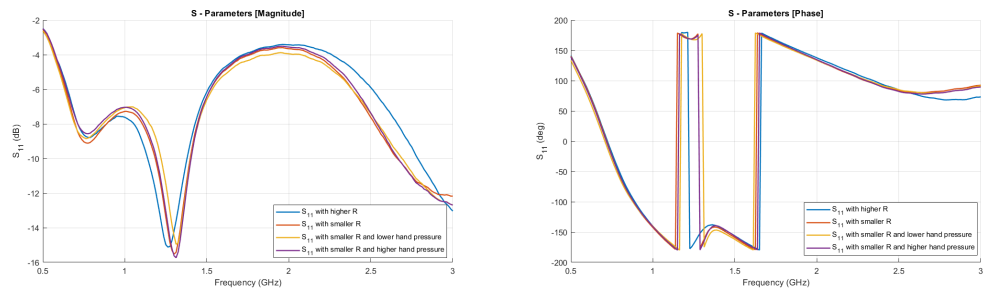
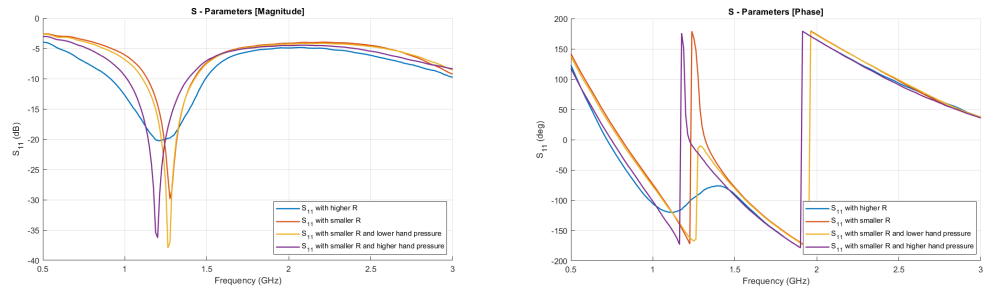
- antenna on bigger curve;
- antenna on small curve;
- antenna on small curve with a small hand pressure;
- antenna on small curve with a high hand pressure.

For the three antennas:

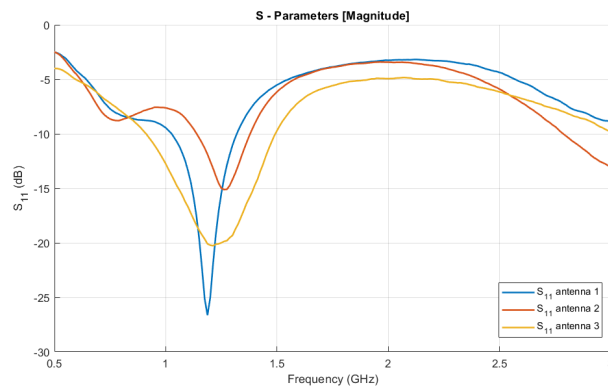


(a)  $S_{11}$  first antenna

Figure 5.12: Measured  $S_{11}$  on jar

(b)  $S_{11}$  second antenna(c)  $S_{11}$  third antennaFigure 5.12: Measured  $S_{11}$  on jar

Comparing the magnitude of them:

Figure 5.13: Comparison of measured  $|S_{11}|$  on jar

From the comparison, it is possible to observe that the three antennas present slightly different behaviour. Anyway, the results allow to affirm that their behaviour is acceptable for the interesting application. This difference can be due to some factors, such as: the antenna position, maybe it is not exactly the same; the tape pressure; welding and connectors; the final result of the production process and tolerances on printed antennas should be slightly different.

Considering figures 5.12, some conclusions can be drawn. First of all, by drastically decreasing the curvature radius, the  $|S_{11}|$  minimum peak moves toward lower frequencies. This behaviour is conformal to the simulated one reported in section 4.3. Moreover, the application of hand pressure, it is possible to affirm that in order to obtain the desired behaviour, it is necessary to apply the right pressure that can be done by using a head cap. This verification was done to ob-

serve that by reducing air pockets, it is possible to obtain better performances. Then, the transmission between the first and the second antenna was evaluated without any target just to observe the behaviour of it. In particular, this evaluation was done by putting the antennas on opposite positions on bigger curvature.

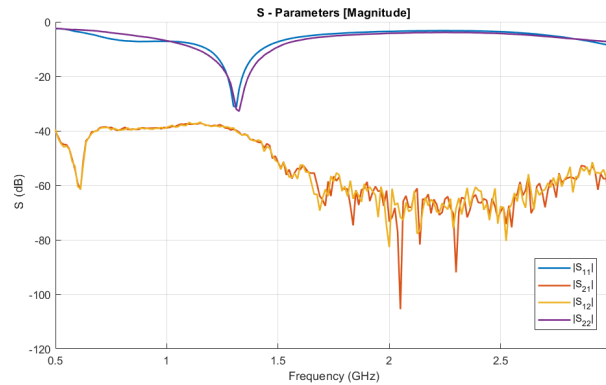


Figure 5.14: Transmission between first and second antenna on jar

After this experiments, the antennas were put close to a 3D phantom head to observe how they work on a more realistic system:



Figure 5.15: 3D phantom head system

The antennas were positioned on phantom head by using elastics that allow to flex them also if pressure is not as the head cap one.

In this situation six antennas were tested. Firstly they were tested singularly to determine if they work properly. Then, they were tested two - by - two studying the transmission coefficients without any target. Finally, the two antennas that

were more compatible, were used to observe transmission introducing an object mimicking blood.

For the single measurements, the antennas  $S_{11}$  parameters are put together to easily compare them. In this way, it is possible to choose which of them should be used to study the transmission with target.

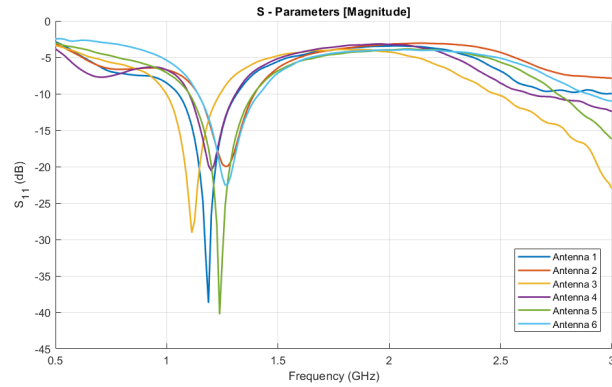
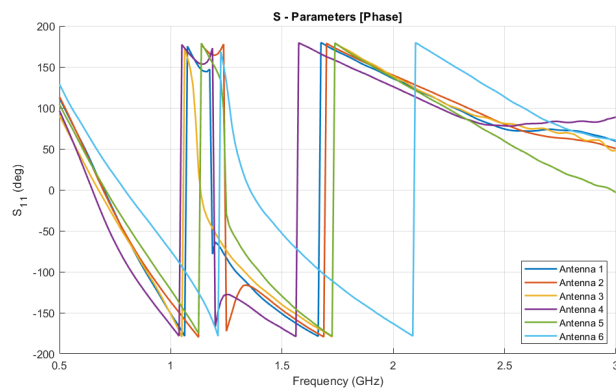
(a)  $S_{11}$  Magnitude(b)  $S_{11}$  Phase

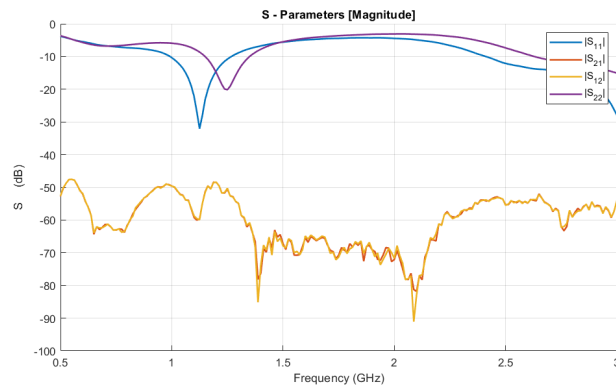
Figure 5.16: Measured  $S_{11}$  for all the realized antenna on phantom head

From the figure above, it is possible to affirm that the antennas activities are acceptable for all of them. Anyway, their behaviour can be improved by considering a better system and by applying the right pressure such that air pocket can be avoid.

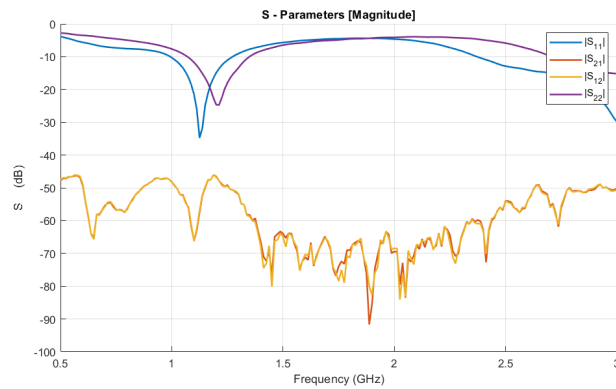
Moreover, by comparing the first three antennas in figure 5.16 with the one in 5.13, it is possible to observe that the behaviour of them is slightly different. This is surely due to the different system.

However, by introducing a second antenna with respect to the condition before, the different position can influence the behaviour of the reflection coefficient. For this reason, it is necessary to observe how they work two-by-two before the target introduction.

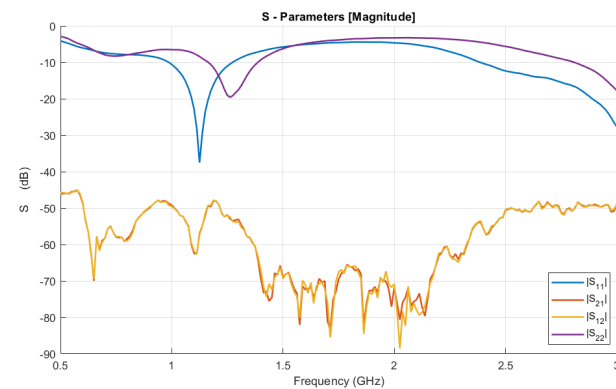
For this part all the combination were observed, but just the more interesting are reported. In this case, the antennas are positioned on the opposite sides of the phantom head, so the higher distance between them is observed :



(a) S - parameters couple Antenna 1 and 2

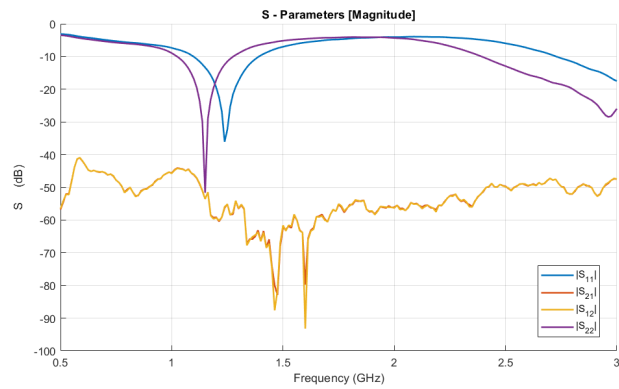


(b) S - parameters couple Antenna 1 and 3

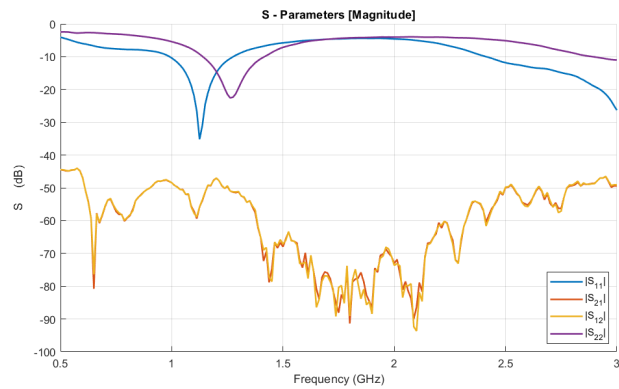


(c) S - parameters couple Antenna 1 and 4

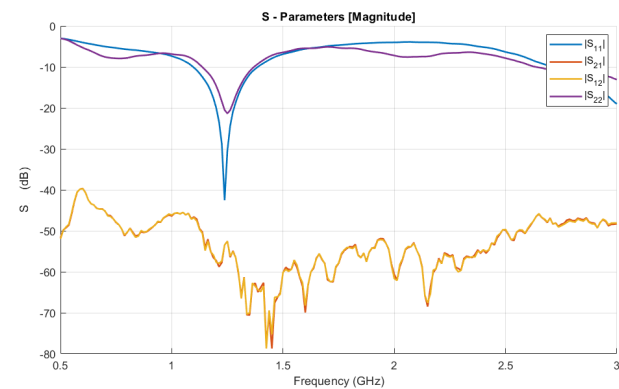
Figure 5.17: Measured S - parameters on phantom head



(d) S - parameters couple Antenna 1 and 5

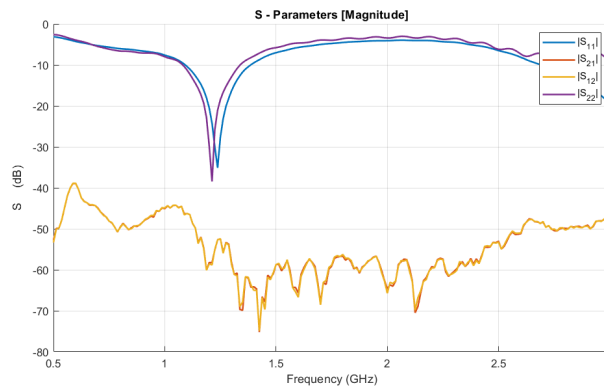


(e) S - parameters couple Antenna 1 and 6



(f) S - parameters couple Antenna 5 and 2

Figure 5.17: Measured S - parameters on phantom head



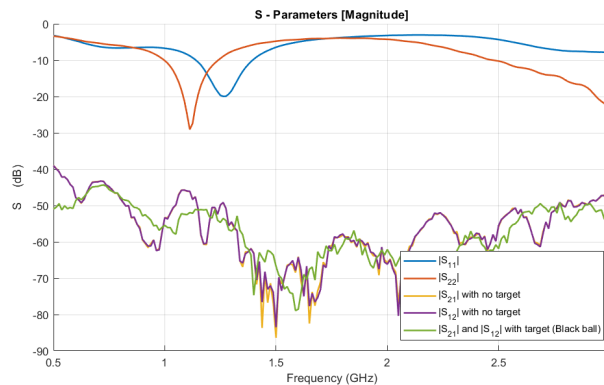
(g) S - parameters couple Antenna 3 and 5

Figure 5.17: Measured S - parameters on phantom head

Some of them are reported just to observe if they present similar behaviour, like figure 5.17g. The others, in particular the one from figure 5.17a to 5.17e, are introduced to observe that the position and pressure influence the final results. Indeed,  $|S_{11}|$  associated to the first antenna, is not always the same in all the conditions.

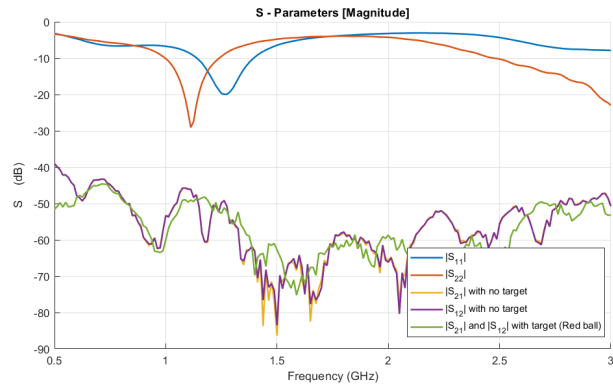
Regarding the transmission coefficients,  $|S_{12}|$  and  $|S_{21}|$ , the positive thing is that the reciprocity theorem can be considered verified since  $|S_{12}| \approx |S_{21}|$ . Moreover, by comparing figure 4.33 (simulation with two antennas and no target) and figures in 5.18a, independently on the spikes due to the noise measurement system device, the trend of the transmission coefficients are compatible and similar. So, it is possible to affirm that the system works as expected.

In simulation, just the blood target was used, but in laboratory different objects are present. In particular, they are made of plastic material with relative dielectric constant  $\epsilon_r = 2.1$ . They are spheres of about 1.20 cm. Hence, they were used just to observe if the measurements reveal the dielectric contrast. In particular, the studied couples were the one composed by: antenna 1 and 2; antenna 1 and 3; antenna 1 and 5.

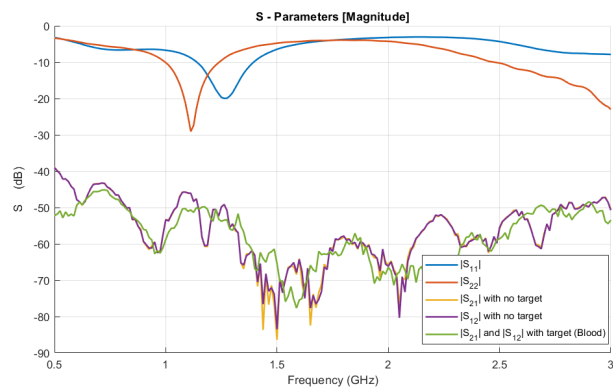


(a) S-parameters with black ball target

Figure 5.18: Measured S-parameters on phantom head couple antenna 1 and 2

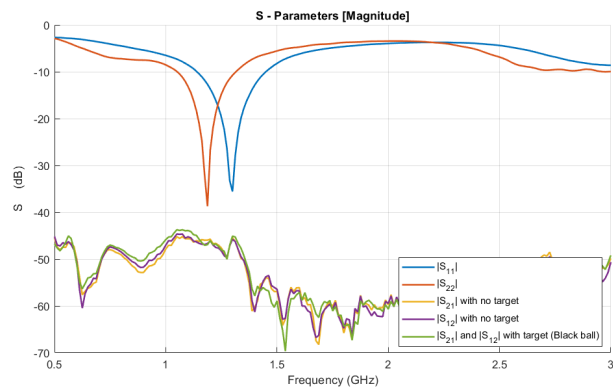


(b) S-parameters with red ball target



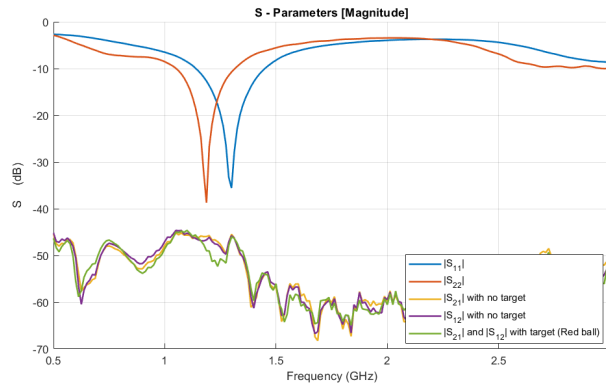
(c) S - parameters couple with blood target

Figure 5.18: Measured S-parameters on phantom head couple antenna 1 and 2

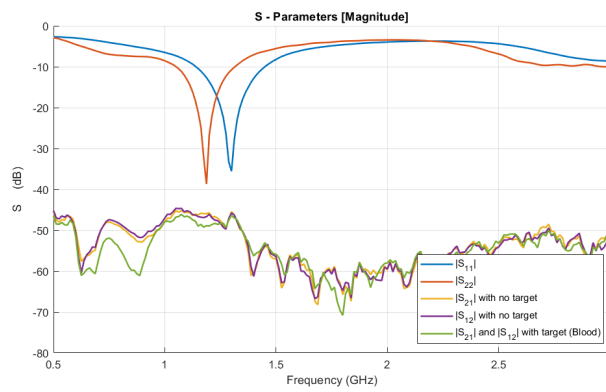


(a) S - parameters with black ball target

Figure 5.19: Measured S-parameters on phantom head couple antenna 1 and 3

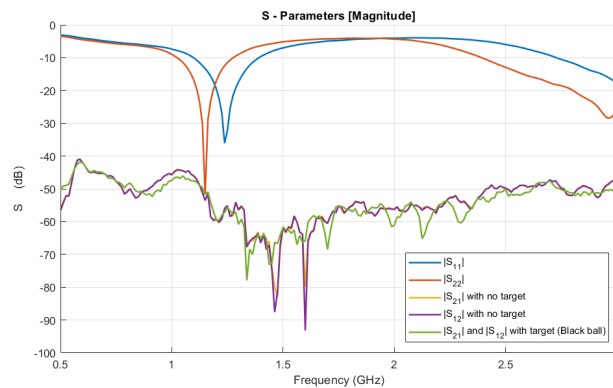


(b) S-parameters with red ball target



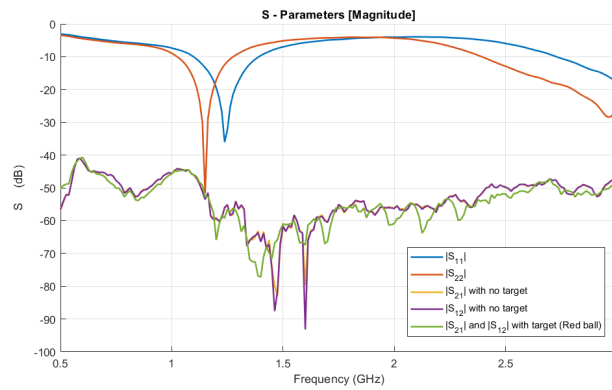
(c) S-parameters couple with blood target

Figure 5.19: Measured S-parameters on phantom head couple antenna 1 and 3

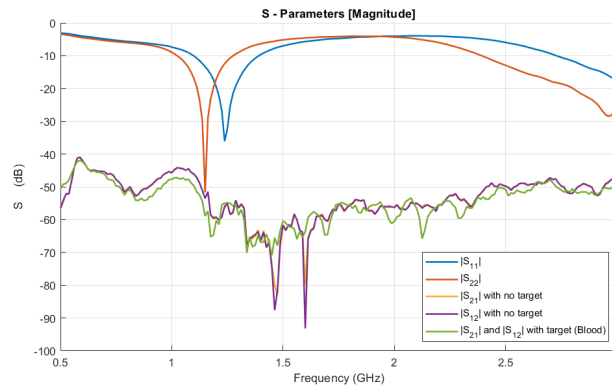


(a) S-parameters with black ball target

Figure 5.20: Measured S-parameters on phantom head couple antenna 1 and 5



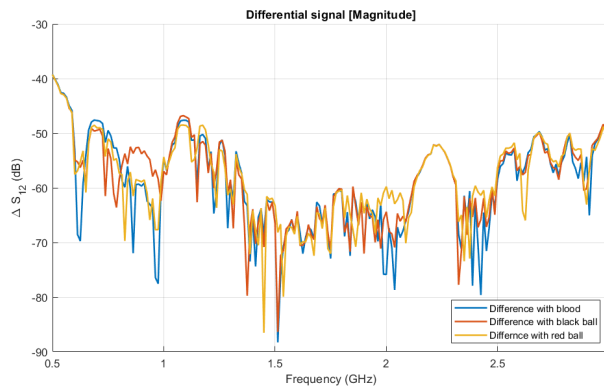
(b) S-parameters with red ball target



(c) S-parameters couple with blood target

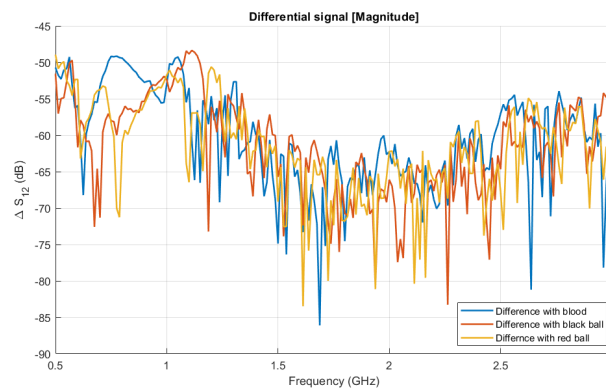
Figure 5.20: Measured S-parameters on phantom head couple antenna 1 and 5

By introducing targets, it is possible to observe that the transmission coefficients of the system, slightly change than the no target system. This means that the antennas are able to transmit information between them. To reconstruct the image, it is necessary to evaluate the S-parameter with and without target and do the difference between them. Their differential signals are:

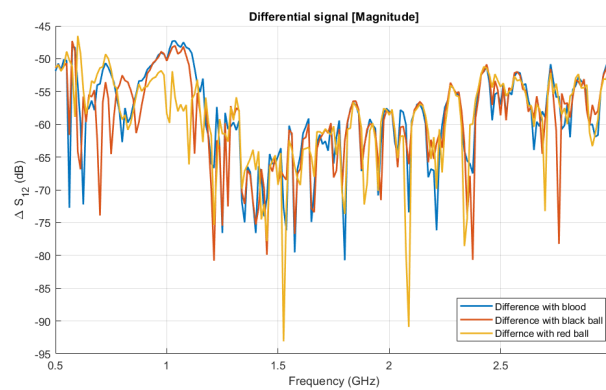


(a) Differential signal for couple antennas 1 and 2

Figure 5.21: Differential signals for the measured antennas



(b) Differential signal for couple antennas 1 and 3



(c) Differential signal for couple antennas 1 and 5

Figure 5.21: Differential signals for the measured antennas

In conclusion, it is possible to affirm that the designed and manufactured antennas are satisfactory since their differential signals allow to detect the dielectric contrast between a target and the surrounded brain tissues liquid. At this point, it is possible to proceed with the data processing to make the reconstruction of the image possible, which is performed at software level using an appropriate algorithm.

## Chapter 6

# Conclusion and future work

In this thesis, after a theoretical review on the TL and brain stroke, the MWI system has been studied such that brain stroke can be detected. In particular, the study deals with the antennas realization that allow to compute the head scanning.

The main goal was to improve the prototype present at the Politecnico di Torino to make it portable, compact and flexible in order to guarantee a pre-hospital diagnosis and higher bending to head. To perform these changes several simulations were done until the specifics verification.

The first modification consists in changing 1.6 mm FR4 substrate with a 150  $\mu\text{m}$  PI one. Obviously, it is necessary to maintain the conductive part of urethane rubber and graphite powder to guarantee matching between the antenna and brain tissues. But, they were simulated such that flexibility can be guaranteed. Moreover, some changes were done on the geometry of the antenna, too. From these analyses, the final antenna presents:

- a bandwidth at  $-10$  dB of about 340 MHz;
- $|S_{11}|$  at 1 GHz of about  $-26$  dB.

These values are optimal considering the fact that they can slightly change on a real system.

Then, some antennas were realized in laboratory to verify the simulation behaviour. Moreover, it was possible to verify their flexibility and compactness, too.

From measurements it can be claimed that most of the antennas present a behaviour similar to those of the simulations. They present a bandwidth around 300 MHz – 400 MHz. Also if their reflection coefficients at 1 GHz are higher than the simulated one, they are below  $-10$  dB. In addition, the variation on the transmission coefficients before and after the introduction of a target, allows to affirm that the antennas are able to reveal the dielectric contrast between the object and the surrounding brain tissues, so to detect a possible stroke.

In conclusion, such structure should be a good candidate for the new prototype. In any case, small optimizations can be contemplated.

However, before making a new prototype, it is important to carry out some small examinations such as:

- adopting measurements that guarantee the right pressure provided by a headset in order to reduce air gaps between the antenna and the head;

- guarantee a good welding and production of the urethane rubber and graphite powder layers that influence the final result;
- performing accurate simulations and measurements of a more complex system that provides for the presence of all 24 antennas with the possibility of observing how they behave with the presence of a target;
- use the manufacturing antennas to realise a 24 antennas prototype in which the measured data will be processed to realise the head image.

# Bibliography

- [1] R. Scapaticci, J. Tobon, G. Bellizzi, F. Vipiana and L. Crocco, "Design and Numerical Characterization of a Low - Complexity Microwave Device for Brain Stroke Monitoring", *IEEE TRANSACTIONS ON ANTENNAS AND PROPAGATION*, VOL. 66 NO. 12, 2018.
- [2] A. Fhager, S. Candefjord, M. Elam and M. Persson, "Microwave Diagnostics Ahead," *IEEE microwave magazine*, 2019.
- [3] A. Berto, "Wideband Fabry - Pérot cavity antenna with overlapping feeds for advanced communications", Master Thesis, Politecnico di Torino, Italy, 2018
- [4] C. A. Balanis, "Antenna theory: analysis and design," *John wiley & sons*, 2016.
- [5] [Online]. Available: <https://ambiente.veniceairport.it/it-it/campielettromagnetici/campovicino-campolontano.aspx>
- [6] R. Orta, Topic: "Lecture Notes on Electromagnetic Field Theory", Department of Electronic and Telecommunication, Politecnico di Torino, Italy
- [7] R. Orta, Topic: "Lecture Notes on Transmission Line Theory", Department of Electronic and Telecommunication, Politecnico di Torino, Italy
- [8] [Online]. Available: <https://www.marionegri.it/magazine/ictus-cerebrale>
- [9] [Online]. Available: [https://www.physio-pedia.com/Epidemiology,\\_Incidence\\_and\\_Global\\_Burden\\_of\\_Stroke](https://www.physio-pedia.com/Epidemiology,_Incidence_and_Global_Burden_of_Stroke)
- [10] W. Johnson, O. Onuma, M. Owolabi and S. Sachdev, " Stroke: a global response is needed", *Bulletin of the World Health Organization*, 2016
- [11] [Online]. Available: <http://www.emro.who.int/health-topics/stroke-cerebrovascular-accident/index.html>
- [12] National Institute of biomedical imaging and bioengineering, "Computerized Tomography," *NIH... Turning Discovery Into Health*, 2019
- [13] National Institute of biomedical imaging and bioengineering, "Magnetic resonance imaging," *NIH... Turning Discovery Into Health*, 2019
- [14] [Online]. Available: [https://en.wikipedia.org/wiki/Microwave\\_imaging#Principles](https://en.wikipedia.org/wiki/Microwave_imaging#Principles)
- [15] Z. Wang, E. G. Lim, Y. Tang and M. Leach, "Medical Applications of Microwave Imaging", *The Scientific World Journal*, 2014

- [16] J. A. Tobon Vasquez, R. Scapatucci, G. Turvani, G. Bellizzi, D. O. Rodriguez-Duarte, N. Joachimowicz, B. Duchêne, E. Tedeschi, M. R. Casu, L. Crocco and F. Vipiana, "A Prototype Microwave System for 3D Brain Stroke Imaging", *Sensors* 2020, 2020.
- [17] Persson M., Fhager A., Trefnà H.D., Yu Y., McKelvey T., Pegenius G., Karlsson J.E., Elam M., "Microwave-Based Stroke Diagnosis Making Global Pre-hospital Thrombolytic Treatment Possible.", *IEEE Trans. Biomed. Eng.* 2014, 61, 2806–2817.
- [18] Candefjord S., Wings J., Malik A., Yu Y., Rylander T., McKelvey T., Fhager A., Elam M., Persson M., "Microwave Technology for Detecting Traumatic Intracranial Bleedings: Tests on Phantom of Subdural Hematoma and Numerical Simulations.", *Med. Biol. Eng. Comput.* 2017, 55, 1177–1188.
- [19] Hopfer M., Planas R., Hamidipour A., Henriksson T., Semenov S., "Electromagnetic Tomography for Detection, Differentiation, and Monitoring of Brain Stroke: A Virtual Data and Human Head Phantom Study." *IEEE Antennas Propag. Mag.* 2017, 59, 86–97.
- [20] A. Alqadami, N. Nguyen-Trong, . B. Mohammed, M. Tobias and A. Abosh, "Compact Unidirectional Conformal Antenna Based on Flexible High Permittivity Custom-made Substrate for Wearable Wideband Electromagnetic Head Imaging System," *Transactions on Antennas and Propagation*, 2019.
- [21] J. Tobon, R. Scapatucci, G. Turvani, G. Bellizzi, N. Joachimowicz, B. Duchene, E. Tedeschi, M. Casu, L. Crocco and F. Vipiana, "Design and Experimental Assessment of a 2-D Microwave Imaging System for Brain Stroke Monitoring", *International Journal of Antennas and Propagation*, 2019.
- [22] R. Scapatucci, L. Di Donato, I. Catapano and L. Crocco, "A feasibility study on Microwave Imaging for brain stroke monitoring", *Progress In Electromagnetics Reserch B*, Vol.40, 305-324, 2012.
- [23] [Online]. Available: <https://omnexus.specialchem.com/selection-guide/polyimide-pi-plastic>
- [24] [Online]. Available: <https://www.franklowe.com/materials/urethane-rubber/>
- [25] G. Malesevic, "Wearable Microwave Antennas for Brain Stroke Imaging", Master Thesis, Politecnico di Torino, Italy, 2019